Maria da Graça Vieira de Brito Almeida
Mestre em Engenharia Electrotécnica e de Computadores

Image Processing for Displacement Measurements

Dissertação para obtenção do Grau de Doutor em
Engenharia Electrotecnia e de Computadores

Orientador: José Manuel Matos Ribeiro da Fonseca,
Prof. Aux., FCT
Co-orientador: Fernando Manuel Fernandes Melício,
Prof. Coord., ISEL

Júri:

Presidente:	Prof. Doutor Luís Manuel Camarinha de Matos
Arguente(s):	Prof. Doutor Agostinho Cláudio Rosa
	Prof. Doutor Arnaldo Joaquim Castro Antunes
Vogais:	Prof. Doutor José Miguel Costa Dias Pereira
	Prof. Doutor Alberto Jorge Lebre Cardoso
	Prof. Doutor Carlos Chastre Rodrigues
	Prof. Doutor André Teixeira Bento Damas Mora
	Prof. Doutor José Manuel Matos Ribeiro da Fonseca

FACULDADE DE CIÊNCIAS E TECNOLOGIA
UNIVERSIDADE NOVA DE LISBOA

Setembro 2014

Image Processing for Displacement Measurements

To my Family

Acknowledgments

The completion of my dissertation has been a long journey. Much has happened in these five years and the conclusion of this thesis was only possible with the support of various people.

I would like to express my very great appreciation to my supervising professor, José Manuel Fonseca, for his patient guidance, enthusiastic encouragement and useful critiques of this research work.

My co-supervisor professor, Fernando Melício, I would like to thank for his help and relevant discussions.

Special thanks goes to professors André Mora and Arnaldo Abrantes for their relevant comments as members of the thesis committee.

I am particularly grateful to professor Carlos M. Chastre Rodrigues from the FCT Civil Department, for supplying valuable data for my research and for his powerful knowledge in several aspects of my research. His suggestions, co-operation and provision of some of the data evaluated in this study were of major interest for this research. His willingness to give his time so generously was very much appreciated. In addition, this project would not have been possible without the tests developed in the Materials Laboratory by Hugo Biscaia, Tiago Carvalho, António Monteiro, Noel Franco, Isabel Borba and Cinderela Silva, where it was possible to get all the images needed for this work. I am very grateful to you all.

I am highly indebted to FCT-UNL, extended to all its staff, who welcomed me in a wonderful way, and the cooperation protocol with Instituto Superior de Engenharia de Lisboa (ISEL).

Of course no acknowledgment would be complete without giving thanks to my parents, brothers and sisters and also my close friends. Thanks for the support and encouragement from the beginning until the end of this work.

Abstract

Since the invention of photography humans have been using images to capture, store and analyse the act that they are interested in. With the developments in this field, assisted by better computers, it is possible to use image processing technology as an accurate method of analysis and measurement. Image processing's principal qualities are flexibility, adaptability and the ability to easily and quickly process a large amount of information.

Successful examples of applications can be seen in several areas of human life, such as biomedical, industry, surveillance, military and mapping. This is so true that there are several Nobel prizes related to imaging.

The accurate measurement of deformations, displacements, strain fields and surface defects are challenging in many material tests in Civil Engineering because traditionally these measurements require complex and expensive equipment, plus time consuming calibration.

Image processing can be an inexpensive and effective tool for load displacement measurements. Using an adequate image acquisition system and taking advantage of the computation power of modern computers it is possible to accurately measure very small displacements with high precision. On the market there are already several commercial software packages. However they are commercialized at high cost.

In this work block-matching algorithms will be used in order to compare the results from image processing with the data obtained with physical transducers during laboratory load tests. In order to test the proposed solutions several load tests were carried out in partnership with researchers from the Civil Engineering Department at Universidade Nova de Lisboa (UNL).

Keywords: Image Processing; Digital Image Correlation; Block Motion Estimation; Displacement and Strain Measurements; Photogrammetry.

Resumo

Desde a invenção da fotografia que o ser humano tem vindo a utilizar a imagem para capturar, armazenar e analisar as situações em que está interessado. Com o desenvolvimento de computadores mais rápidos e potentes é possível utilizar o processamento de imagem como método de análise e de medição. Diversos exemplos de aplicação deste método podem ser encontrados na biomedicina, indústria, vigilância, aplicações militares e mapeamento. Igualmente alguns prémios Nobel foram atribuídos a cientistas que utilizaram o processamento de imagem nos seus estudos.

Flexibilidade, adaptabilidade e capacidade de processar grandes quantidades de informação são algumas das qualidades do processamento de imagem. A medição precisa de deformações, deslocamentos, campos de tensão e defeitos de superfície são um desafio em muitos ensaios de materiais em Engenharia Civil onde, tradicionalmente, estas medidas exigem equipamentos complexos e caros e demorados de calibração.

O processamento de imagens é um meio barato e eficaz para efectuar medições de deslocamento em ensaios de carga. Utilizando um sistema de aquisição de imagem e um computador adequados é possível medir com alta precisão pequenos deslocamentos. Apesar de no mercado já existirem vários pacotes de programas comerciais estes são comercializados a um preço elevado.

Neste trabalho serão utilizados algoritmos de estimação de movimento, sendo os resultados comparados com os dados obtidos pelos transdutores físicos. A fim de testar as soluções propostas foram realizados vários testes laboratoriais em parceria com investigadores do Departamento de Engenharia Civil da Universidade Nova de Lisboa (UNL).

Palavras-chave: Processamento de Imagens; Correlação Digital de Imagem; Algoritmos de Estimação de Movimento; Mapas de deslocamento e de tensão; fotogrametria;

Abbreviations and Notations

ARPS - Adaptive Rood Pattern Search Algorithm

c1, c2, c - Constants of the PSO algorithm

CC - Cross Correlation

CCD - Charge Coupled Device

CF - Cost Function

C_{ij} - Pixel intensities in the current block

$\bar{C}$ - Mean of all pixels in the current block

cmax - Number of block columns analysed by the algorithm

d - Displacement

DIC - Digital Image Correlation

2D-DIC - Two Dimensional Digital Image Correlation

E- - Elastic modules

F - Tensile Force

MAD - Mean Absolute Error

MAX - Number of images analysed by the algorithm

lmax - Number of block lines analysed by the algorithm

L - Original specimen length

LVDT - Linear Variable Differential Transformers

ME - Motion Estimation

MME - Minimal Matching Error

MPEG - Moving Picture Experts Group

MSE - Mean Square Error

MV - Motion Vector

N - Pixel line per block

NS - Number of steps

NTSS - New Three Step Search

RGB - Red Green Blue colour model

ROI - Region of Interest

TSS - Three Step Search Algorithm

SES - Simple and Efficient Search Algorithm

S_S - Step Size

PSCH - Pattern Signature Correlation Histogram

PSO - Particle Swarm Optimization

r, r1, r2 - Random number in range [0,1]

R_{ij} - Pixel intensities in the reference block

$\bar{R}$ - Mean of all pixels in the block reference

RP–PSO - Rood Pattern-Particle Swarm Optimization

w - Search window

W - Inertia weight of PSO algorithm

ε - Extensional strain

γ - Distortion angle

σ - Tensile stress

τ - The size of ARPS rood pattern

List of Contents

List of Figures

List of Tables

Chapter 1

Introduction

The aim of this section is to present the motivation for this research. The research question and the hypothesis are described. The structure of the thesis is also presented for a better comprehension.

1 Introduction

1.1 Motivation

Since the invention of photography (at 1826) humans have used images to capture, store and analyse acts that they are interested in. With the developments in this field (particularly digital photography from 1957 and the invention of Charge Coupled Device (CCD) in 1969) supported by better computers, it is nowadays possible to use image processing technology as an accurate method of analysis and measurement. Successful examples of applications can be seen in several areas of human life such as: biomedicine, industry, surveillance, military and mapping. This is so true that several Nobel prizes have been given related to image analysis.

The principal qualities of image processing are flexibility, adaptability and an ability to easily and quickly deal with a large amount of information.

Digital Image Processing is more and more frequently used as an additional power tool in various Civil Engineering areas, such as load tests, crack measurements and material test inspections. Normally, to take measurements load cells, linear variable differential transformers (LVDT) and electrical strain gauges are used. With this traditional methodology a lot of equipment and a very complex procedure are required.

Using image processing techniques it is possible to measure the whole area of interest and not just a few points of the material under test as happens with traditional methodology. Image processing allows for a significant improvement in this area because a single camera and a simple computer can do both the data acquisition and the analysis of the whole area of the material under study without the need for any additional equipment as in the traditional method.

When conventional methodology is used, the number of measured points takes on a huge importance because as they increase so the need for hardware, setup time and costs also increases. Increasing the number of measured points

may corrupt the experiment as it is an intrusive method. Using image analysis techniques the density of the measured points can be very high without any changes to the equipment. As an example, a trivial image of 1024 × 1024 pixels can be used to obtain a continuous information field with more than 300 analysis points.

Digital Image Correlation (DIC) is a method that examines consecutive images taken during the deformation period, and detects the movements based on a mathematical correlation algorithm. This is accomplished by taking two digitized images representing the non-deformed and the deformed stages. In many situations a random pattern is imposed or special target points are inserted for a more efficient correlation. Image Correlation is also very flexible because it is possible to apply this technique to several types of digital image such as photography, optical and microscopy.

Since the 1980's when DIC was first conceived(Peters and Ranson 1982; M. Sutton et al. 1983; Chu, Ranson, and Sutton 1985), several studies have been developed to obtain an optimized and accurate algorithm.

With DIC in planar components (2D-DIC) it is possible, among others, to:

- understand various materials' deformation behaviours (metals, plastics, wood, ceramics and tensile loading of paper) (Dai et al. 2012; Huang, Liu, and Sun 2014; Iyer and Sinha 2006; Nishikawa et al. 2012; Park et al. 2007);
- measure the material properties of a beetle wing (Jin et al. 2009);
- do full-field measurement of transient strain in various board assemblies subjected to shock in various orientations (Lall et al. 2007);
- calculate real time full-field deformation analysis on the Ballistic Impact of Polymeric Materials (Yu et al. 2009).

Only in the late 1990s did researchers apply 2D-DIC to study damage in composites and concrete as mentioned in (M. A. Sutton, Orteu, and Schreier 2009).

Fracture mechanics is often studied because many objects are made of steel and/or concrete and this material can break when it is subject to cyclic

loads that can cause fatigue cracks. Theoretical predictions on crack growth can be done based on fracture mechanic approaches in conjunction with traditional experimental observations. Material composition and the end-shear confinement were found to affect the non-uniform deformations observed in the early stages of loading (Carvalho et al. 2010; Choi and Shah 1998; Nishikawa et al. 2012).

It is therefore very important to investigate new methods to inspect these materials. In this thesis three different algorithms were used along with data obtained in real tests, and they were presented in different scientific conferences: the Simple and Efficient Search (SES) algorithm (G. Almeida et al. 2010), the Adaptive Rood Pattern Search (ARPS) algorithm (Graça Almeida et al. 2011), the studies of using different block sizes (Graça Almeida, Melicio, and Fonseca 2011) and the changes in Particle Swarm Optimization algorithm in order to grow to Rood Pattern - Particle Swarm Optimization (RP-PSO) algorithm (G Almeida, Melicio, and Fonseca 2012).

One important issue is the impact of the random pattern on the resulting measurements. Different specimens were studied in the five years of tests done in partnership with researchers from the Civil Engineering Department of the Universidade Nova de Lisboa (UNL). These specimens were concrete beams (3m and 0.6m wide), carbon fibre reinforced polymer (CRFP) and specimens of Plexiglas, balsa wood and PVC. Figure 1-1 shows the experimental setup.

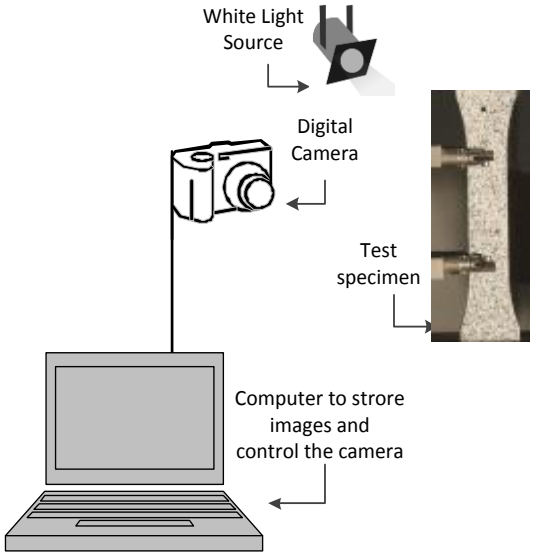

Figure 1-1. Experimental Setup

1.2 Research

The main research objective is to produce a system able to perform data acquisition and analysis with high accuracy, low cost and easy setup for use in stress tests.

The proposed system aims to contribute to monitoring load tests that are able to:

- Acquire the data;
- Process the information in different regions of interest;
- Analyse the results, such as stress and displacements maps.

Through this system an improvement in the research on the behaviour of materials is possible since it is not limited to the number of sensors and this may enable a complete study of the material rather than just a small region of it. The combination of traditional measurements with image analyses techniques can give an improvement in high precision structural analysis in environments such as material research laboratories.

The major research questions that have to be answered by this study are:

- Are Block Matching Algorithms suitable to get the displacement map?
    - What kind of correlation technique is most efficient?
    - What should the relationship between the entire image and the number of target points be?
- Is it viable to use edge information for a fast search on global areas and block matching for detailed processing on restricted areas?
- Is a random pattern preferable to a regular pattern?
    - How does the speckle pattern affect the results?
    - Is it possible to increase the accuracy of the system without significantly increasing the computation time?

In order to answer these research questions the following items were taken into consideration:

- Identification and characterization of the problems associated with images subject to thresholding;

- Identification of the best block-matching algorithm possibility combined with other types of algorithms;
- Identification of the best system parameters: cost function, block size and pattern qualification;

The data obtained in real tests with different specimens and different speckle patterns was used in this work. It was therefore possible to compare the image processing results with the information obtained by physical sensors.

As a result, the main outcomes of this thesis include:

- An algorithm able to deal with small and large displacements;
- Definition of the best block size in function of the current speckle pattern;
- Adjustment of the number of target points in function of the size of the beam;
- Calculation of the strain map for the entire concrete beam;
- A tool that can be used in Civil Engineering laboratory research.

1.3 Validation Methodology

In this thesis two common block matching algorithms (the Simple and Efficient and the Adaptive Rood Pattern Search) are compared with the new Rood Pattern-Particle Swarm Optimization algorithm (RP-PSO) as well as the Pattern Signature Correlation Histogram algorithm (PSCH). The evaluation of these algorithms is based on real test data. This work shows the performance improvement of the block motion algorithms in respect to the choices of the parameters to become completely independent of the random pattern applied, the focal distance or the lighting conditions.

This study compares the results of the image processing approach with the data acquired by physical sensors. Throughout the tests it became clear that the sensors often had some error caused by calibration problems or sensor placement. As such a new method of validating the data obtained by either physical sensors or by the image processing algorithms was needed.

For this new validation methodology a specific program was prepared in order to present an image-time series to a trained researcher. The researcher starts by choosing a particular point in the first image and identifies the same point throughout the entire image-time series. Each sequence is classified three times and the average is adopted as the reference value called Golden Standard (GS). This methodology is replicated for each physical sensor used on the test.

To analyse the algorithm's performance the number of computations (number of calls to the cost function i.e. the number of evaluated blocks) and the computation time were measured.

Four papers were presented in different scientific conferences:

- Almeida, Graça; Biscaia, H.; Chastre C.; Melicio, F, Fonseca, J., " Displacement Estimation of a RC Beam Test based on TSS algorithm", IEEE xplore digital library, 11497923, ISBN: 978-1-4244-7227-7, Information Systems and Technologies (CISTI), 2010 5th Iberian Conference on, 16-19 Jun.
- Almeida, Graça; Melicio, Fernando; Chastre, Carlos; Fonseca, José, "Displacement Measurements with ARPS in T-Beams Load Tests", Springer, Volume 349, Chapter 31, Pages 286-293, 01/01/2011, ISBN: 978-3-642-19169-5, DOI: 10.1007/978-3-642-19170-1_31, Editor: Springer Berlin Heidelberg.
- Almeida, Graça; Melicio, Fernando; Fonseca, José, "Displacement measurements with block motion algorithms", Computational Vision and Medical Image Processing Conference, Pages 155-160, ISBN: 9780415683951, September 28, 2011 by CRC Press.
- Almeida, Graça; Melicio, Fernando; Fonseca, José, "Block Matching Algorithms for Load Test Evaluation", Civil-Comp Press, 2012 Proceedings of the Eighth International Conference on Engineering Computational Technology, DOI:10.4203/ccp.100.57, B.H.V. Topping, Civil-Comp Press, Stirlingshire, UK.

Two journal papers are in the review process awaiting the final decision:

- Almeida, Graça; Melicio, Fernando; Fonseca, José, "Structural Deformation Measurements by Image Block Matching Algorithms", International Journal of Structural Integrity
- Almeida, Graça; Biscaia, Hugo; Chastre Carlos; Melicio, Fernando, Fonseca, José, "In-Plane Displacement and Strain Image Analysis", Computer-Aided Civil and Infrastructure Engineering.

1.4 Thesis Structure

This thesis is organized in five chapters.

The initial chapter is the introduction (Chapter 1) where the motivation, the research question and the validation methodology are presented.

In Chapter 2 a review (State-of-the-Art) of the more important concepts in block motion, and three of the most commonly used block matching algorithms are described.

In Chapter 3 the developed algorithms and the Civil Engineering theory applied to digital image analysis are presented.

The results of the most relevant tests are exposed in Chapter 4 and in the final chapter the conclusions and future work are presented.

Chapter 2

State-of-the-Art

This section contains the literature review supporting the research proposed in this document. Chapter 2 is divided into two main parts. Firstly, a brief introduction to block motion concepts followed by presentation of the algorithms. Secondly the trends in displacement measurements are surveyed to better contextualize the current status.

2 State-of-the-Art

2.1 An Introduction

Buildings suffer damage that can produce significant degradation due to harsh environments. As such they need inspection in the early stages of degradation. Image inspection is very effective mainly because of its non-intrusive nature. Aggressive weather conditions such as rainwater, earthquakes and salt erosion cause concrete degradation, a material often used for buildings, with obvious consequences to their desired qualities.

Instrumentation and measurements of Civil Engineering tests usually require considerable time and very complex procedures (Chastre and Silva 2010; Biscaia, Chastre, and Silva 2013). The setup and calibration associated with displacement transducers and electrical gauges, in addition with the risks to their physical integrity when the specimen breaks, requires rigorous alternative measurement solutions. Both Computer Science and Electronic Engineering have made considerable contributions to Civil Engineering tests, instrumentation and measurements. Sutton (Peters and Ranson 1982; M. Sutton et al. 1983; Chu, Ranson, and Sutton 1985) started to study image correlation techniques for photogrammetry in the early 1980s. Since then photogrammetry has been increasingly used as an additional tool in various Civil Engineering tests, such as load tests, crack measurements, bridge deformation measurements and material test inspections (Albert et al. 2002; U. Hampel and Maas 2003; Maas and Hampel 2006; H. Hampel and Maas 2009; Dai et al. 2012; Iyer and Sinha 2006; Nishikawa et al. 2012; Park et al. 2007).

Using digital photography and image processing algorithms it is possible to automatically measure deformations, displacements, strain fields and surface imperfections in many material tests and analyse not only a restricted area but the entire area of interest with simple procedures and without physical contact. Using this methodology the number of measured points can be decided after the tests without requiring their repetition. The displacement along the image-

time series is calculated following small areas containing random patterns called blocks.

The usefulness of the natural pattern depends on the material it is made of. However, it is possible to create an adequate pattern by applying random speckled black ink over a white background layer. The size and density of the speckle, the width and the height of the specimen, the camera resolution, the lens focal length, the distance between the camera and the specimen and the interval between photos are all crucial for the resulting accuracy.

Using a simple digital camera it is possible to take photos at regular time intervals before loading (reference images) and during (deformed images) thus documenting all the structural deformation. After collecting the image-time series one can calculate the displacements between consecutive images using mathematical correlation algorithms to obtain the measurements of the material under study. The image distortion can induce errors but they are small if the distance between the blocks is small (M. A. Sutton, Orteu, and Schreier 2009).

This approach, when compared with classical measurement techniques in Civil Engineering tests, drastically increases the number of measured points and reduces cost and complexity. It is also possible to adjust the number of measured points and the region of interest even after the test has been completed with the additional advantage of obtaining complete documentation of the test.

Image processing can be a major improvement because a simple camera does the data acquisition and the analysis of the data can be done using image processing techniques (Hussain 1991; Bhaskaran and Konstantinides 1997; Acharya and Ray 2005; Sonka, Hlavac, and Boyle 2007; Gonzalez and Woods 2007) developed on a mathematical package software like MATLAB (Asundi Ananda 2002).

Despite the fact that there are several commercial software packages on the market, they lack flexibility and/or are sold at a high cost.

In order to detect motion between two images, several methods can be used: differential, template matching or block functions. Block motion algorithms are widely accepted by the video compressing community and have

been used in implementing various standards ranging from MPEG1/H.261 to MPEG4/H.263 (Al-Mualla, Canagarajah, and Bull 2007; Barjatya 2004).

2.2 *Block Motion Estimation*

A block motion algorithm divides each image into small blocks and follows the blocks under study along the image sequence, matching each block in consecutive images using pixel intensity as the single feature. The basic idea of block motion estimation is to divide each image into a matrix of non-overlapping $N \times N$ pixels (also called blocks, macro-blocks, sub-picture or subset) and then compare these blocks with the previous image in order to calculate the motion vectors (MV). It is assumed that all block pixels have the same motion vector. Block-based motion estimation assumes that objects' moves are translational. The current block is searched for in the reference image in a delimited search area of w pixels around the position of the current block (see Figure 2-1).

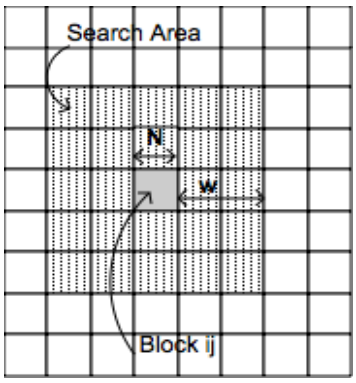

Figure 2-1. Block matching consists mainly in a block of side N pixels and a search area, w pixels around that block

The capability of the block matching algorithms to correctly identify each block in the next image of the time-series greatly depends on its pattern. For each block the algorithm will find a matching block in the previous image within a search area surrounding the block (see Figure 2-2).

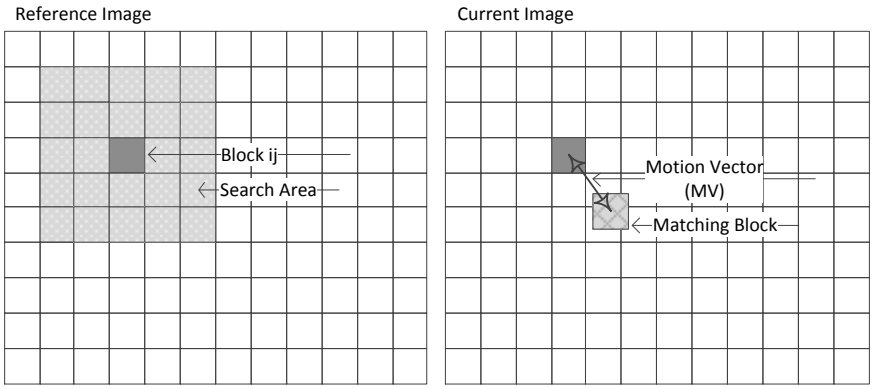

Figure 2-2. Reference and current image

Concrete is a material commonly used in Civil Engineering structures that has an inherently adequate texture. However, it is better to apply a speckle pattern to concrete surfaces in order to increase contrast and obtain images that are easier to process. A good random speckle pattern must have a large quantity of black speckles of different shapes and sizes. In Figure 2-3, it is possible to see an example of two consecutive images with the 50 × 50 pixel grid and the random speckle pattern applied.

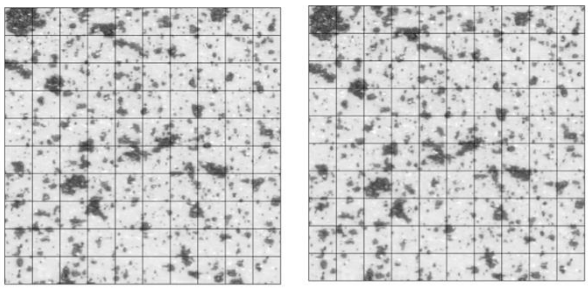

Figure 2-3. Two consecutive images and the matrix of blocks applied to follow the pattern

The singularity of each block to its neighbourhoods is an important factor to reduce block tracking error. The displacement estimation methodology is based on pixel intensity with the unique pattern in each block making it possible to find the correct displacement between consecutive images.

Whichever block matching algorithm is in use, the matching criteria is based on a minimum cost function value. The most common functions for block comparison are the Mean Absolute Difference (MAD) (2.1), the Mean Square Error (MSE) (2.2) and the minimum Cross Correlation (CC) (2.3). In order to avoid multiplications and to achieve the same performance as the MAD function sometimes only the sum of absolute difference are used.

$$MAD = \frac{1}{NN}\sum_{i=1}^{N}\sum_{j=1}^{N}\left|C_{ij} - R_{ij}\right| \tag{2.1}$$

$$MSE = \frac{1}{NN}\sum_{i=1}^{N}\sum_{j=1}^{N}\left(C_{ij} - R_{ij}\right)^2 \tag{2.2}$$

$$CC = \frac{\sum_{i=1}^{N}\sum_{j=1}^{N}\left(C_{ij} - \bar{C}\right)\left(R_{ij} - \bar{R}\right)}{\sqrt{\sum_{i=1}^{N}\sum_{j=1}^{N}\left(C_{ij} - \bar{C}\right)^2 \sum_{i=1}^{N}\sum_{j=1}^{N}\left(R_{ij} - \bar{R}\right)^2}} \tag{2.3}$$

where N is the size of one side of the block, C_{ij} and R_{ij} are the pixel intensities in the current and the reference blocks, and $\bar{C}$ and $\bar{R}$ are the mean for all C_{ij} and R_{ij} respectively.

Computational complexity is a key criterion for the evaluation of block motion algorithms. The Number of Computation (2.4) can be an evaluation criterion. Another possible measure is the computation time i.e. the time spent on each algorithm, but this measure depends much on the computer used.

$$Number\ of\ Computation = \frac{Number\ of\ Evaluated\ Blocks}{Total\ Number\ of\ Blocks} \tag{2.4}$$

2.3 *Block Motion Algorithms*

2.3.1 The Simple and Efficient Search algorithm

The Simple and Efficient Search algorithm (SES) presented by (Lu and Liou 1997) is a variation of the classical Three-Step Search algorithm (TSS). SES reduces the computational complexity of motion estimation because, as in TSS, a unimodal error surface is assumed and it is impossible to have two minimums in opposite directions. Therefore the 8 search directions used in TSS are reduced to 3 in the SES algorithm. In Figure 2-4 the three phases (circles, triangles and squares) are shown where it is evident that SES requires less computational time thus speeding up TSS by a factor of two while preserving its performance and regularity.

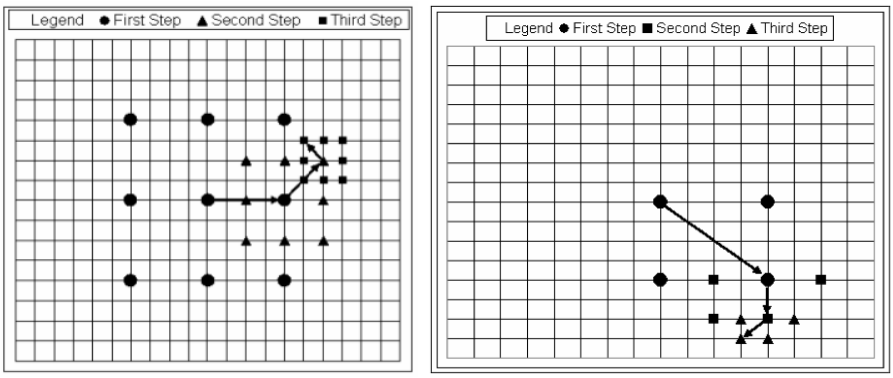

Figure 2-4. The three different phases of the TSS (at left) and SES (at right) algorithms from (Barjatya 2004)

Like TSS, the SES algorithm has 3 steps, each step with two phases. Initially it selects a region for a global search and then in each step the region is reduced. The search area is divided into four quadrants. The first phase consists of selecting the search direction quadrant. It starts by calculating the cost function for three points: *A* that is the current block in the window search centre and *B* and *C* that are other blocks that will help decide the best quadrant for the matching (see Figure 2-5). The second phase finds the location of the

block with the smallest error considering the quadrant selected in the first phase.

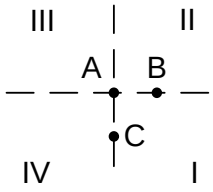

Figure 2-5. The SES first phase search direction

In the first phase the cost function (CF) for the black dots' points (points *A*, *B* and *C* of Figure 2-5) is computed. With this information the most promising quadrant is selected with the following four rules:

- If CF(A) ≥ CF(B) and CF(A) ≥ CF(C) quadrant I is selected;
- If CF(A) ≥ CF(B) and CF(A) < CF(C) quadrant II is selected;
- If CF(A) < CF(B) and CF(A) < CF(C) quadrant III is selected;
- If CF(A) < CF(B) and CF(A) ≥ CF(C) quadrant IV is selected.

Several cost functions can be used, for example: mean square error, the mean absolute difference or the cross correlation (equation 2.1 to 2.3)

In the second phase, the additional white squares' locations are used to identify the new centre for the next step (see Figure 2-6). The point with the smallest cost function value becomes the new search origin and the step size is half of the last iteration.

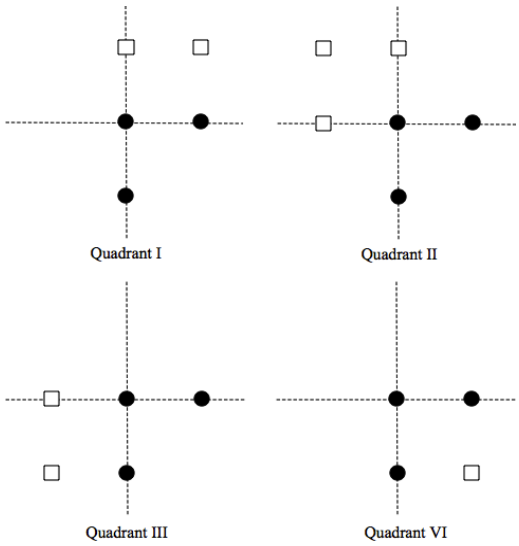

Figure 2-6. The initial search points of phase 1 (black circle) and the new search points of phase 2 (white squares), for each quadrant

In each phase the number of steps is dependent on the search window. A search window w pixels wide requires NS steps and the distance between the pixels in a search step is named a Step size (S_S). Equations 2.5 and 2.6 show how to calculate the number of steps and the step size for the nth step.

$$NS = \frac{log_{10}(w+1)}{log_{10}(2)} \tag{2.5}$$

$$S_S = 2^{NS-n} \tag{2.6}$$

Assuming that the search window is 7 pixels wide (w = 7), the matching block is searched in a constrained area of up to 7 pixels on all the four sides of the block. This corresponds to 3 *steps* (NS = 3) and 4 *Step size* ($S_S = 4$) i.e. the block to search is located at point *A* and points *B* and *C* are located +/- 4 pixels away from *A*. The cost functions for these points are calculated and the best quadrant is chosen. The step size is reduced to $S_S = S_S/2$ at each step repeating all the processes until $S_S = 1$.

2.3.2 *Adaptive Rood Pattern Search*

For the initial search the Adaptive Rood Pattern Search (ARPS) algorithm evaluates the four endpoints in a symmetrical rood pattern, plus the predicted motion vector. The information of the predicted motion vector allows going directly to the useful area even if it is far from the centre.

Block-based motion estimation assumes that objects move in a translational direction, usually in a coherent motion. In most cases adjacent blocks have similar motions and with this information it is possible to predict the next motion. The blocks on the immediate left, above, above-left and above-right of the current block are the most important ones to calculate the predicted Motion Vector (MV) (Nie and Ma 2002). Four types of region of interest (ROI) can be used (see Figure 2-7). Type D requires less memory and that is why it is often selected.

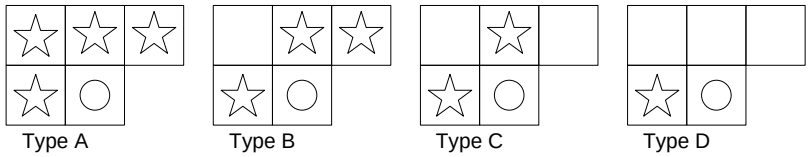

Figure 2-7. Regions of support: the blocks market by "O" the current block and the blocks marked with a star are used to predict the MV

The initial size of the rood pattern is approximately equal to the length of the predicted motion vector (i.e. the motion vector to the immediate left of the current block). The size of the rood pattern Γ is calculated as in (2.7),

$$\Gamma = round\left|\overrightarrow{MV}_{predicted}\right| = round\left[\sqrt{MV^2_{predicted(x)} + MV^2_{predicted(y)}}\right] \quad (2.7)$$

The square and the root square operations shown in (2.7) require considerable computational time. Therefore, instead of (2.7) it is common to use a simplification that only requires the highest magnitude of the two components of the predicted MV (2.8).

$$\Gamma = Max\left(\left|\overrightarrow{MV}_{predicted(x)}\right|, \left|\overrightarrow{MV}_{predicted(y)}\right|\right) \quad (2.8)$$

When it is impossible to have the predicted MV (blocks in the first column), an arm length of 2 (Γ=2) is chosen.

Figure 2-8 shows the four arms of the rood pattern whose length is the maximum of the predicted motion vector. The Minimal Matching Error (MME) point found in the current step will be the starting search centre for the next phase. In the second phase a refined local search uses a unit-size rood pattern to find the best motion vector. This step is repeated until the MME is found at the rood's centre.

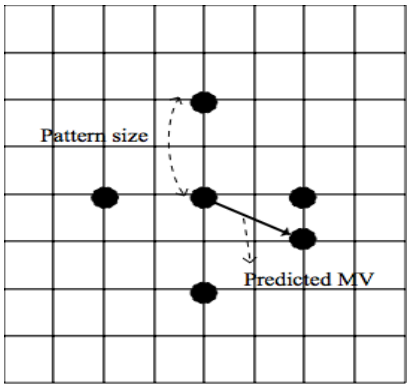

Figure 2-8. Adaptive rood pattern plus the predicted motion vector

If this algorithm is applied to a video sequence where there are an important number of blocks without motion in adjacent frames, it is useful to improve it with zero motion detection in order to reduce computation time. It is considered that a block is static if the matching error is smaller than a predefined threshold. In this situation the minimum search point is already in the centre of the rood pattern and the algorithm is stopped in the first phase.

2.3.3 *Particle Swarm Optimization*

Particle Swarm Optimization (PSO) is a stochastic optimization algorithm designed and proposed by (J. Kennedy and Eberhart 1995). Particle Swarm Optimization is an extremely simple algorithm that is effective for optimizing a wide range of functions. It requires only primitive mathematical operators and is computationally inexpensive in terms of both memory requirements and speed (J. Kennedy and Eberhart 1995).

This adaptive algorithm is based on the simulation of the social behaviour of organisms such as a flock of birds or a school of fish. In order to seek food or avoid predators animals adjust their physical movement. The movement adjustments are based on environment parameters, physical neighbours' behaviours and group direction.

In a computer simulation a population is composed of particles with initial positions randomly initialized. The particles fly through a multidimensional space with their motion updated at each iteration based on their best position as well as the best group positions. The metric used to decide the best position depends on the problem in question. Each particle remembers its best position and the global best position i.e. the best position ever visited. With this information the velocity of each particle is updated and the new position of a particle is influenced by the best position visited in its neighbourhood.

In (Shi and Eberhart 1998) a new version of PSO was proposed by adding a new inertia weight to the original algorithm. Each particle is represented in the *D* multidimensional search space with i^{th} particle represented as $X_i = (x_{i1}, x_{i2}, \dots, x_{id}, \dots, x_{iD})$. The best position for any particle is recorded and represented as $P_i = (p_{i1}, p_{i2}, \dots, p_{id}, \dots, p_{iD})$. The index of the best particle among all the population is represented by the symbol g. The rate of the position change (velocity) for particle i is represented as $V_i = (v_{i1}, v_{i2}, \dots, v_{id}, \dots, v_{iD})$. The particles are manipulated according to the following equations:

$$v_{id} = W\, v_{id} + c_1\, r1\, (p_{id} - x_{id}) + c_2\, r2\, (p_{gd} - x_{id}) \quad (2.9)$$

$$x_{id} = x_{id} + v_{id} \quad (2.10)$$

where c_1 and c_2 are two positive constants, *r1* and *r2* are two random numbers in the range [0,1], and *W* is the inertia weight number.

Equation (2.9) is used to calculate the particle's new velocity according to its previous velocity, its current position, the best experience and the group's best experience. Then the particle flies towards a new position according to equation (2.10). The second part of equation (2.9) represents the "cognition" i.e. the private experience of the particle itself. The third part is the "social" part that represents the collaboration among the particles. Without the first part of equation (4.5) all the particles will tend to move towards the same position (Shi and Eberhart 1998).

The role of inertia, *W*, is to balance the global and local searches. Large inertia weights force a larger exploration, while small inertia weights focus the search in small areas. (Shi and Eberhart 1998) said "a time decreasing inertia weight from 1.4 to 0 is found to be better than a fixed inertia weight. This is because the larger inertia weights at the beginning help to find good seeds and the later small inertia weights facilitate fine search". c_1 and c_2 are usually 2 as recommended by the authors as on average it makes the weights for the "social" and "cognition" parts to be 1.

The common neighbourhood topologies are *star* and *ring*. The choice of neighbourhood topology has a profound effect on the propagation of the best solution found by the swarm (Omran, Engelbrecht, and Salman 2006). Also in (James Kennedy and Mendes 2002; Bakwad et al. 2008; Ranganadham, Gorpuni, and Panda 2009) a *Von Neumann* topology is proposed. In this topology each particle is connected to its four neighbouring particles (above, below, right and left particles).

2.4 Related Work

Several works have been under development in this area, namely at Dresden University of Technology (H. Hampel and Maas 2009), Waseda University (Yamaguchi and Hashimoto 2006) and Lulea University of Technology (Carolin, Olofsson, and Taljsten 2004).

Cracks in concrete structures are important diagnosis indicators studied by many researchers. However, to detect them with conventional methods is not an easy task and their detection in the earliest stage is extremely difficult.

The detection of early cracks can be seen in (H. Hampel and Maas 2009). The authors developed and tested a cascade image analysis aiming to detect fine cracks in the micrometre range. Their paper started with a review of related work in three categories of methods to automatically detect cracks in a concrete surface: edge detection techniques, targeting and full field displacement vector analysis.

By applying edge detection techniques such as Sobel or Canny filters, it is possible to see the cracks. This technique is very simple and can be realized with many image processing software packages. Despite that, the edge detection technique is very dependent on the lighting conditions, but it can detect cracks with a width of one or more pixels. The concrete probe was studied via discrete targets affixed to it (see Figure 2-9). With the use of this target point technique, cracks will be shown as an increase in the distance between neighbouring targets. The major handicap of using target points is that:

- it leads to a strong generalization of the crack position because it cannot be located exactly but always referred to the neighbour target points;
- it is a huge effort to signalize the specimen with all the necessary targets;
- it is impossible to distinguish multiple cracks between two targets.

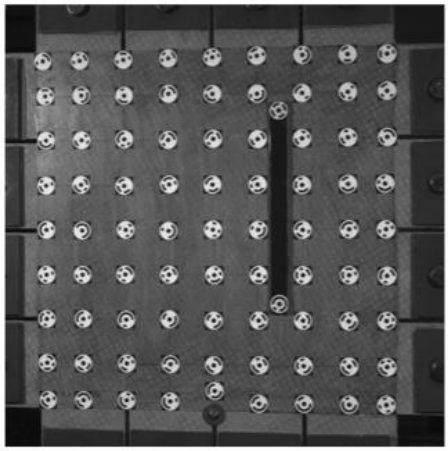

Figure 2-9. Concrete with a matrix of discrete targets from (H. Hampel and Maas 2009)

The full field displacement vector analysis is accomplished by applying image-matching techniques which use the natural or artificial texture of the specimen. The cascade image analysis initially applied image-matching techniques to consecutive images of an image sequence to generate the displacement vector fields. This methodology is computationally expensive because a displacement field must be generated for every pixel. The vector length is the attribute used to make a vector length image which contains accumulated displacement vectors over the whole specimen. In the second step, with the Sobel operator, an image containing information about the position and width of each crack is obtained.

An early paper by the same authors (Maas and Hampel 2006) identifies the major hardware and software issues for building a toolbox based on image processing for Civil Engineering material testing. "The use of photogrammetry in material testing experiments will generally allow for the simultaneous measurement of deformations or displacements at an almost arbitrary number of locations over the camera's field of view". The data acquisition systems, the data processing techniques and some real application examples are presented in this paper.

In (Yamaguchi and Hashimoto 2006) a new crack detection method for a concrete surface image based on a percolation model is introduced. "Percolation is a physical model based on the natural phenomenon of liquid permeation". This model uses edge information to reduce the number of

starting points for percolation processing. For the edge detectors they use seed information from several sources such as the Sobel filter, the Canny filter and the morphological gradient.

The authors use edge information for the choice of applicable seed pixels reducing the number of starting points for the process instead of repeating the process starting from every pixel. In the region growing method the process starts from one pixel of the previously given seed pixels and compares it with neighbouring pixels. The crack region is grown from the seed pixel by adding neighbouring pixels. In tests the methodology for crack detection was applied to 10 images of real concrete surface (see Figure 2-10). The size of the images was 500×500 pixels corresponding to an area of approximately 250×250 mm.

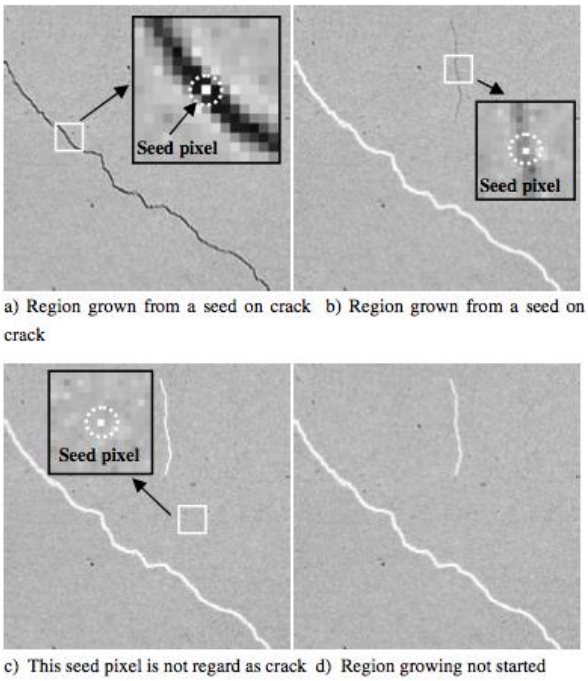

a) Region grown from a seed on crack b) Region grown from a seed on crack

c) This seed pixel is not regard as crack d) Region growing not started

Figure 2-10. Images of crack region growth from (Yamaguchi and Hashimoto 2006)

In the work of (Carolin, Olofsson, and Taljsten 2004) a non-contact strain measurement method that covers a pre-defined area is presented. Several tests were carried out on reinforced concrete beams with a span of 4.5 m and the results were compared with the traditional electrical strain gauges. In this study

a speckle pattern correlation was used and a photo was taken every 30 kN until rupture. In their tests a film camera was used with the film being scanned by a high quality scanner. The picture was divided into blocks of 128×128 pixels and then a threshold was used to binarize the image (see Figure 2-11).

Figure 2-11. Block after a threshold from (Carolin, Olofsson, and Taljsten 2004)

After binarization the centre of gravity of every block is calculated. The authors considered that larger blocks lead to better accuracy. Following this methodology, and using speckle correlation, it was possible to find the same block in the second loading condition. The authors found the use of 128×128 pixels was satisfactory with 128 pixels between centres, but they found their method was very dependent on the camera resolution, the studied area and the pattern. The test was also monitored with 35 strain gauges but no comparison was shown between the data obtained by the sensors and the data obtained by image processing.

This methodology was duplicated in the FCT Laboratory with a photo sequence image-time series of TSC1 test taken every 30 s instead of load stage and monitored with 5 physical sensors. Despite the respectable results obtained when compared with the physical sensor, the achieved accuracy depends significantly on the illumination conditions requiring frequent threshold adjustments. This test also revealed the necessity of reducing the photo intervals in order to detect the fine details at rupture time.

One of the major problems related to strain measurements with spatial resolution is result validation because the strains given by the physical sensors are global and not local. Therefore only a few points can be compared with the spatial distribution obtained by image processing analysis.

In (Koljonen, Kanniainen, and Alander 2007) an implicit error estimation approach based on statistical analysis was used. To validate the performance of the digital image correlation algorithm an accurate reference method was needed because strain gauges have poor spatial resolution and are point-wise. In this work it was assumed that the principal strains in a transversal intersection are uniform. The images were divided into a regular grid and the strain fields were computed. The strain error was estimated by the standard deviation of strains measured. After this, images were translated by a few pixels and the strains were calculated again. This small translation does not affect the strain measurements because the uniformity of the strain field and the error estimates should remain unaltered. The standard deviation gives confidence intervals for the error estimates.

The Digital Image Correlation (DIC) technique is applied in (Kurtz, Balaguru, and Helm 2008). Before loading, a random black and white speckle pattern was painted on the surface of the specimen and an unloaded image taken. At each load stage additional images were acquired. The images were divided into several grey level blocks. Each block was then compared with the second image using the cross-correlation error function. This process was repeated for all blocks in the area of interest resulting in a full-field map of the surface displacements. Two different groups of beams, one for the DIC tests and another for the strain-gauge tests, were used in this study. The authors found that both methods provided similar results. The principal advantage that DIC offers for strain analysis is that the displacement measurement is continuous over the entire specimen, while strain gauges provide values at single points leaving the data that is between the gauges to be assumed rather than determined. But when other methodologies are used it is necessary to be sure of the implemented algorithms. In order to validate those algorithms their results are compared with the results from the strain gauges. However, as Kurtz says (Kurtz, Balaguru, and Helm 2008), this comparison is only possible

at single points. This paper also mentions the analytical solutions normally used in Civil Engineering.

The contribution of several factors such as resolution versus specimen dimensions, focal length and distance between camera and specimen, distortion effects and speckle pattern are very important to parameterize the image processing algorithms. All these considerations can be found in (Cintrón and Saouma 2008) and also in (Bornert et al. 2009) where the general procedure to evaluate the measurement errors of digital image correlation is discussed. The authors used synthetic images and evaluated the displacements with six software DIC packages.

In order to establish digital image correlation as a standard measurement technology it is important to determine the relationship between the uncertainty and the experimental setup of the cameras and speckle pattern. "Image Correlation has experimentally proven itself to be accurate based on direct tests comparing vision-based measurements to strain gauges". Optimizing the image contrast plus choosing an appropriate speckle and block size are some aspects that increase accuracy (Reu et al. 2009).

One of the first issues related to digital image correlation is to choose the best characterization of the speckle pattern and for that particular speckle pattern what the block size must be. In (Lecompte et al. 2006; Reu et al. 2009) the influence of the speckle size on displacement accuracy is also analysed. For this study the authors used images with speckle patterns generated numerically and each speckle pattern image suffered a mathematical deformation. The authors found that the larger the block the more accurate the measured displacements are and where a small block is used, the most precise results are obtained with small speckles. Therefore an optimal compromise between pattern and speckle size should be achieved. In Figure 2-12 it is possible to see the sprayed speckle pattern with three different zooms, yielding three speckle patterns.

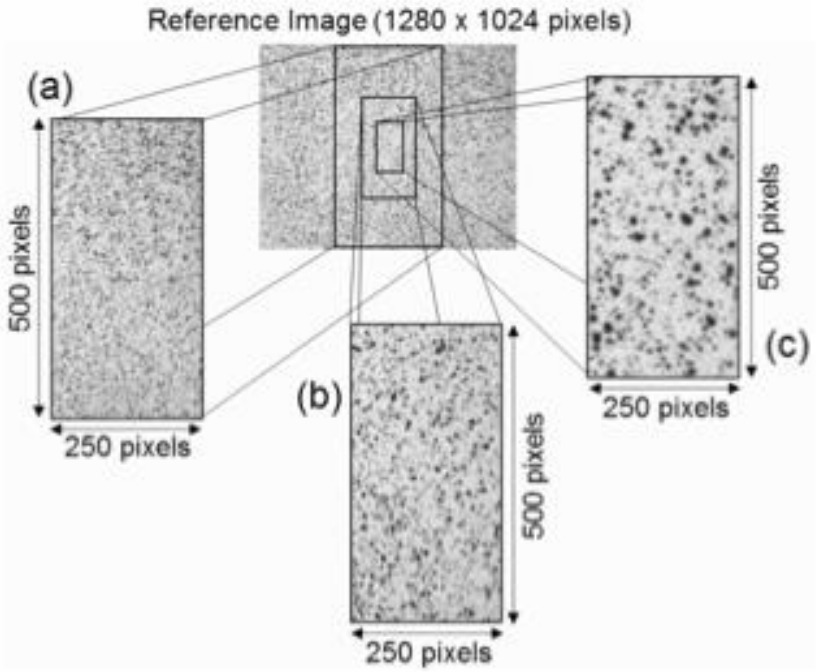

Figure 2-12. Sprayed speckle pattern with three different zooms (Lecompte et al. 2006)

In (Pan et al. 2008) the problem of block size selection for the digital image correlation technique is also investigated. In this paper three reference images were used (see Figure 2-13) and in order to simulate the image noise random Gaussian noise was added to the speckle images to form the deformed images. An algorithm based on the sum of squared differences of block intensity gradients with the cross correlation criteria and using blocks from 17×17 to 71×71 pixels was proposed.

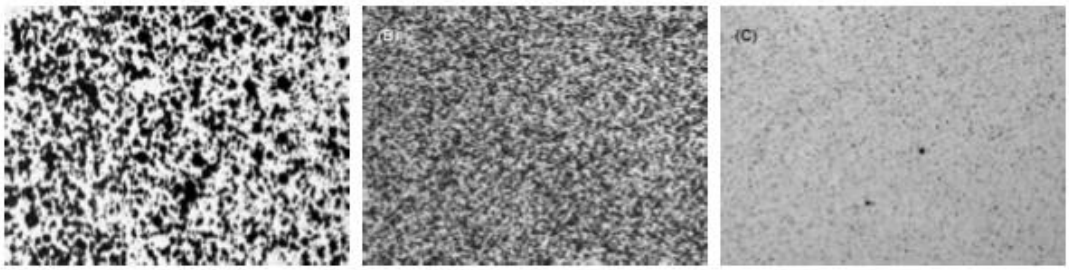

Figure 2-13. Three reference images used in the experimental validation (A- left, B- middle, C- right) (Pan et al. 2008)

In Figure 2-14 it is possible to see the standard deviation of the vertical displacement (v-displacement). The standard deviation error decreases as the block size increases for all three test images studied. "It can be also observed that errors of the displacement calculated from test image pairs C are much larger than those obtained from test image pairs A and test image pairs B. This can be explained by the fact that the image contrast of the speckle pattern in pairs C is much lower than those of the speckle images in pairs A and B". The authors claimed that different random speckle patterns must have different block size images in order to have identical accuracy. Images with higher contrast allowed smaller blocks to achieve higher accuracy of displacement measurements.

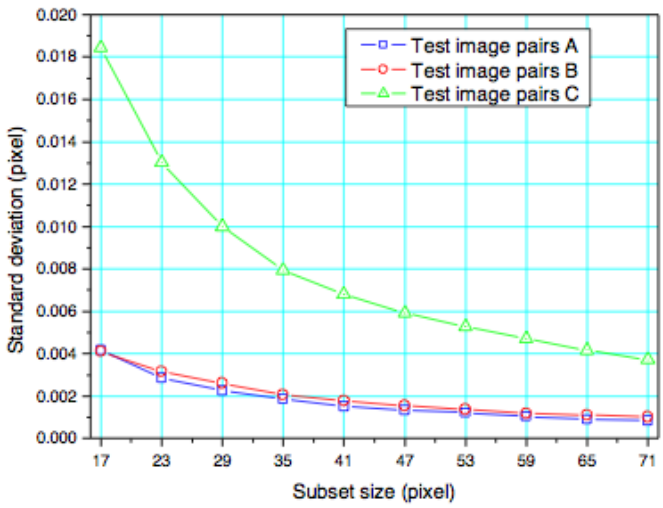

Figure 2-14. Standard deviation of v-displacement with different block sizes (Pan et al. 2008)

Also (Barranger et al. 2012; Barranger et al. 2010) presented a study on the influence of the rigid and deformable pattern and its influence on digital image correlation. Their numerical simulation study points out that a rigid pattern has influence on the uncertainty of the digital image correlation. However, their experimental tests showed that rigid and deformed patterns give similar results. "This study was conducted in 2D cases in order to show the influence of the powder in the speckle pattern on the evaluation of displacement by digital image correlation linked to the choice of the type of interpolation and lighting".

The speckle patterns were created on the surface of a transparent silicone specimen. It was manufactured in-situ and had a section of 6x10 mm^2. To conduct experiments, direct light on the specimen surface was avoided. "Indeed, shadow phenomenon appears on speckle patterns made of powder with straight lights oriented directly on them which would have generated variations in grey levels on the surface of the specimen between the reference and deformed images". As such only diffused lights were used for these experiments. Three different kinds of speckle patterns were created on the specimen: black paint, white paint and a spread of 150 μm calibrated polyamide particles (see Figure 2-15).

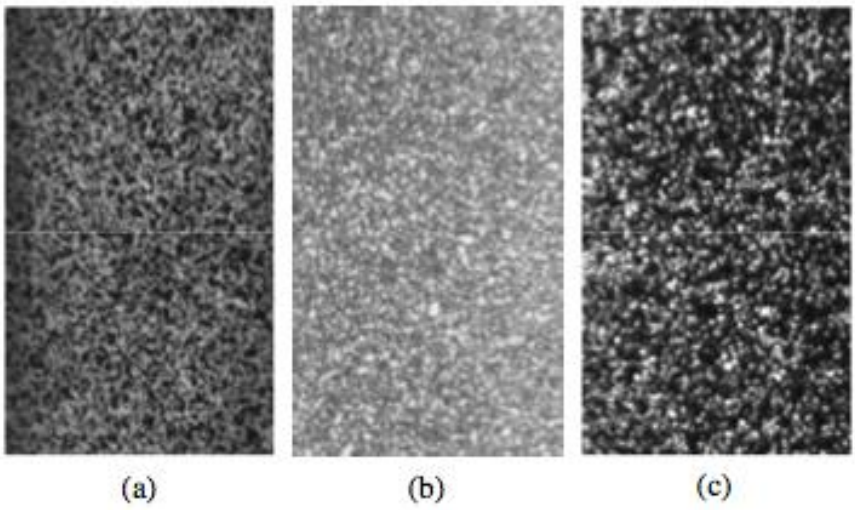

Figure 2-15. Black paint (a), white paint (b) and spread powder (c) speckle patterns from (Barranger et al. 2010)

The authors concluded that "painted speckle patterns give similar results to those obtained by the mark tracking technique, whereas the speckle patterns made of powder underestimate strain values. Contrary to the paint, particles remain rigid during the whole experiment, which means that the grey level distribution is not uniformly deformed". This is prevalent especially for the large strains.

The limits of accuracy of the optical strain measurement system are presented by (Jerabek, Major, and Lang 2010) using polypropylene (PP) and PP

composites in the pre and post-yield regimes. The pattern was sprayed with black graphite (see Figure 2-16).

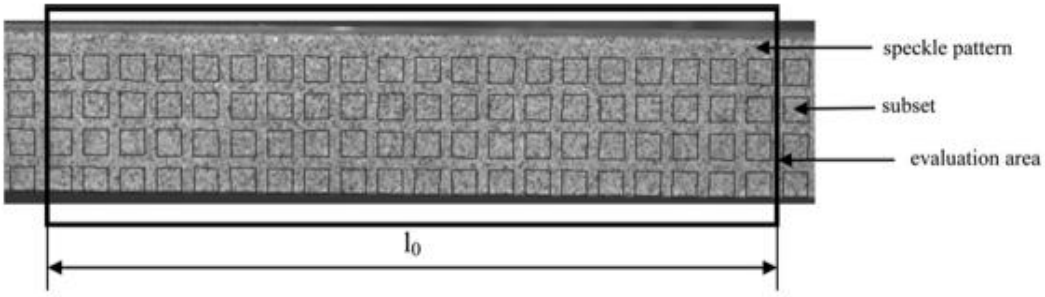

Figure 2-16. The random speckle pattern and the predefined blocks positioned by the software ARAMIS from (Jerabek, Major, and Lang 2010)

Using ARAMIS, a commercial software developed by Gesellschaft für Optische Messtechnik (Gom 1990), to compute the Digital Image Correlation (DIC) measurements, it was shown that a fine speckle pattern and a light intensity just below over-exposure provided the best results. Several test setup parameters were studied: light intensity, speckle pattern, temperature chamber and shutter time.

Polymeric materials deform relatively homogeneously up to the yield point but at large strains, in the yield and post-yield regimes, heterogeneous deformations are expected. So the mechanical extensometers can be used in the first phase but they are inadequate in the second phase. With DIC it is possible to have complete information of the test and the specimen surface. Their best result was achieved with overexposure, a shutter time of 20 ms and fine speckle patterns. Up to the yield point both strain determination (DIC and clip-on extensometer) exhibit good agreement. However, beyond the yield point the clip-on extensometer delivers higher strains than the DIC system. This is because the extensometer obstructs the spontaneous material deformation.

The work by Czaderski and Motavalli (Czaderski and Motavalli 2010) shows how to measure full-field displacements in the longitudinal and out-of plane directions of pull-off tests. Pull-off tests are tensile tests on fibre reinforced polymer (FRP) strips that are glued to concrete blocks. The electronic

transducers and strain gauges normally used have the disadvantage of only measuring local results in specific positions. In this work the authors also used ARAMIS (Gom 1990) in order to obtain the Digital Image Correlation information. Some measurements were taken from the front view and some from the side view that provided the observation of the characteristic stage of the pull-off tests: initiation of the first crack, ignition of de-bonding and failure (see Figure 2-17).

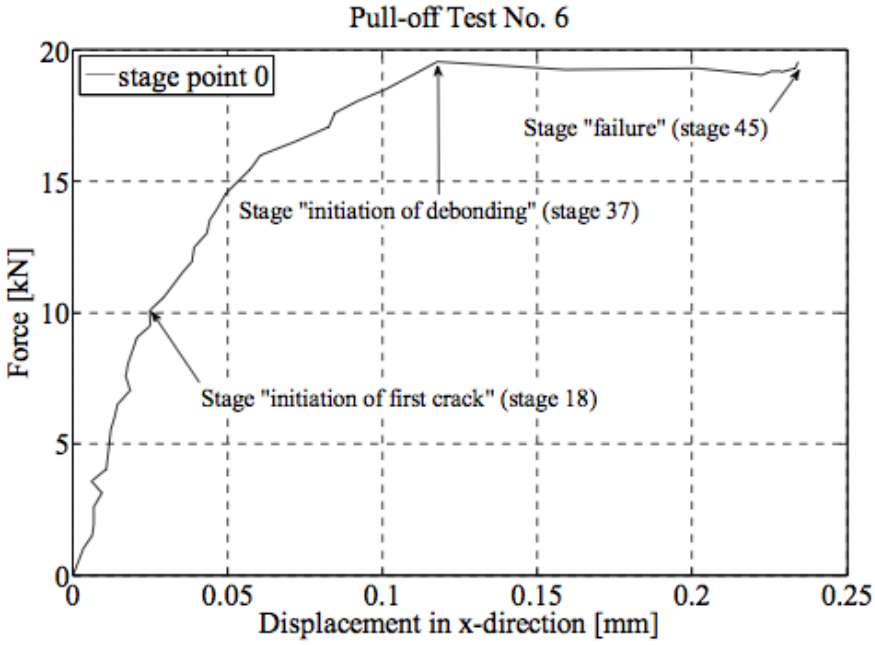

Figure 2-17. Development of longitudinal (X) displacements during the loading of pull-off test from (Czaderski and Motavalli 2010)

Another example of Digital Image Correlation (DIC) application is the work by (Lee, Chiou, and Shih 2010) where the strength and stiffness of the beam–column joint was studied. With DIC the authors measured and observed the full strain field of the joint. In Figure 2-18 it is possible to see the system setup with two cameras: one in front of the specimen that focussed on the centre of the beam-column joint zone and another placed to cover the entire test block measuring the beam and column deflection.

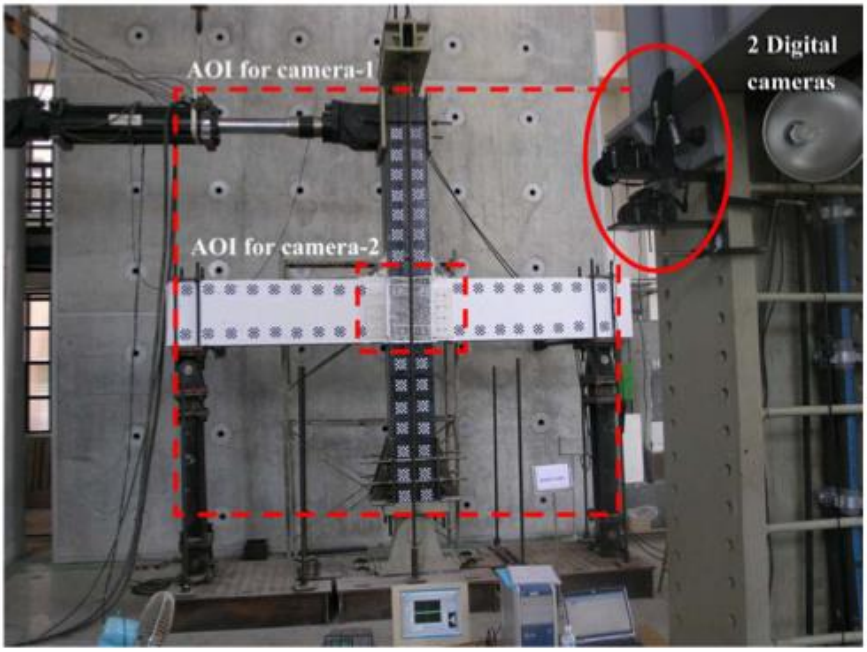

Figure 2-18. Experimental system setup, from (Lee, Chiou, and Shih 2010)

The authors used a random speckle pattern on the surface of the specimen with 50×50 pixels blocks and a resolution of 0.3012 pixel/mm (see Figure 2-19).

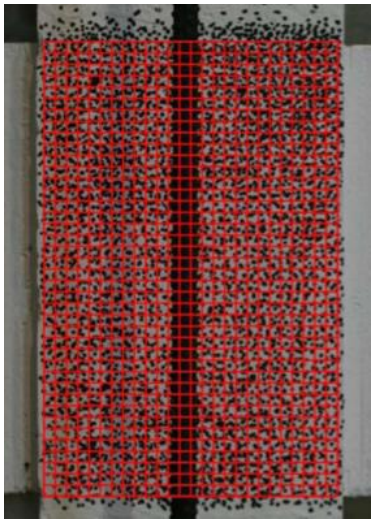

Figure 2-19. Mesh example with 50x50 pixel per block, from (Lee, Chiou, and Shih 2010)

The results from the DIC measurements were presented but not compared with physical sensor measurements. With DIC information it was possible to

understand particular situations, namely the anchor zone, which was not possible with the traditional sensors.

In (Jianguo, Xiaolin, and Min 2010) Hybrid PSO (an image matching method based on PSO, Population Category Evolution and Simulated Annealing) was proposed. With Hybrid PSO it is possible to speed up the convergence and improve the premature convergence associated with an evolutionary algorithm. The fitness function used was the cross-correlation. Combining simulated annealing with PSO it is possible to classify and adopt different update strategies in order to speed up the convergence and improve the phenomenon of premature convergence. Other similar applications of PSO can be seen in (Liu et al. 2009).

(Bakwad et al. 2008) proposed the Small Population based Modified Parallel Particle Swarm Optimization (SPMPPSO) algorithm for motion estimation in a video sequence. The authors only used 4 neighbours (particles) and this allowed a fast convergence. The proposed method saved computational time when compared with Adaptive Rood Pattern Search but showed lower accuracy (Peak Signal to Noise Ratio - PSNR). The authors compared the results of the proposed method with the Exhaustive Search, Simple and Efficient Search, Three Step Search, New Three Step Search, Four Step Search, Diamond Search and Adaptive Road Pattern Search.

In (Yuan and Shen 2008) a fast block matching algorithm for motion estimation was proposed and the algorithm was compared with other popular fast block-matching algorithms (Exhaustive Search, Simple and Efficient Search, Three Step Search, New Three Step Search, Four step Search and Diamond Search). The authors used PSO in order to accelerate the matching search and reach the best motion estimation. Their improved PSO algorithm is based on initializing the particle velocity with the motion vector of the previous adjacent block. The minimum of Mean Absolute Difference was used to search for the best position in the search window. The Exhaustive Search has the highest computational complexity while the block-matching algorithm based on PSO is the faster and more efficient algorithm. The authors applied their algorithms to a video sequence obtaining a slight improvement when compared to the traditional PSO.

The paper of (Ranganadham, Gorpuni, and Panda 2009) proposed a methodology based on a PSO algorithm to calculate the bi-directional motion in a video sequence. In a video sequence there is a higher number of static blocks with small or no movement. Their algorithm predicted these movements before starting the motion estimation procedure which allows accelerating the algorithm and saving memory. The matching errors were based on the sum of absolute difference between the block in the current frame and the block at the same location in the reference frame. They are then compared to a predetermined threshold. If the matching error is smaller than a certain value they assume that the block has no movement. They put four particles in a cross shape with size one, and four particles in a cross shape with size two, and then they rotated it by angle $\pi/2$. With the shape having particles in 8 directions they tried to balance the global exploration and local refined search in order to create a larger search space as well as higher matching accuracy. The authors claimed that this technique is superior to the existing bi-directional motion compensation methods.

Block matching algorithms are used to estimate motion. These algorithms are very popular because of their simplicity, robustness and ease of implementation.

In this thesis two block motion algorithms are used, the SES and the ARPS, and the results are compared with the new algorithms (RP-PSO and the PSCH). The RP_PSO combines the ARPS and PSO algorithm. The PSCH uses the histogram information for the block comparison. A random or regular pattern is imposed on all the materials under test achieving a reinforcement of the natural material pattern.

The main idea is to use real data and not a mathematical image deformation. All the results obtained by the algorithms were compared with the physical sensors and with the Golden Standard. Load tests with concrete beams of 0.6m to 3m, load tests with standard specimens of different materials and pull-off tests of CRFP in concrete and steel were all used. The major difficulty was sensor validation because sometimes the acquisition system lost the sensors' signal and/or the sensors moved from their initial position presenting erratic behaviour.

Chapter 3

RP-PSO and PSCH Algorithms

This section describes two new algorithms especially designed for this case study: the Rood Pattern – Particle Swarm Optimization (RP-PSO) and the Pattern Signature Correlation Histogram (PSCH) algorithms. While RP-PSO is a combination of the ARPS and PSO algorithms, PSCH uses the histogram block information as its feature instead of pixel intensity.

3 RP-PSO and PSCH Algorithms

3.1 Introduction

Image processing applied to Civil Engineering problems allows better accuracy and information detail without consuming the time and hardware required by physical sensors. Block-based motion estimation is suitable for load test analysis where objects usually move in a translational direction with coherent movement. Therefore, the study of random patterns with different load test conditions encourages the introduction of a new algorithm (RP-PSO) based on the ARPS and PSO algorithms. A regular grid pattern was added to the random pattern making it possible to use another method for motion estimation where the feature used was not the pixel intensity but the block histogram. The histogram peaks correspond to the regular grid and between these maxima is the signature of the random pattern. The Pattern Signature Correlation Histogram algorithm (PSCH) is based on both histogram information and block motion algorithms.

3.2 Rood Pattern – Particle Swarm Optimization (RP-PSO)

The Rood Pattern-Particle Swarm Optimization (RP-PSO) algorithm combines the ARPS and PSO algorithms with each particle corresponding to an $N \times N$ pixels block. The position of a particle is influenced by the position of the best particle in its neighbourhood. Particle swarms are initially arranged in a rood pattern according to the strategy of the ARPS algorithm. After this initial arrangement the particles fly according to the PSO algorithm.

In RP_PSO seven particles (square points in Figure 3-1) are organized around the point where calculation of the motion vector is required: four particles are positioned close to the central point and the other three particles are positioned outward (east, south, and west) at the distance of the last motion vector (MV).

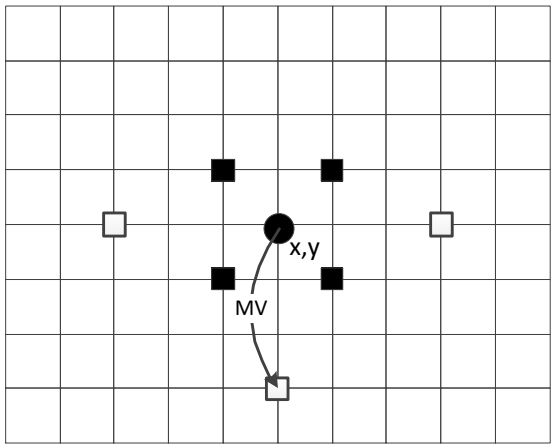

Figure 3-1. The particle (x,y) represents the centre of the current block. The black squares represent the centre of the blocks at a unitary distance around the current block and the white squares represent the centre of blocks at the distance of MV (last known motion vector)

For each neighbourhood the local best particle (lbest) can be determined by searching the minimum of a cost function (MAD, MSE or CC). The initial velocity is given by the motion vector of the left block. At image boundaries where this information is unavailable zero is adopted. In order to avoid going beyond the boundaries of an image a maximum value must be chosen to limit the velocity vector. With this organization it is possible to cover a large area in all directions using less iterations.

The particles' velocity and position functions are:

$$\mathbf{v}' = W\mathbf{v} + cr(\text{lbest} - \mathbf{x}) \tag{3.1}$$

$$\mathbf{x}' = \mathbf{x} + \mathbf{v}' \tag{3.2}$$

where $\mathbf{v}'$ and $\mathbf{x}'$ are the new velocity ($\mathbf{v}$) and position ($\mathbf{x}$) vectors, c is a positive constant, r is a random number in the range [0,1], W is the inertia weight, *lbest* is the position with the best matching criteria and vectors $\mathbf{v}$ and $\mathbf{x}$ are the velocity and position for all particles.

In the RP-PSO algorithm the velocity function only uses local information without requiring global best information because particles are first positioned close to the central point that will be searched.

The RP-PSO block motion algorithm follows the steps:

- Initialize the swarm's particle position according to Figure 3-1;
- Initialize the velocity of the swarm's particle according to the motion vector of the left block;
- Repeat the following steps until a fixed number of iterations is achieved:
    - evaluate the fitness function for each particle using the cost function (MAD, MSE or CC);
    - compute Estimate the value that minimizes the cost function which is the local best particle (lbest);
    - update the velocities and positions for all particles using equations (3.1) and (3.2).

3.3 Pattern Signature Correlation Histogram (PSCH)

The Pattern Signature Correlation Histogram (PSCH) algorithm was created to deal with regular patterns. To apply this algorithm a regular grid is imposed on a specimen with a random pattern (see Figure 3-2).

Figure 3-2. Example of an image with both a random and a rectangular pattern

So far the pixel intensity was chosen as the feature but PSCH uses the histogram of the pattern as the feature. For each block the horizontal and vertical sum of the pixels' intensity is calculated. Using these histograms a fingerprint pattern is obtained for each block and with this information it is possible to match the block in the next image with the cross correlation

methodology. Although it is possible to apply this algorithm even if only a regular pattern is applied, the regular pattern facilitates and improves the accuracy of the block detection. Figure 3-3 and Figure 3-4 show an example of horizontal and vertical histograms.

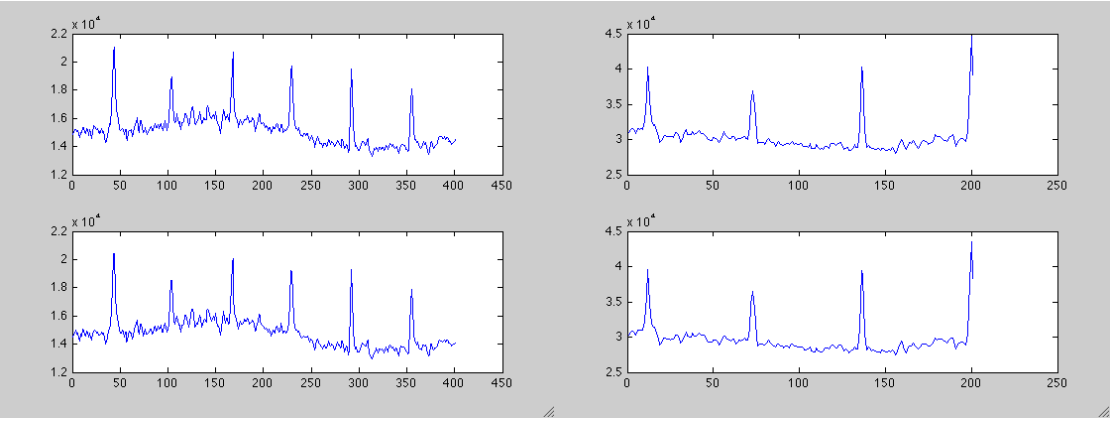

Figure 3-3. Horizontal (left) and vertical (right) histograms between consecutive images

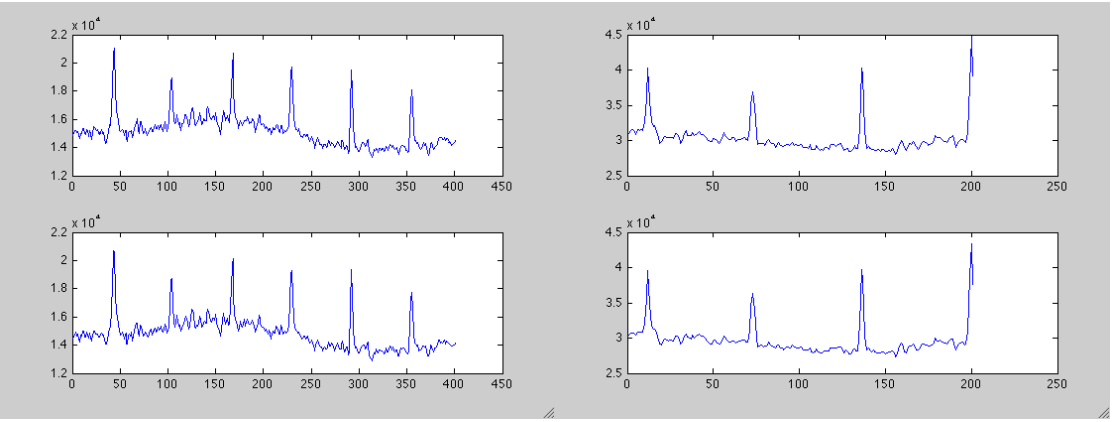

Figure 3-4. Horizontal (left) and vertical (right) histograms between the first and the 10th image

The fingerprint pattern methodology was also applied to the block motion algorithms studied in the previous section. For each block the histogram is calculated and this feature is used to match the blocks. Finding a block matching consists of finding a block that has the most similar histogram. The computational time is improved and the searching is optimized following the ARPS and RP-PSO algorithms.

3.4 *Deformation of an Infinitesimal rectilinear parallelepiped*

Some aspects studied in this thesis are related to the materials and structures in Civil Engineering e.g. rupture displacements, deformations and strain calculations. The deformations and displacements are obtained directly from the algorithms presented in the previous sections but the strain calculus uses the theory of an infinitesimal material element.

For each test a sequence of *MAX+1* images is obtained. The first image corresponds to the initial situation (non-deformed phase) and the subsequent images follow the specimen deformation. In all the algorithms the image is divided into a grid with *N*×*N* pixel blocks forming a matrix of *lmax* block lines by *cmax* block columns. The algorithm analyses all the blocks and searches for a block in the next image that is as similar as possible to the current block. When a block match is found the distance between the coordinates in the current image and the coordinates in the previous image is recorded.

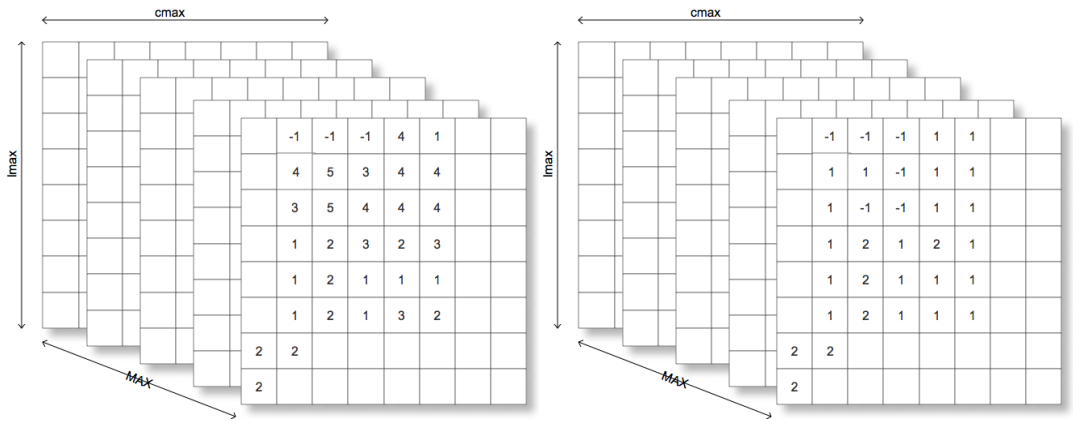

Figure 3-5. Arrays of vertical (left) and horizontal (right) displacements obtained by processing multiple images

After processing all the images, *MAX* horizontal and vertical displacement matrices are computed (see Figure 3-5). The displacements in the x-direction and in the y-direction are stored in two separate sets of matrices. The cumulative values of the block displacement, from the first to the last image, are also useful for the design of a temporal displacement graph and for the total displacement calculation (Figure 3-6).

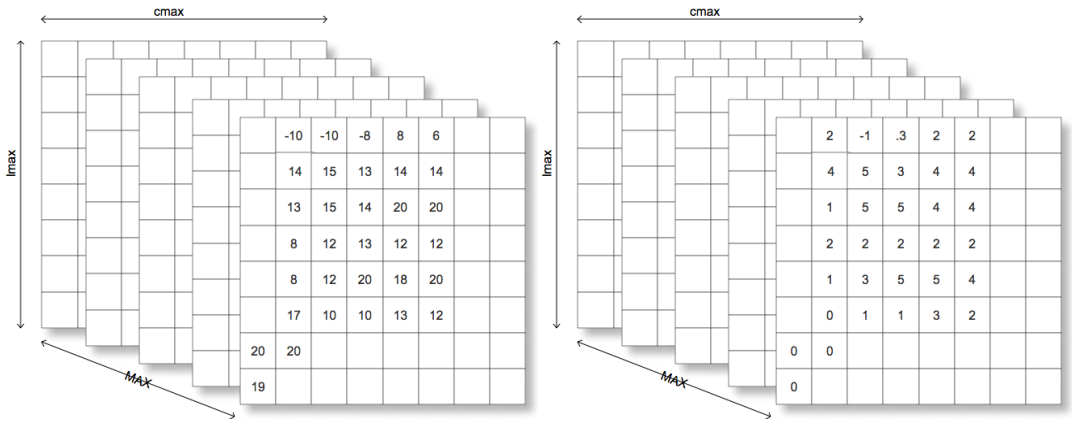

Figure 3-6. Displacement accumulations from the first to the last image

For the graphs' analysis it is important to mention:

- The edges values (first and last columns and lines) should be removed because, in most cases, they show inconsistencies due to the lack of surrounding information;
- Filters like neighbourhood average or median can be applied in order to remove values inconsistent with their neighbours;
- Displacement blocks are converted in terms of image coordinates and stored in two arrays, *X* (columns co-ordinates) and *Y* (lines co-ordinates);
- The central column was normally used to compare with the physical sensor data located in the centre of the specimen.

With all of these considerations, the theory of infinitesimal displacements is applied considering each $N \times N$ block as a corner of a rectangle [A B C D] that is deformed into a new geometric form [a b c d] (see Figure 3-7). The point A displacement is $\vec{u}$. AXY, AXX, AYY and AYX are the elongations of each side of the rectangle. For infinitesimal deformations the displacement gradients are small when compared to unity.

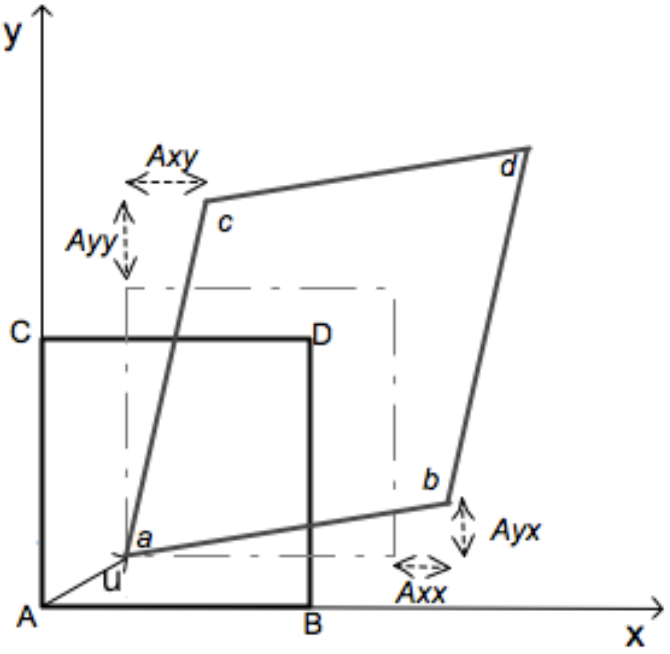

Figure 3-7. Infinitesimal initial block [A B C D] and its deformation, block [a b c d]

The normal strain in the x-direction, extension of $\overline{AB}$, is:

$$\varepsilon_{xx} = \frac{\overline{ab} - \overline{AB}}{\overline{AB}} \tag{3.3}$$

Once that $\overline{AB} = N$ it results in:

$$\varepsilon_{xx} = \frac{N + \frac{\partial u_x}{\partial_x} N - N}{N} = \frac{\partial u_x}{\partial_x} \tag{3.4}$$

The normal strain in the y-direction, extension of $\overline{AC}$, is:

$$\varepsilon_{yy} \frac{\overline{ac} - \overline{AC}}{\overline{AC}} \tag{3.5}$$

In this case $\overline{AC} = N$ and therefore:

$$\varepsilon_{yy} = \frac{N + \frac{\partial u_y}{\partial_y} N - N}{N} = \frac{\partial u_y}{\partial_y} \tag{3.6}$$

Consider now the change in the angle formed by the edges AB and AC. This angle change is called the distortion angle and is calculated as:

$$\gamma_{xy} = \frac{\partial_{u_x}}{\partial_y} + \frac{\partial_{u_y}}{\partial_x} \tag{3.7}$$

This study is applied in the next section to several real tests for validation purposes where the information obtained by the image processing analysis is compared with the physical sensor data.

Chapter 4

Results Evaluation

In this section the most relevant tests are presented and discussed. The algorithm results are compared with the data obtained from physical sensors and with the Golden Standard (GS). A detailed list of all experimental tests carried out is also presented.

4 Results Evaluation

Several laboratory tests were carried out in order to validate the adopted approach and measure the efficiency of the solution. Those tests were possible because several students from the FCT Civil Engineering Department agreed to develop their tests together sharing the information acquired by the traditional sensors and adapting the specimens with a pattern adequate to the image processing analysis.

Four different materials were tested until rupture: concrete beams (small and large), small specimens of wood, Plexiglas and PVC. For all the tests it was possible to compare the results from the image processing to the sensors' data since the tests were simultaneously monitored by the image acquisition system and by the sensors traditionally used in Civil Engineering tests.

Before data acquisition it was necessary to prepare the specimens for the image acquisition system and for the sensor data acquisition system. Two different situations can be seen in Figure 4-1. All the digital measurement was done at a distance without any particular calibration, with low cost support and very easy setup.

Figure 4-1. Example of two image acquisition system

Some initial tests were carried out with a virtual displacement where an image was mathematically transformed. In a second phase a micrometre was used (at ISEL Automation Laboratory) and finally the tests were carried out in

the Materials Laboratory of the FCT Civil Engineering Department. An overview of some specimens can be seen in Figure 4-2 where it is possible to see the variety of imposed patterns.

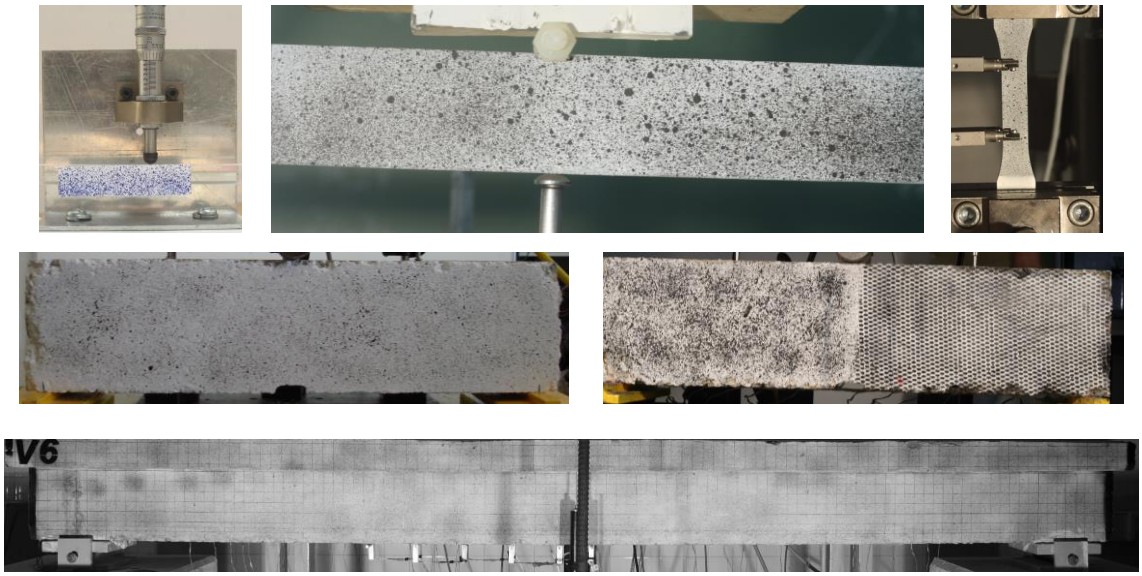

Figure 4-2. Different speckle patterns with different materials

4.1 Validation Methods

The physical sensors' data was used to validate the information obtained by the image processing analysis. Small capacitive sensors, a universal tensile machine (Zwick) and LVDT sensors were the physical sensor data sources. The Zwich was used for standard specimens. With concrete beam load tests the deflection measurement was measured by standard 100 mm/50 mm LVDT sensors located along the longitudinal direction of the beam. The data from the LVDT sensor at the mid-span was used for comparison with the data obtained from the image analysis system. LVDT sensors require a considerable time to assemble and calibrate and they can be easily damaged at concrete beam rupture. This is one of the advantages of the photometric approach since it doesn't require any physical setup on or even close to the specimen. All the measurements were done at a distance without any particular calibration. In

order to get a visual photometric reference an ordinary ruler was used on a sample photo as a reference for all the other photos.

Beyond the sensor data, the images were also used to get a Golden Standard (GS). In order to obtain the GS three trained users classified each image-time series manually three times. This information will be shown in a box plot - the yellow spots represent the average of the Golden Standard (an example can be seen in Figure 4-3). In some situations the information obtained by image processing is different from the physical sensors' data but it is in accordance with the manual measurements (GS). This happens because the material has initial accommodations and it is also due to the asynchronies between the two data acquisition systems.

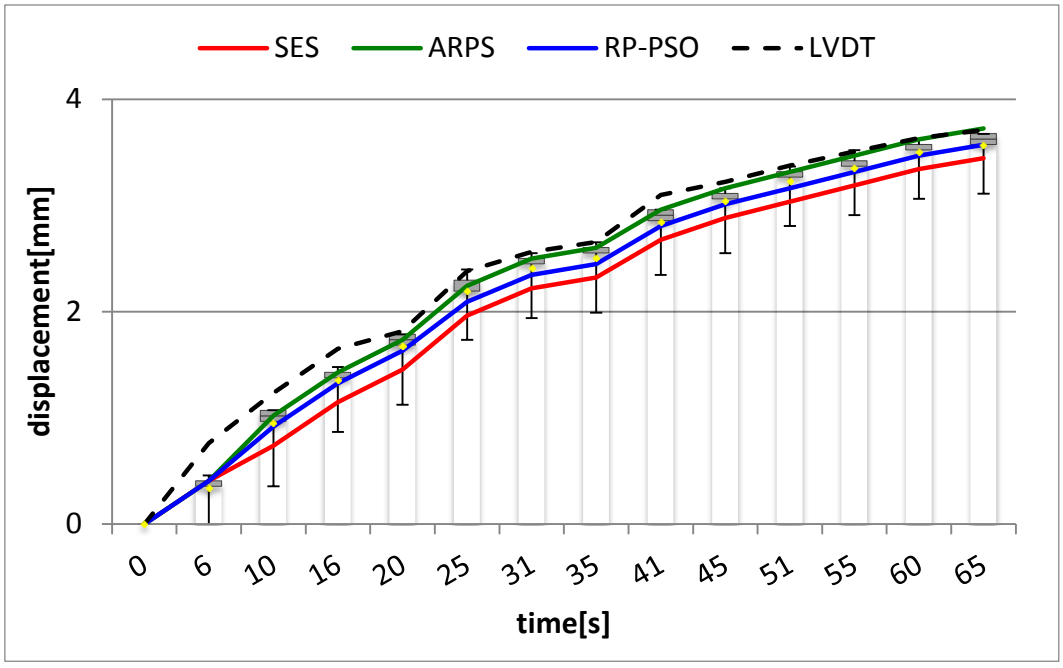

Figure 4-3. Example of a box plot graph where the data from the sensor is worse than the data obtained by image processing

4.1.1 Image Datasets Acquisition

Images were initially captured by a Cannon EOS 400D digital camera (3888×2592 pixels resolution) with a 50-70 mm lens. Two 500W spotlights were

used for structured lighting. The last tests used a Canon EFS 60 mm f/2.8 Macro lens with a single spotlight. All the images were captured in RAW format and then convert to TIFF format. The image processing analysis and the program were developed using the MATLAB environment from MathWorks.

The specimens were initially prepared with an underlying cover of matt white ink with a superimposed random speckle pattern manually applied using a large brush and matt black ink. The paint was applied with an ink spray on the bar specimens.

4.1.2 Test Chronology

The first algorithm implemented was the Simple and Efficient Search algorithm which was tested with virtual displacement using a large 3 m wide concrete beam. The image sequence was initially taken with the camera shutter remotely triggered by an operator. However, this was not found to be the best option and after the Canon remote control software was used.

The tests in the first two years were dedicated to building and testing the block matching algorithms, firstly with virtual displacement images and then with real tests. During these two years data from the tests on five 3 m wide reinforced concrete beams, ten 0.60 m wide concrete beams and from the tests with the micrometre was used. In June 2010 image tests were kindly provided by Civil Engineering students but they proved inappropriate because they were taken by directly triggering the camera causing additional image shaking that caused errors in the image processing analysis. Those tests were pull-off tests with small concrete blocks and load tests with small concrete beams. The pull-off tests had very small displacement. Some problems of image resolution, velocity of the tests and triggered camera occurred so no image processing data was viable.

More than 5000 images were processed and Table 4-1 and Table 4-2 show the test's chronology during the development of this thesis. Each test was stored on an Excel file where the data from the physical sensors were recorded every second. As the image time series are taken every 20 s, 10 s or 5 s, those files

were manipulated to extract the necessary lines for the algorithms' data evaluation.

Table 4-1. 2009 and 2010 tests chronology

Reference	Number of Images	Test duration [min]	Date/Material
TSC1	40	45	**June 2009 concrete beams 3m wide**
TSC2	34	30	
TSC4	54	30	
HB1	21	30	
HB2	64	120	
MAR 10000/05	77	10	**April 2010 concrete beams 0.6m wide**
NS 10000/04	72	10	
T++ 10000/05	49	10	
T-+ 10000/04	40	10	
MAR 10000/04	73	10	
NS 10000/05	93	10	
T++ 10000/04	51	10	
T-+ 10000/05	65	10	
Concrete boxes	*213*	-	*June 2010*
Concrete beams	*395*	-	
Virtual Images	178	**-**	**September 2010**
ISEL1	9	60	**November 2010 Micrometre Plexiglas bars**
ISEL2	9		
ISEL3	9		
ISEL4	10		
ISEL5	13		
ISEL6	15		
ISEL7	18		
ISEL8	22		
Test1	48	20	**November 2010 concrete beams 0.6m wide**
Test2	56	10	
Test3	57	20	
Test4	59	20	

In 2011 a test with a video camera was done but the camera quality was unacceptable for the proposal of this thesis and it was discarded. The last three years' accumulated experience results in more viable tests. Some of the tests were also specifically planned for this thesis. Specimens with standard dimensions were used as it was much easier to do several tests on the same day with the same conditions while easily changing the pattern and the specimen material. At the end of 2012 two large concrete beams were also tested.

The July 2014 tests are related to two Master students' theses that needed the image processing information because if they used the physical sensors, with the corresponding costs, the work was financially not viable. The goal was

to know what happened along the specimen when pulled. If physical sensors were to be used, 5 to 8 transducers would be necessary for each test (with no possibility of re-use). So two tests (one for each student) were monitored by both physical sensors and image analyses and the remaining eight were done using only the image acquisition system (two global LVDT sensors were used for each test). Those tests were pull-off tests that have the particularity of presenting very small displacement. A Carbon Fibre Laminate (CRFP) was glued on a concrete and a steel surface.

Table 4-2 2011 to 2014 tests chronology

Reference	Number of Images	Test duration [min]	Date/Material
2011 January video camera tests			
Test 1	38	20	**February 2011 specimens of Plexiglas (43x3.2mm; 71x1.7mm;54x1.2mm)**
Test 2	60		
Test 3	22		
Test 01	16	30	
Test 02	23		
Test 03	33		
Test 04	33		
Test 05	33		
Virtual Images	105	-	**December 2011**
V5	710	90	**October 2012: concrete beam 3m wide**
V6	780	60	**November 2012: concrete beam 3m wide**
Plexiglas	105	120	**December 2012 standard specimens with different materials**
PVC	146		
Wood	89		
Plexiglas	168	140	**April 2013 standard specimens with Plexiglas and PVC**
PVC	175		
IB_01	312	240	**July 2014 Carbon Fibre Laminate (CFRP) on steel/concrete**
IB_02	175	15	
IB_03	116	15	
CS_01	116	45	
CS_02	105	10	
CS_03	42	15	
CS_04	83	15	
CS_05	88	20	

4.2 Results from the most relevant tests

In this section some tests were selected because it is monotonous to provide all the results. The selection invites us to look at each particular

discussion related to image processing analysis: parameters of block matching algorithms, image-time interval, different patterns and data validation.

4.2.1 *The micrometre tests*

The tests done with a micrometre were essential to validate the implementation of the SES and ARPS algorithms and also to validate the initial results with virtual image displacements. The results were achieved using 25×25 pixels/block and a random pattern printed and glued on the surface of the specimen. After each displacement a photo was taken with a 20.2 pixels/mm resolution. Two different materials were used: balsa wood (lightweight with a density of 0.16 g/cm^3) and Plexiglas (with a density of 1.18 g/cm^3).

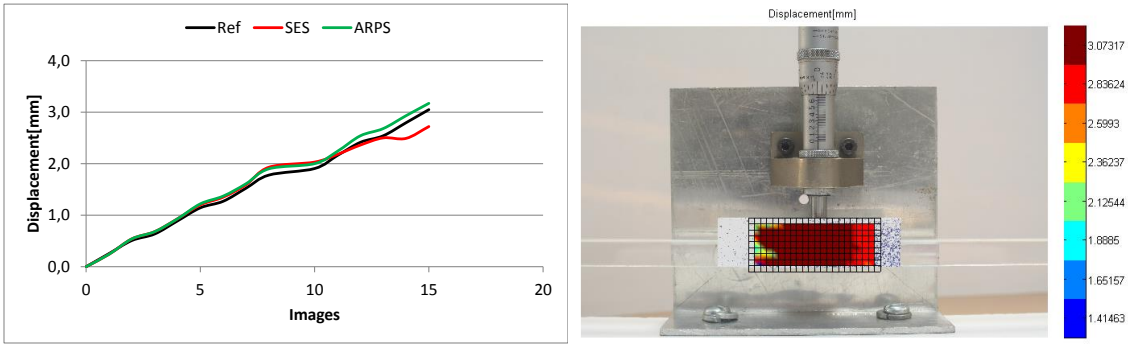

Figure 4-4. The displacement vs. images and the ARPS map displacement achieved with a micrometre for the Plexiglas bar

The displacement graph for both the SES and ARPS algorithms are shown in Figure 4-4 and Figure 4-5. In these figures the measurement provided by the micrometre is also shown (*Ref* line). On the right of these figures it is possible to see the displacement maps for both materials with the ARPS algorithm. The SES algorithm showed lower accuracy with both materials and for this reason the displacement map is shown only for the ARPS data.

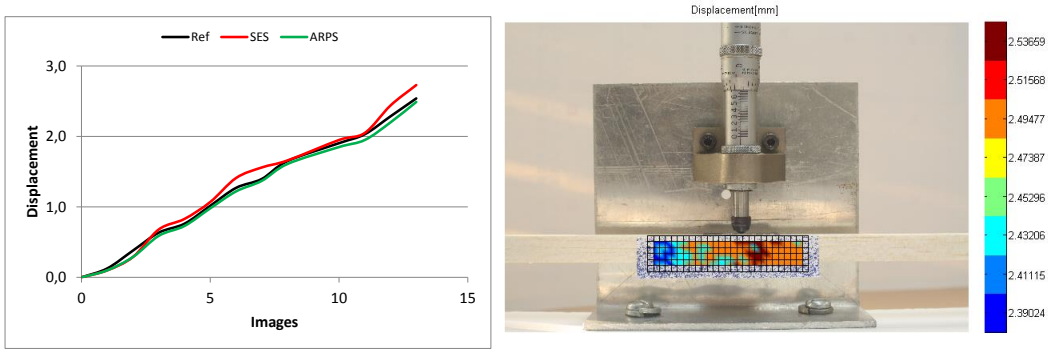

Figure 4-5. The displacement vs. images and the ARPS map displacement achieved with a micrometre for the balsa wood bar

As the balsa wood is more flexible it is possible to see different regions with different displacements. In the Plexiglas example the displacement map is more uniform.

4.2.2 *The load tests until rupture*

In this section an example (NS10000/04) of the tests done in April 2010 is presented. The experiments with 0.6 m wide concrete beams were done until rupture in a destructive test. The image data acquisition had a resolution of 9.5 pixels/mm and the interval between images was s.

Initially, the image time intervals were 2 s and 1 s. This was inadequate due to the large displacement that occurred at the end of the test. The time interval between photos was then reduced to 5 s allowing the system to follow the major displacements.

In Figure 4-6 it is possible to see the displacement vs. time graph where *d_sensor* is the data obtained with the physical sensor and *d_image* is the data obtained by the image processing system.

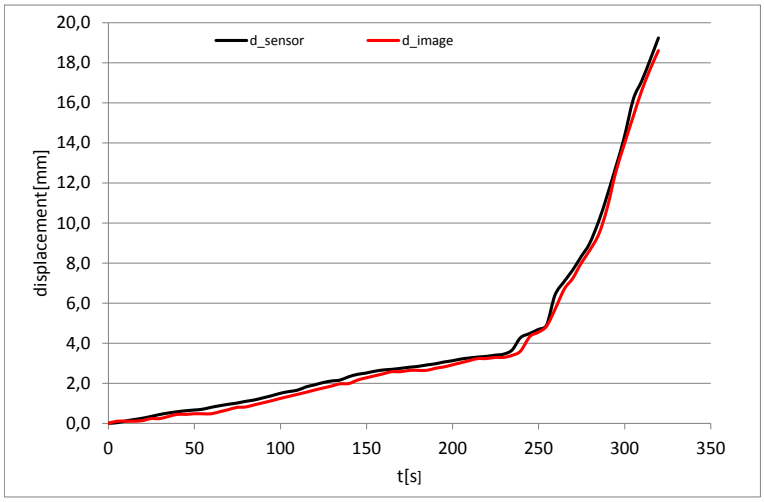

Figure 4-6. Displacement vs. time for NS10000_04 beam

In Figure 4-7 (left) a displacement map is shown. Blue indicates regions with low displacement and red regions with high displacement. A grid of 50×50 pixels blocks was used, corresponding to an area of 5.26×5.26 mm for each block. The beam was broken in the middle with the right side of the beam sliding to the right because it was free. The major displacements occurred with the slide to the right which explains why there are more red regions on the right of the image.

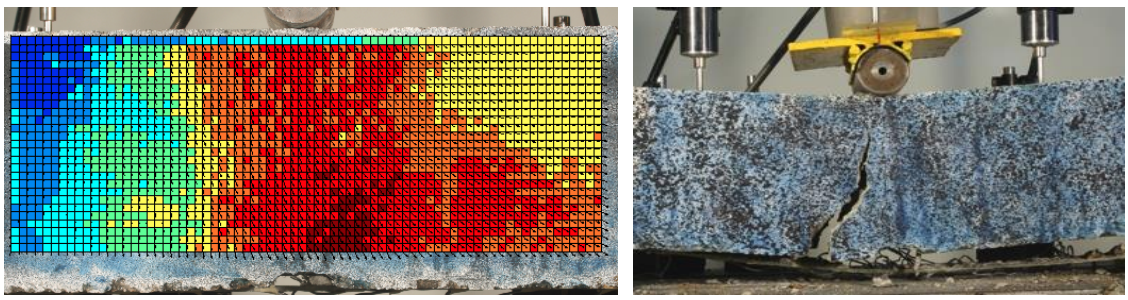

Figure 4-7. Displacement map for the entire region of interest (left) and the rupture (right)

It is also possible to see the displacement vector in each block (see Figure 4-8 for a zoom of the central part of the displacement map). This displacement vector was consistent with the onset of breaking. The advantage of the complete

displacement map is to show the regions where the major stress occurs in the earlier stages of the tests.

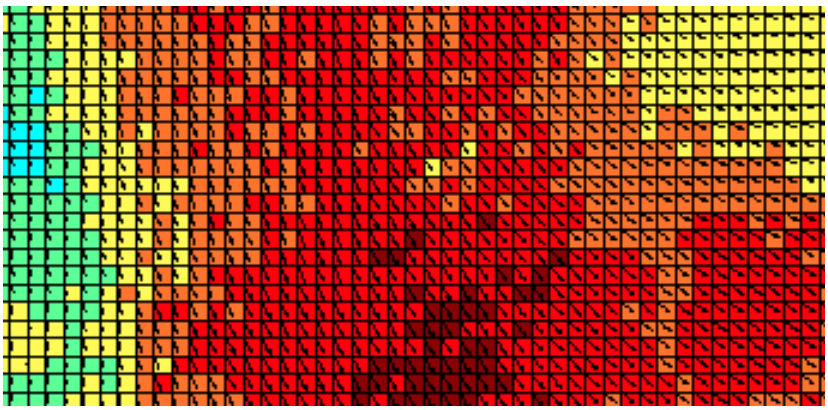

Figure 4-8. Zoom central displacement map

Another situation of a test of rupture can be seen in Figure 4-9. In this case the T++10000_05 data test was used. The acquisition was done with 10 s image interval and 42 images were used with a resolution of 8.4 pixels/mm. The beam was prepared with an underlying layer of matt white ink on top of which a superimposed random speckle pattern was manually applied using a large brush with matt black ink.

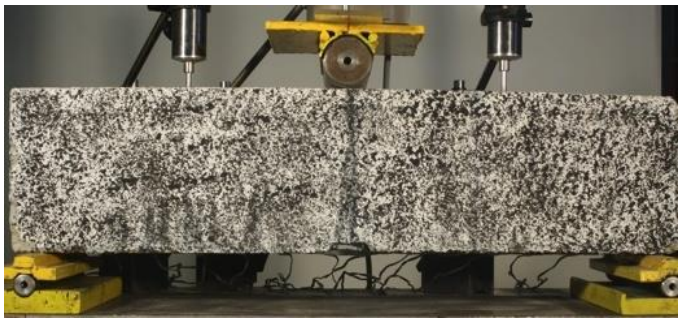

Figure 4-9. Example of the random pattern applied to the T++10000_05

The complete displacement map calculated by the SES, ARPS and RP-PSO algorithms is shown in Figure 4-10, using 128×128 pixels/block. The red blocks correspond to larger displacements.

The SES algorithm is the most sensitive but it is unable to follow the rupture zone. The RP-PSO shows better dynamics for all block sizes with greater capacity to follow the rupture zone.

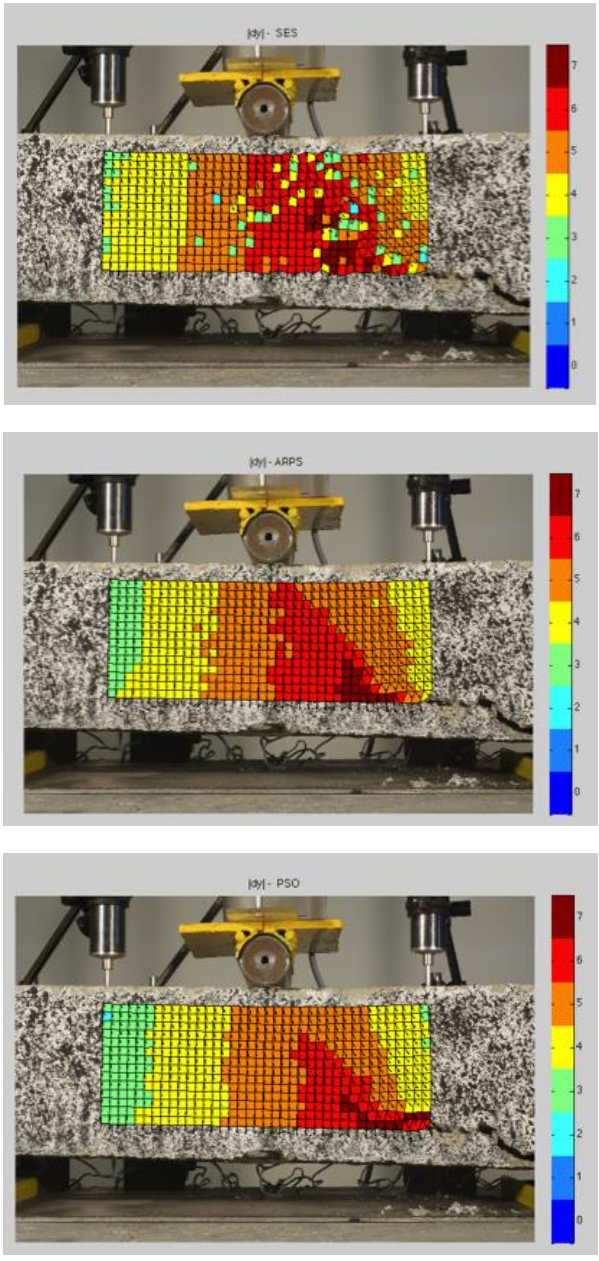

Figure 4-10. Displacement in the y-axis for the T++10000_05 using SES (at top), ARPS (in middle) and RP-PSO (at bottom) with block size of 128×128 pixel

Figure 4-11 shows the d×t and F×d graphs using the information from the sensor placed at the centre of the specimen plus the information of the three

algorithms in the same spot. The results from the three algorithms (*d_SES*, *d_ARPS* and *d_RP_PSO*) are shown together with the sensor data (*d_Sensor*). The RP-PSO algorithm is best able to follow the larger displacements and is the one closest to the displacement indicated by the physical sensor.

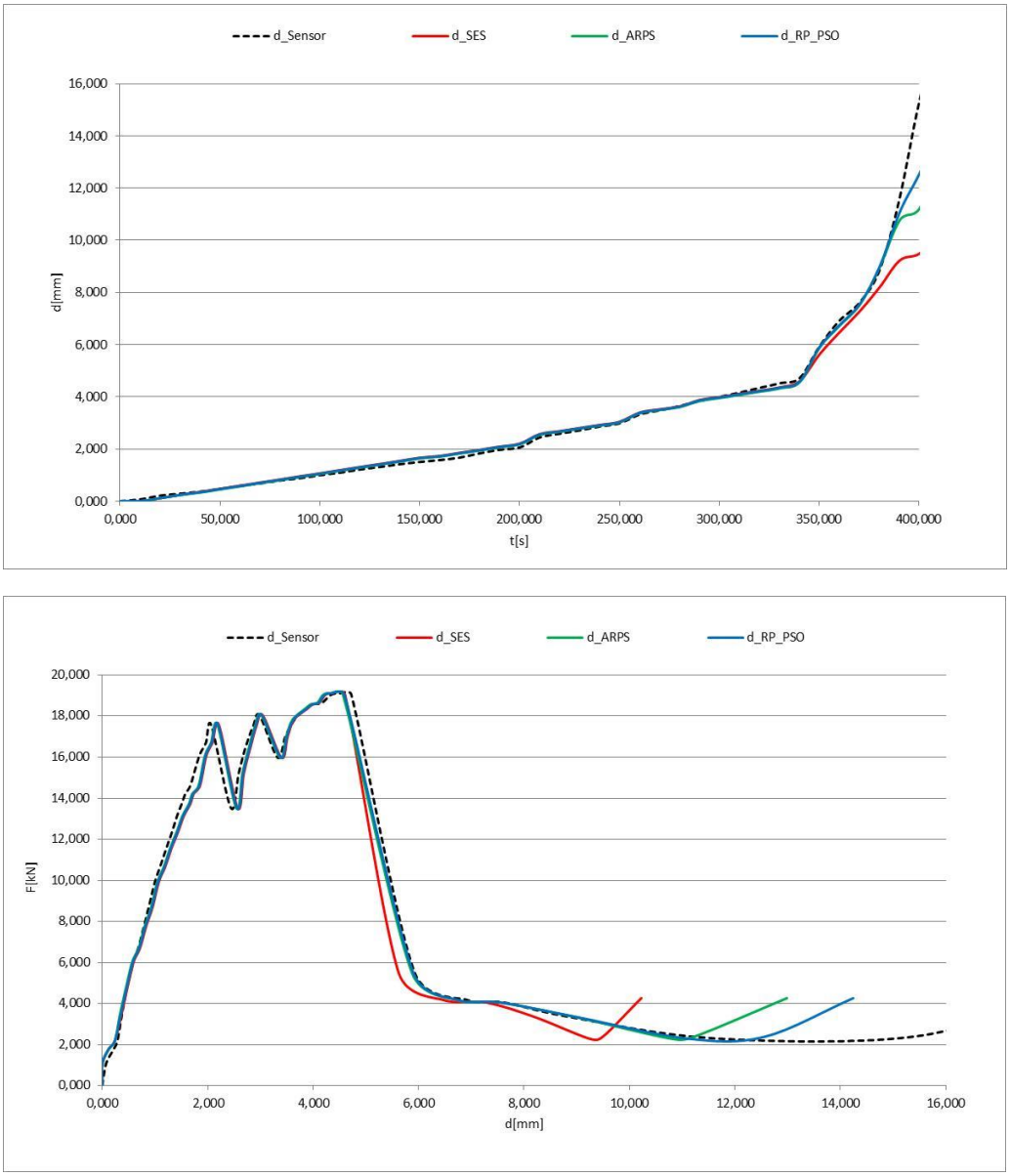

Figure 4-11. Graph displacement versus time (at top) and Force versus displacement (at bottom) for the T++10000_05 concrete beam

In these graphs it is possible to see the algorithms' incapacity to follow the large displacements, especially the SES algorithm. This is due to the 10 s image interval that was revealed to be insufficient for the last period the test.

4.2.3 Influence of the Block Size

Several tests were done with a Plexiglas specimen in order to study the random speckle pattern variety and the best block size to use in the block matching algorithms. Using this small bar it was much easier to repeat tests due to the shorter setup time and inexpensive samples. In Figure 4-12 it is possible to see the data acquisition setup.

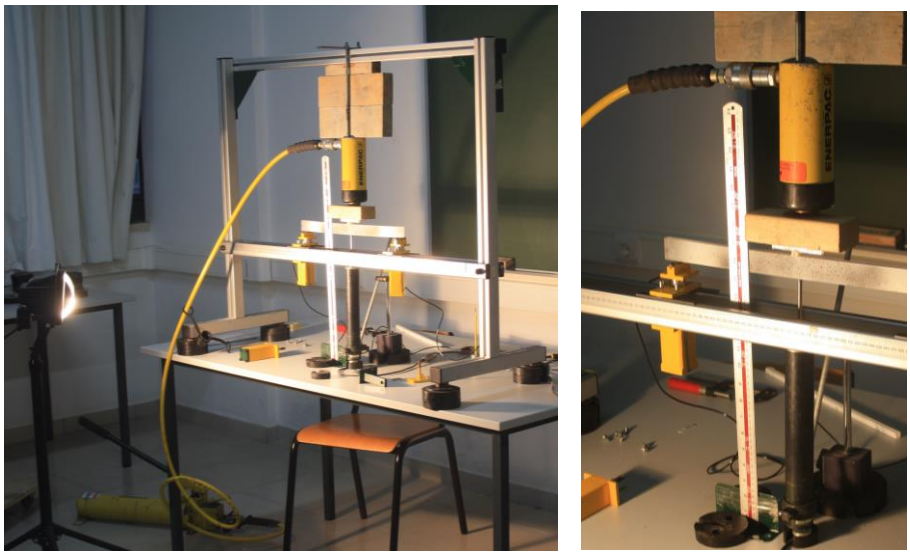

Figure 4-12. System acquisition data with small bars of Plexiglas

Plexiglas bars (an example can be seen in Figure 4-13) were used to create a more controllable environment where the different speckle patterns were easily changed. Displacement was measured by LVDT sensors for the algorithm's validation. The results shown in this section were based on 33 image tests taken with an interval of 5 s and a resolution of 20.5 pixels/mm.

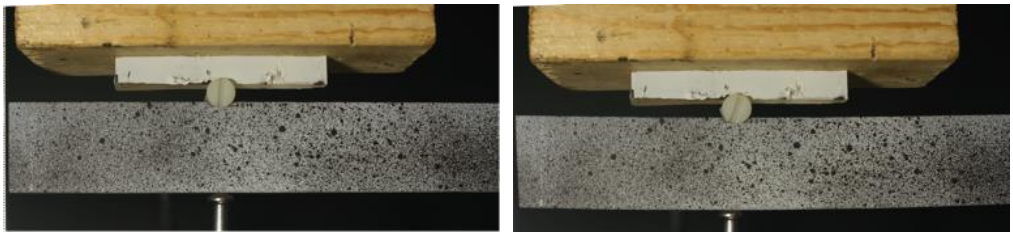

Figure 4-13. Images of the Plexiglas bar: initial shape (left) and final shape (right)

Figure 4-14 shows the displacement versus time with different block sizes compared to the data obtained from the LVDT sensor. The region of interest was in the middle of the specimen, i.e. the same spot as the sensor. The ARPS algorithm was applied using different block sizes. The data obtained with 32×32 pixels/block was identified by *b_32* at the graph. The same terminology was used for blocks with the size of 50, 64 and 100 pixels (referred in the graphs as *b_50*, *b_64* and *b_100*).

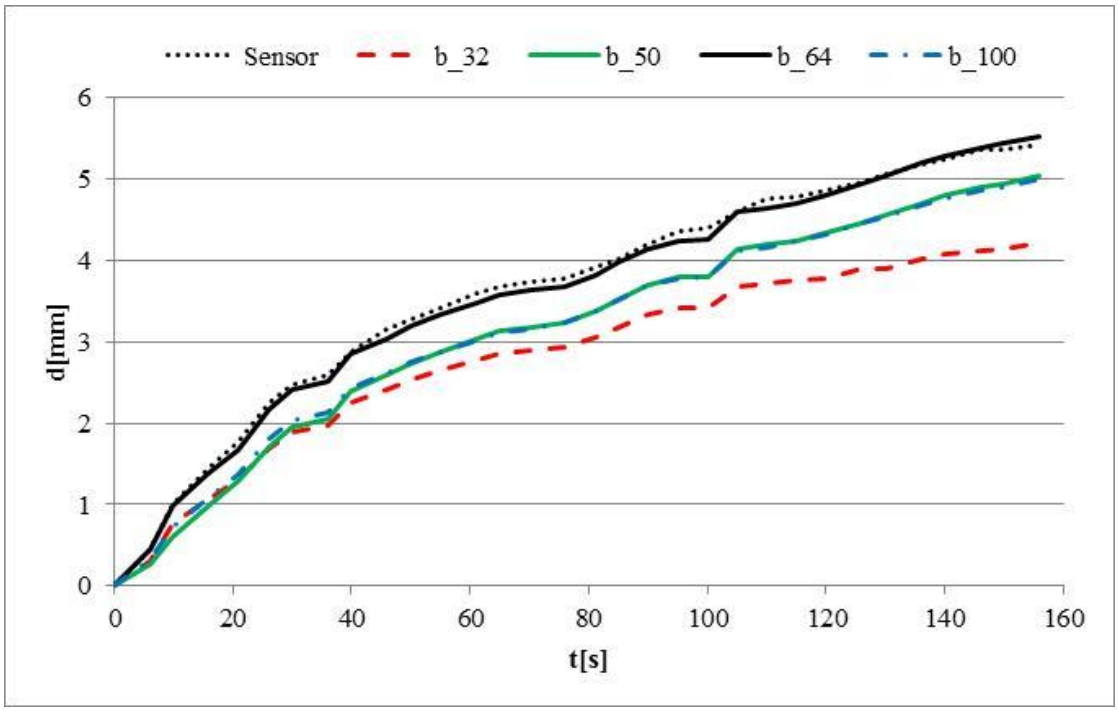

Figure 4-14. Displacement vs. time with ARPS algorithm for different block sizes

The pattern applied and the block sizes adopted are related and both are important for achieving accurate results. With a large pattern and a small block

size it is impossible to follow the displacement because the pattern is often unrecognisable. Further, if a small pattern and a small block size are chosen, the computation time can be too high. For the same pattern and for each block motion algorithm there is an ideal size of block. The best results were achieved with a block size of 64.

4.2.4 The Golden Standard Study

One of the major problems found in the different tests was the synchronization between the start time of the image session and the start time of the sensors' acquisition. Even if both starts are synchronised there are important initial accommodations on the test's specimens and on the pneumatic equipment. It was found that both data values (sensor and algorithm data) are similar but sometimes delayed in time. In other situations the algorithms' data was significantly different from the sensor's data.

In order to validate the algorithms results a Gold Standard (GS) was obtained by manual analysis of the images using dedicated software. In this analysis the user manually points out the consecutive position of each point under analysis over the entire image time series. Each of the three trained users classified the image series three times.

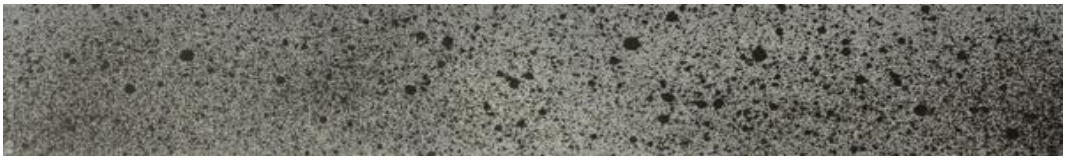

Figure 4-15. Example of the random pattern used in the Golden Standard study

Figure 4-15 shows the random pattern example for the GS study. The results obtained with the LVDT sensor were compared with those obtained in the middle of the beams by the image processing. In all the comparative figures the yellow spots represent the average of the Golden Standard that is represented in a box plot. The tests were done with the SES, ARPS and RP-PSO algorithms.

Figure 4-16 shows the results for the Plexiglas with 64×64 and 128×128 pixels/block. With 64×64 pixels/block the RP-PSO algorithm shows better results than ARPS, and the SES algorithm diverges from the Golden Standard. With blocks of 128×128 pixels the results of the three algorithms were more similar.

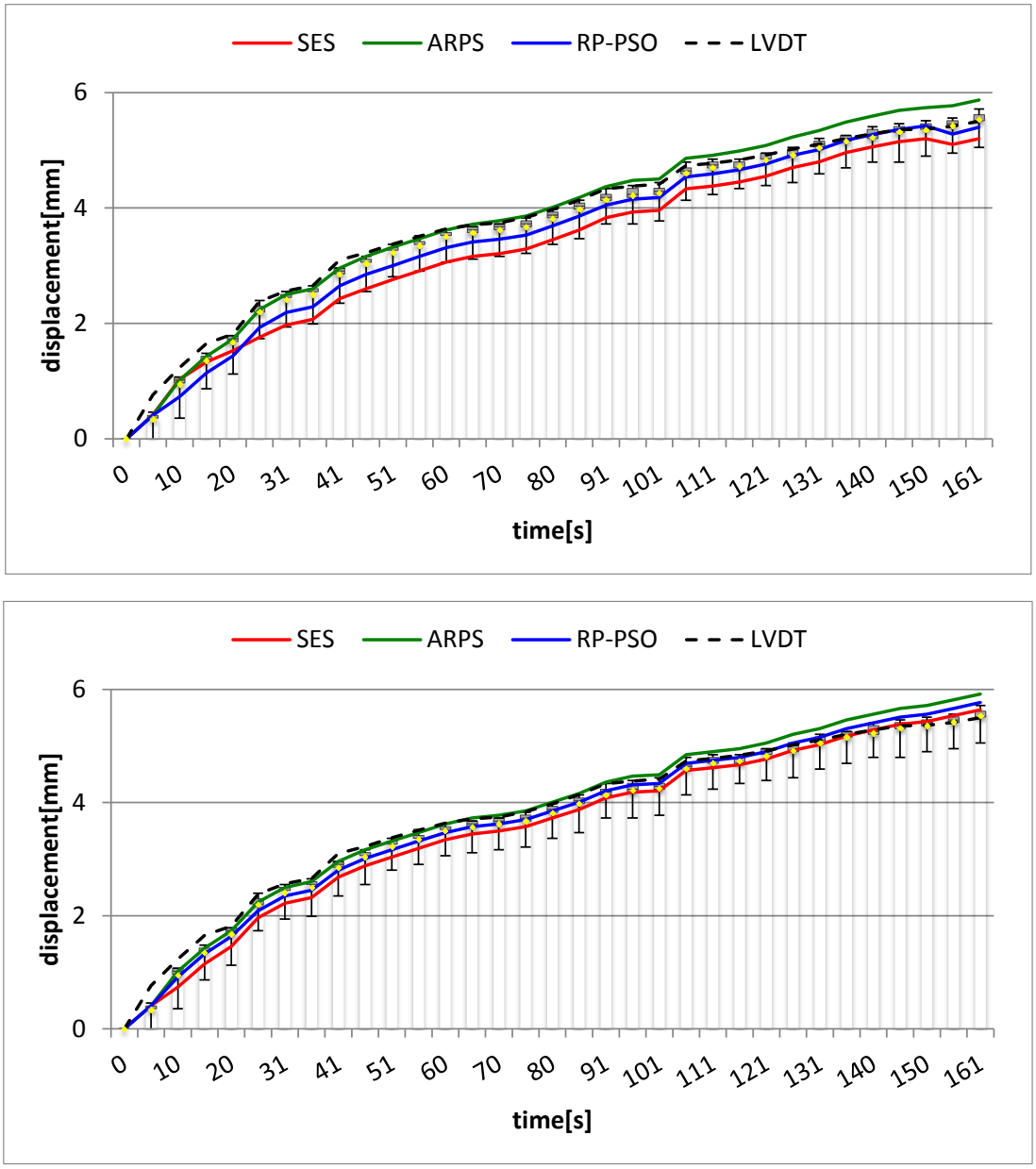

Figure 4-16. Plexiglas Golden Standard compared with LVDT and image processing algorithms with a block size of 64×64 (at top) and 128×128 (at bottom)

Other differences between the physical sensors and the Golden Standard are presented in section 4.2.6.

4.2.5 The Large Concrete Beam Test

The large concrete beam used was 3 m wide. With samples of this size, if only one camera is used the resolution is reduced. The last two tests with large concrete beams (V5 and V6 tests) were photographed with two cameras: one took photos of the complete beam and the other a half of the beam. With these photos it was possible to analyse the beam with two different resolutions. In addition, on the V6 beam a regular grid was superimposed over the random pattern. The results were obtained with 75×75 pixels/block for the half beams and 50×50 pixels/block for the entire beams.

In Figure 4-17 it is possible to see the general views (half and full size) of V5 concrete beam. In this test the manual crack classification was done. In those moments the test was stopped (the test took 90 minutes to complete). The maximum load was 96.9 kN with a displacement of 19.2 mm and then reduced to 0 kN.

Figure 4-17. A partial view (left) of V5 beam and the complete view (right)

The random pattern for V5 and V6 beam was different as can be seen in Figure 4-18. The V5 concrete beam only has the random pattern while with the V6 concrete beam a regular black grid was applied over the random pattern.

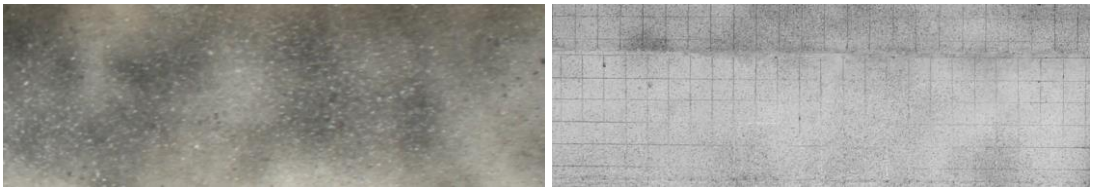

Figure 4-18. The V5 beam pattern (left) and the V6 beam regular and random pattern

Figure 4-19 shows the first and the final images of the V6 beam. In this beam a regular grid was superimposed over the random pattern. This test took approximately 30 minutes and the goal was to achieve beam rupture. That occurred at 140 kN with 42 mm displacement.

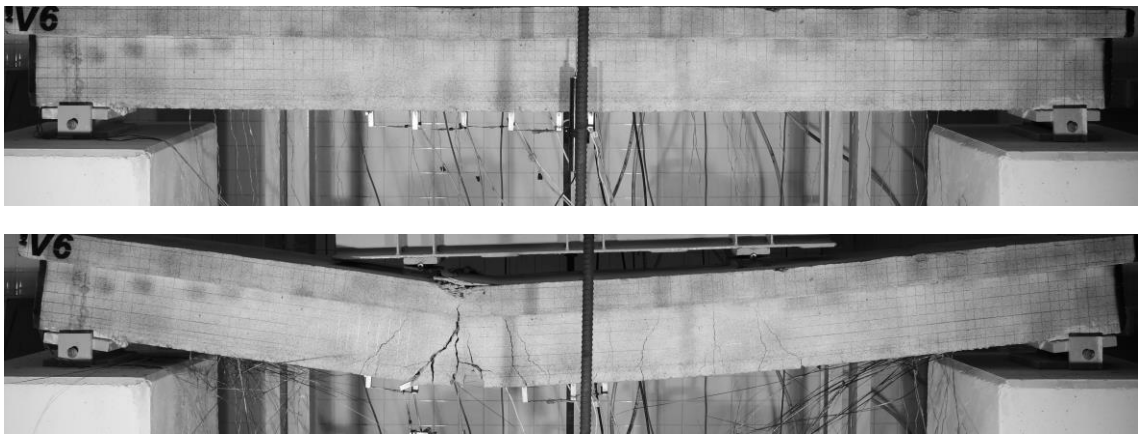

Figure 4-19. First (top) and final(bottom) images of V6 beam

A support bar on the specimen's front-centre was placed for its stability but this produced some inconsistencies in the centre of the displacement map (in that zone no displacement movements were calculated).

4.2.5.1 Analyses with the random pattern

With the full view of the beam several analyses can be done: deflection shape, the motion vector and the stress distribution in a uniform cross section. Some problems occurred with the complete V5 beam due to its poor definition pattern, low image contrast and resolution. For this reason each algorithm shows a distinct displacement map (see Figure 4-20). The red zone represents

the major displacements and the blue zone the minimum displacements. Also, as already mentioned, the specimen front bar becomes a blue zone in the displacement map centre.

Another conclusion is that the Cross Correlation (CC) (eq. 2.3) cost function has better results with this pattern than with the Mean Absolute Difference (MAD) (eq. 2.1). Therefore, all the results presented with the random pattern use the CC function as the metric to compare two consecutive images. In other tests, with high contrast patterns, the use of MAD or CC does not interfere with the results.

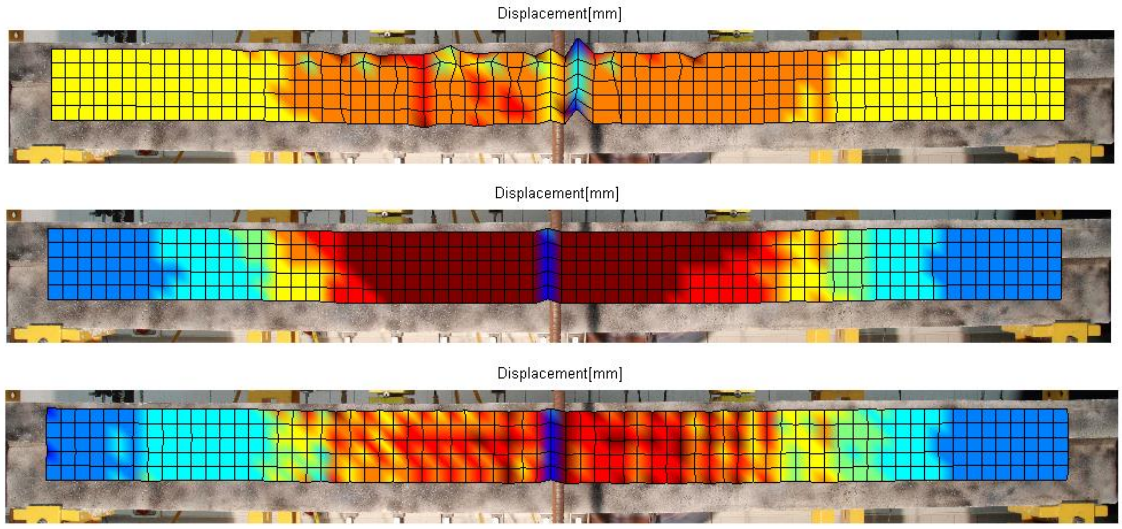

Figure 4-20. The complete displacement map results with the three algorithms: SES (top), ARPS (middle) and RP_PRSO (bottom)

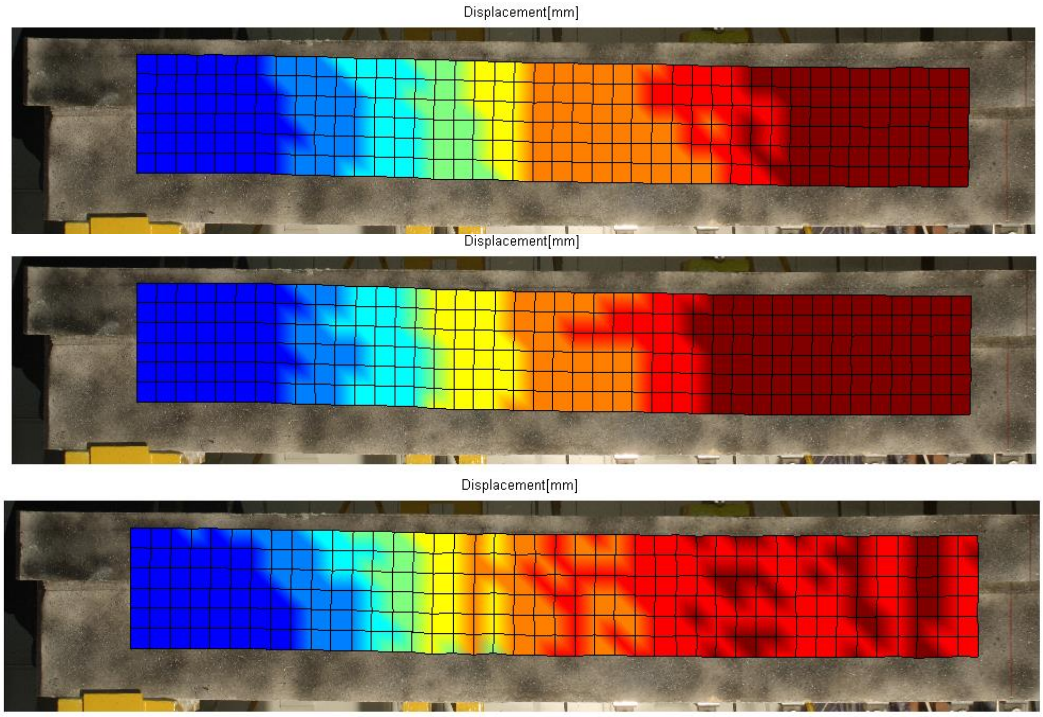

Figure 4-21. Displacement map with the SES (top), ARPS (middle) and RP-PSO (bottom) algorithms

If the half beam image time-series is used the displacement maps are similar for all three algorithms because in this situation the resolution is higher. Figure 4-21 shows the displacement maps for each algorithm. Although the numerical results of different algorithms may be similar as they are achieved in a particular region, normally the same spot as the physical sensor, it is through the displacement map that it is possible to see the algorithms' slight differences. In this case the RP_PSO is shown to be the most sensitive.

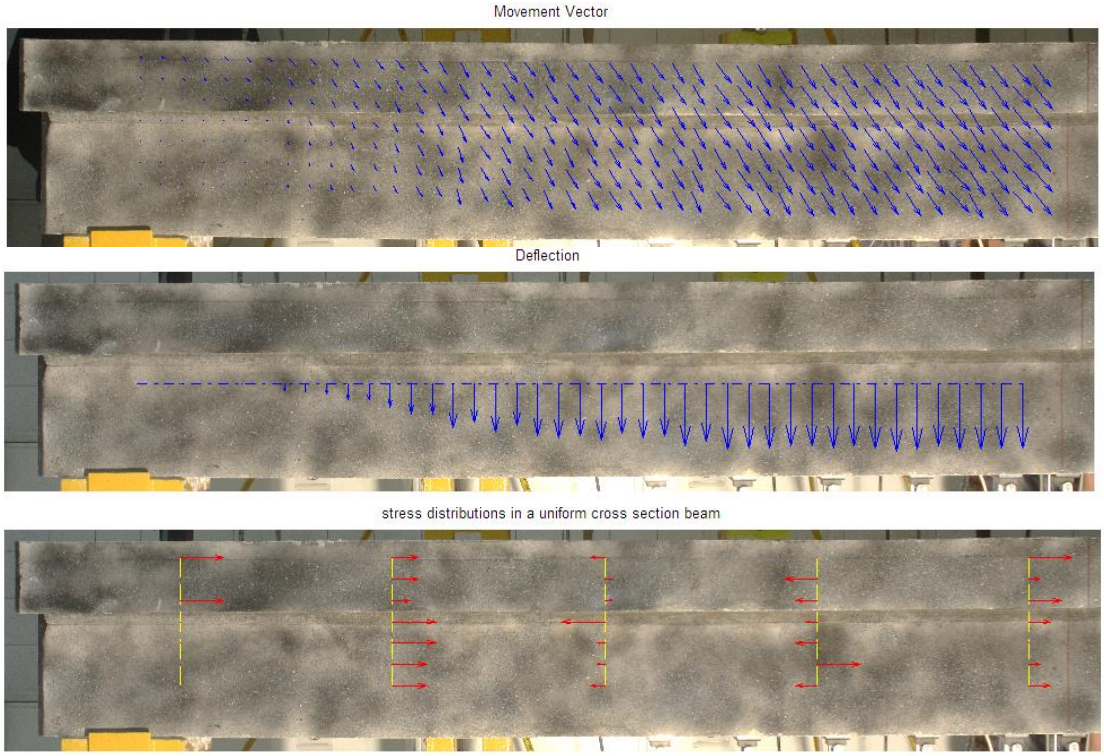

Figure 4-22. The movement vector map, the deflection of the beam and the stress distributions in a uniform cross section with the RP_PSO data

The movement vector map, the deflection of the beam and the stress distributions in a uniform cross section are types of information that can be obtained through digital image correlation. Figure 4-22 shows those maps with the RP_PSO data. The red region displacement maps correspond to higher movement vector and deflection.

The V6 beam has a better random pattern and for this reason it is possible to use the full size beam results (see Figure 4-23). The ARPS data algorithm was used to show the complete maps of displacement, strain, movement vector, deflection and stress distribution.

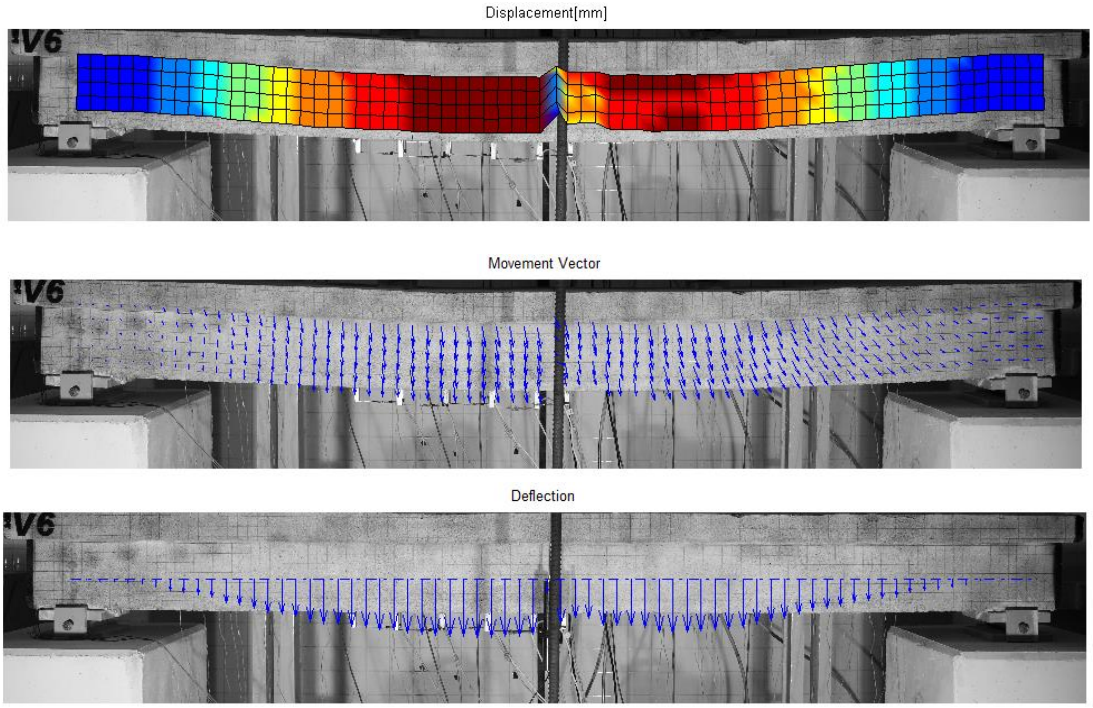

Figure 4-23. Maps of displacement, movement vector and deflection obtained with the ARPS data

In Figure 4-24 the same information sequence is shown using the data obtained with the RP_PSO algorithm.

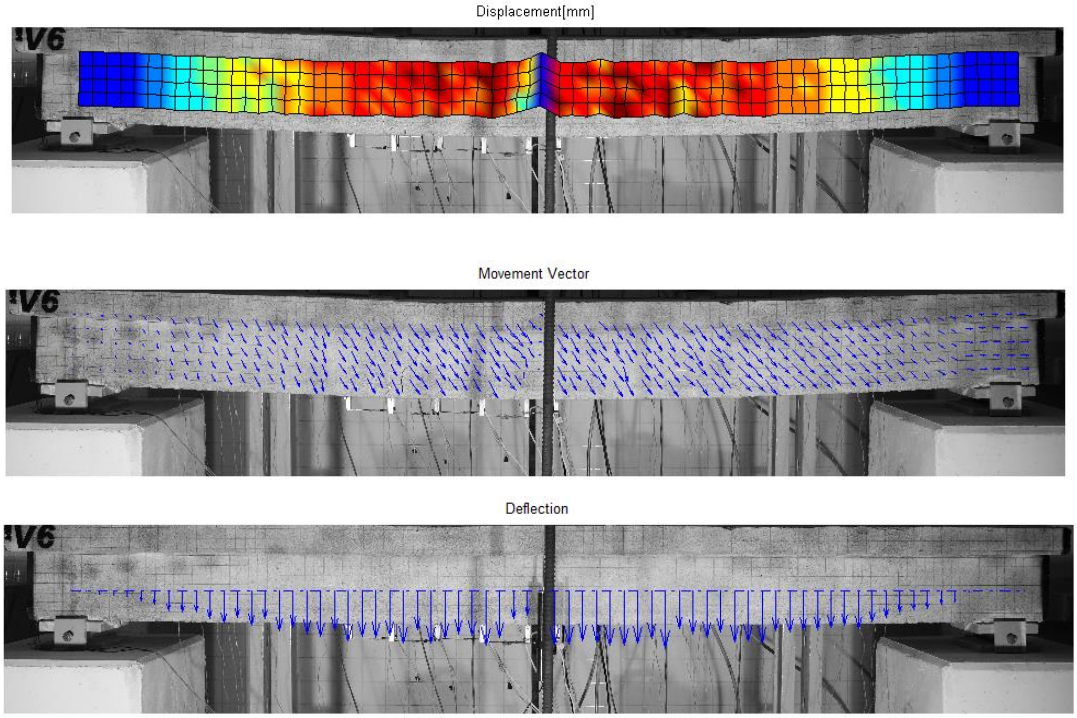

Figure 4-24. Maps of displacement, movement vector and deflection obtained with the RP_PSO data

4.2.5.2 Analyses with PSCH

The Pattern Signature Correlation Histogram algorithm (PSCH) can be combined with a block motion algorithm. For this example the V6 image-time series was used.

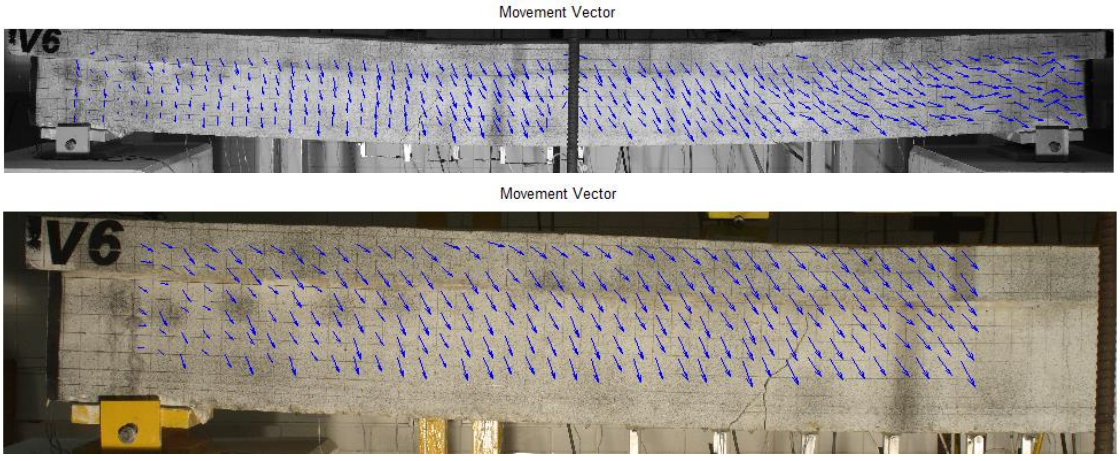

Figure 4-25. The movement vector map with PSCH algorithm for both views (full and half view)

In this situation the Cross Correlation cost function was used between the two block histograms instead of using the pixel intensity as the feature. The movement vector map seems more realistic when compared with Figure 4-19.

The time spent on the regular grid was excessive and did not compensate the results when compared with the facility of a random pattern and its results.

4.2.6 The Specimen Tests

Several specimens were carried out in tension, in accordance with standards ASTM -D 638 – 00 (Astm 2014). The specimens' dimension can be observed in Figure 4-26. With these specimens it was much easier to study different materials (balsa wood, PVC or Plexiglas) and to impose different patterns.

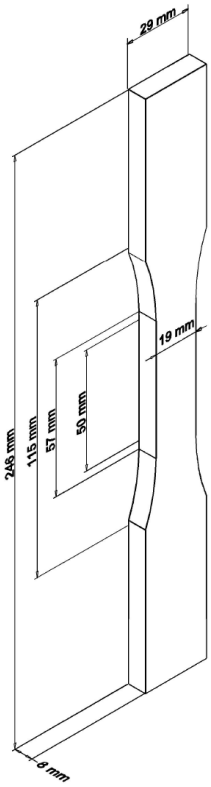

Figure 4-26. Example of a specimen used in the tests

In this section the results of two different types of material are used. The manufacturer classified fragile material A as Plexiglas and the ductile material B as PVC. A total of 10 flat specimens (5 Plexiglas specimens - A1 to A5 - and 5 PVC specimens - B1 to B5) were tested. Zwick, a universal tensile machine, was used with a capacity of 50 kN. The test speeds were 0.02 mm/s and 0.05 mm/s.

In Table 4-3 it is possible to see the image series' acquisition conditions. All the digital measurements were done at a distance without any special calibration using a low cost tripod. The image acquisition was done with a Canon EOS 550D digital camera with a Canon EFS 60mm f/2.8 Macro lens. Artificial lightning was used in order to maintain a constant light environment using a 100 W tungsten spotlight. Images were captured with 3456×5184 pixels at intervals of 5 s resulting in sequences of 22 to 100 photos depending on the test speed. All the images were captured in RAW format in order to avoid any image compression and/or particular camera settings and then converted to TIFF format for image processing with MATLAB.

Table 4-3. Image series acquisition conditions used by the different algorithms

	A1	**A2**	**A3**	**A4**	**A5**	**B1**	**B2**	**B3**	**B4**	**B5**
Speed test [mm/s]	0.02	0.02	0.02	0.02	0.02	0.02	0.05	0.05	0.05	0.05
Number of Images	38	42	22	54	36	233	79	97	100	100
Resolution [pixel/mm]	232.0	82.1	84.2	82.6	85.3	85.7	85.0	75.5	54.0	56.1

To produce a random speckle pattern the PVC was manually sprayed with matt black ink and the Plexiglas specimens were prepared with an underlying layer of matt white ink on top of which a random speckle pattern was manually sprayed with matt black ink. Figure 4-27 and Figure 4-28 show the diversity of the random pattern applied. The entire area was not considered as the camera was placed very close to specimen A1 in order to have the best possible resolution.

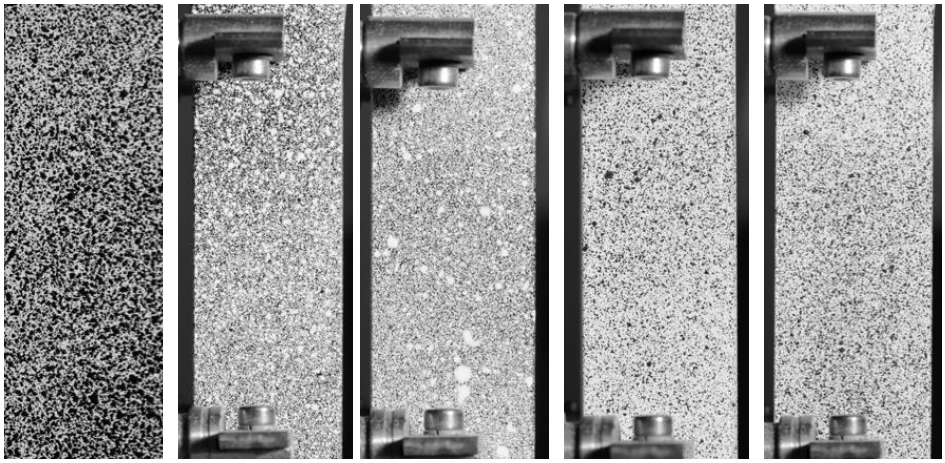

A1 A2 A3 A4 A5

Figure 4-27. Detail of the pattern applied to the five specimens (A1 to A5) of fragile material

In order to classify the random pattern applied, the percentage of black pixels and the borderline pixel were considered. As an example, the percentage area occupied by black pixels was 55.1% for A1, 15.5% for A4 and 10.8% for B2. The number of edging pixels was 3.2% for A1, 2.7% for A4 and 4.3% for B2.

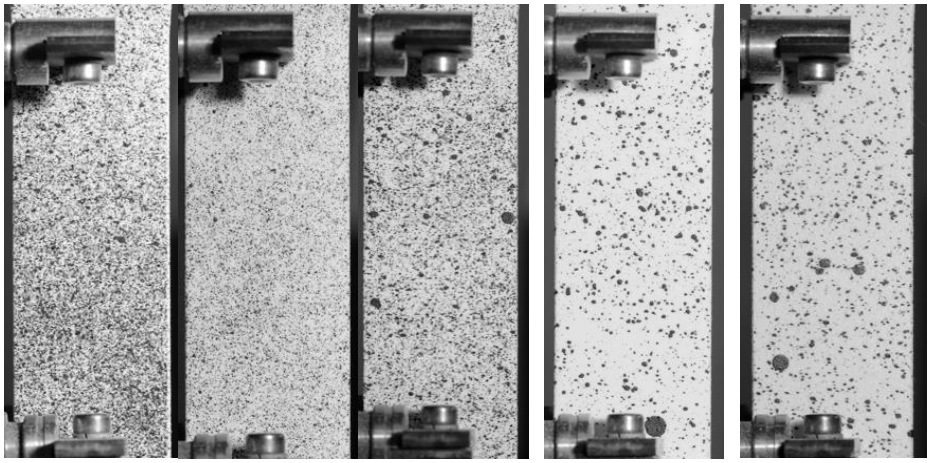

B1 B2 B3 B4 B5

Figure 4-28. Detail of the pattern applied to the five specimens (B1 to B5) of ductile material

The image-time series were tested with three different algorithms. The search area is the area around the current block where it is expected to find a block match between two consecutive images. This value was empirically

found as 15 for all the algorithms. In the RP-PSO algorithm two iterations were done, the maximum velocity vector allowed was 15, *c* was 1.8 and the inertia weight, *W*, was 1.1. In all the algorithms the matching criterion was the Mean Absolute Difference (MAD) (equation 2.1) function where only the pixel intensity was used as a feature. Block sizes of 150×150, 100×100 and 50×50 pixels were tested.

During the experiments only one fragile specimen broke in the middle but almost all the ductile specimens broke in the middle (B4). Figure 4-29 shows the specimens' fracture points.

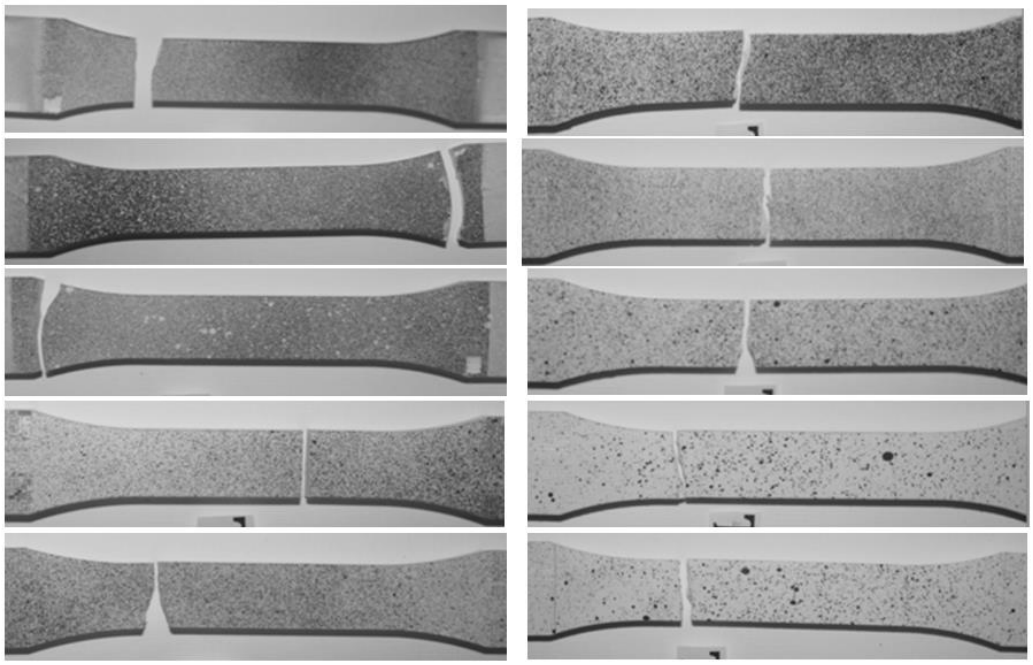

Figure 4-29. Detail of the broken specimens of materials A (left - top left A1 sequentially to A5 bottom left) and B (right - top right B1 sequentially to B5 bottom right)

4.2.6.1 Global Results

The SES algorithm has the highest number of computations followed by the ARPS and the RP-PSO. Figure 4-30 shows the number of computations required by each algorithm using 100 pixels per block. The values in this chart were taken from an area of 600×600 pixels in each specimen.

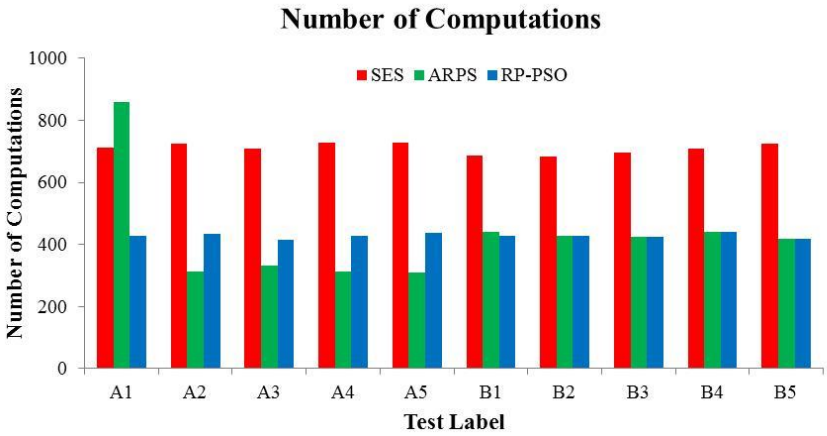

Figure 4-30. Number of computations for the three algorithms using 100×100 pixels/block

The SES algorithm takes longer to calculate due to the higher number of computations. The RP-PSO algorithm, despite in some tests having a higher number of computations than the ARPS, takes almost the same time as the ARPS.

Table 4-4 shows the elastic modulus (*Ei*), tensile strength (*Fr*), displacement (*dr*) and strain (*εr*) at break for the sensor; the elastic modulus (*Ei*) is calculated with information of the graph Force × displacement.

Table 4-4. Results from the physical sensor data for each specimen

	A1	**A2**	**A3**	**A4**	**A5**	**B1**	**B2**	**B3**	**B4**	**B5**
Ei [MPa]	727	701	749	**704**	727	122	**106**	94	102	123
Fr [N]	6886	8324	5502	**9401**	7801	907	**924**	938	992	988
dr [mm]	3.3	4.2	2.2	**5.6**	3.6	23.3	**19.8**	24.3	25.0	25.0
εr [%]	8.3	10.5	5.5	**14.0**	9.0	58.3	**49.4**	60.6	62.5	62.5

With the data obtained by each algorithm (d_{Alg}) it is possible, for each specimen, to calculate the average deviation error (*av_error*), elastic modulus (*E*) and strain (ε_{Alg} or ε_{Sensor}) as:

$$av\_error = \frac{\sum_{i=1}^{MAX} \frac{|d_{Alg} - d_{Sensor}|}{d_{Sensor}}}{MAX} \tag{4.1}$$

$$E = \frac{\sigma_2 - \sigma_1}{d_2 - d_1} \tag{4.2}$$

$$\varepsilon_{Alg} = \frac{d_{Alg}}{L} \tag{4.3}$$

$$\varepsilon_{Sensor} = \frac{d_{Sensor}}{L} \tag{4.4}$$

where MAX is the number of images considered, L the specimen's original length, d_{Sensor} and d_{Alg} the displacement achieved by the sensor and by the image processing algorithm. Equation 6.2 is calculated by collecting two points on the Force × displacement graph: σ_1 and σ_2 are the force values at 10% and 30% of the rupture point, d_1 and d_2 are the corresponding displacement values. Table 4-5 shows the results obtained with each algorithm for block sizes of 100 pixels.

Table 4-5. Results achieved by different algorithms using blocks of 100x100 pixels

	A1	A2	A3	**A4**	A5	B1	**B2**	B3	B4	B5
Elastic module [MPa]										
SES	741.4	601.8	702.0	**686.8**	660.8	117.0	**93.0**	87.0	85.0	84.0
ARPS	741.4	601.8	702.0	**654.9**	660.8	117.0	**97.0**	85.0	86.0	84.0
RP-PSO	802.6	576.4	631.0	**647.3**	718.6	124.0	**106.0**	88.0	98.0	84.0
Displacement at rupture [mm]										
SES	3.5	4.9	2.5	**6.1**	4.1	23.4	**19.3**	22.0	26.8	26.6
ARPS	3.4	4.9	2.5	**6.2**	4.1	23.5	**18.4**	22.0	26.9	26.6
RP-PSO	3.4	5.0	2.6	**6.2**	4.2	23.1	**18.4**	21.9	22.6	24.9
Strain at rupture [%]										
SES	8.9	12.1	6.2	**15.3**	10.2	58.5	**48.1**	55.1	67.1	66.5
ARPS	8.5	12.1	6.3	**15.4**	10.2	58.7	**46.0**	55.0	67.2	66.5
RP-PSO	8.4	12.5	6.6	**15.4**	10.4	57.6	**45.9**	54.7	56.5	62.3

Figure 4-31 shows the average error achieved by each algorithm using 100 pixels per block. For the fragile material the average errors are high. The A1

specimen has the highest resolution but the entire central area was not considered. The second best was the A4 specimen that was unique in breaking in the middle. The average error found for the ductile material was slightly better than for the fragile material. Ductile material B2 also broke in the middle and achieved a lower mean error deviation.

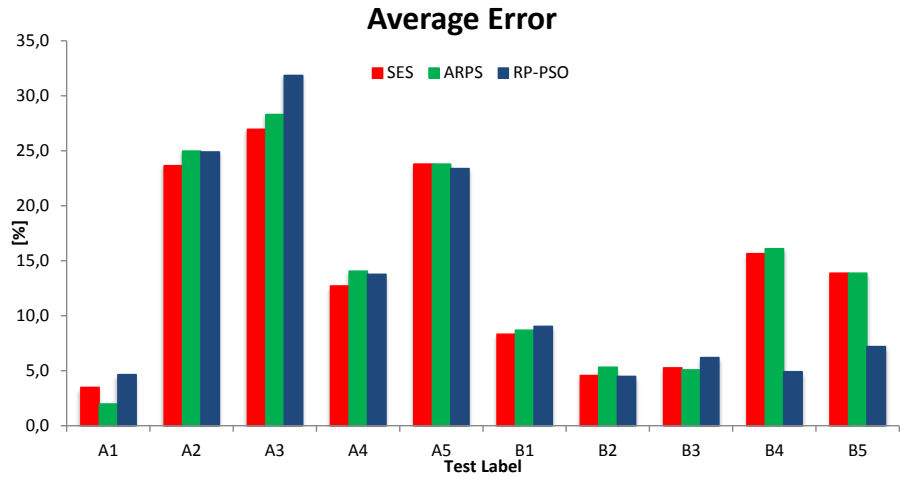

Figure 4-31. The average error achieved by different algorithms with 100 pixels per block

Figure 4-32 shows the average error for different block sizes for the two specimens A4 and B2. The RP-PSO algorithm achieved the best or at least identical results as the ARPS. For the fragile material the SES algorithm has worse results as the block size increases. The ARPS and the RP-PSO have equivalent performance.

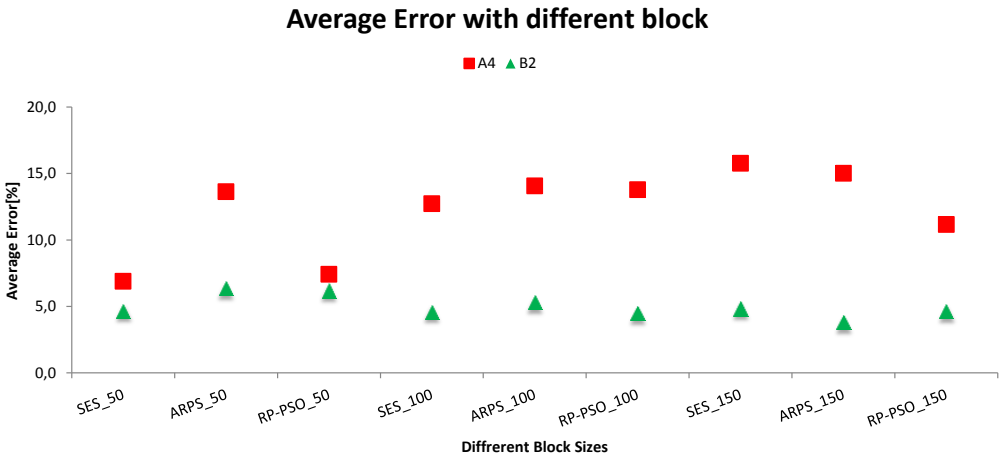

Figure 4-32. Average error for the specimens A4 and B2, with different algorithms and block sizes

For the ductile material the block sizes do not significantly influence the results. The RP-PSO's best results were achieved with the ductile material. These results show that it is impossible to choose an algorithm independently of the material. In order to see other characteristics of those materials the A1 specimen was chosen (better resolution) as well as specimens A4 and B2 because they have the smallest average error. The data from 100×100 pixels/block was used to plot the graphs of Stress vs. Displacement, Stress vs. Strain and the complete maps of displacement and strain in the next sections.

4.2.6.2 A1 Specimen

In A1 (Plexiglas specimen) the best resolution (232 pixels/mm) was achieved. Figure 4-33 shows the displacement and strain maps in y and x directions for the A1 specimen. The displacement map shows that the displacements are not uniform throughout the specimen as is assumed in many theoretical representations in Civil Engineering.

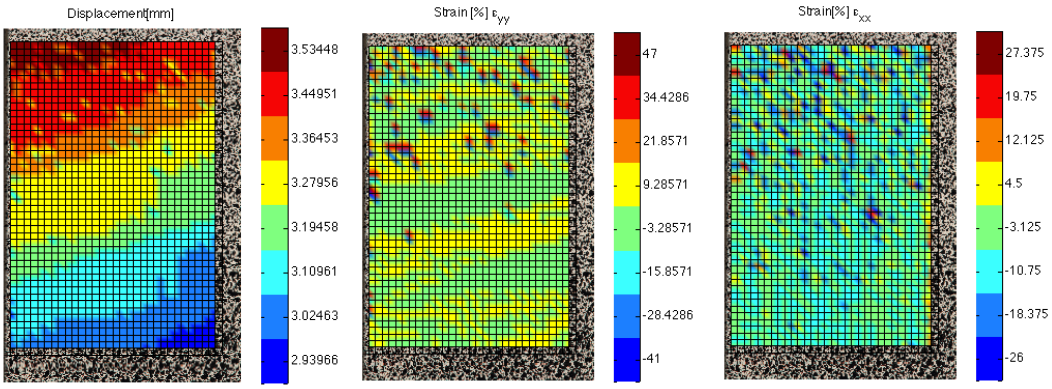

Figure 4-33. Maps of displacement and strain in y and x directions for the A1 specimen

4.2.6.3 A4 Specimen

The A4 fragile material images have a resolution of 82.6 pixels/mm. In Figure 4-34 the displacement and the strain per block is shown. The strain map shows larger values in the middle where the specimen broke.

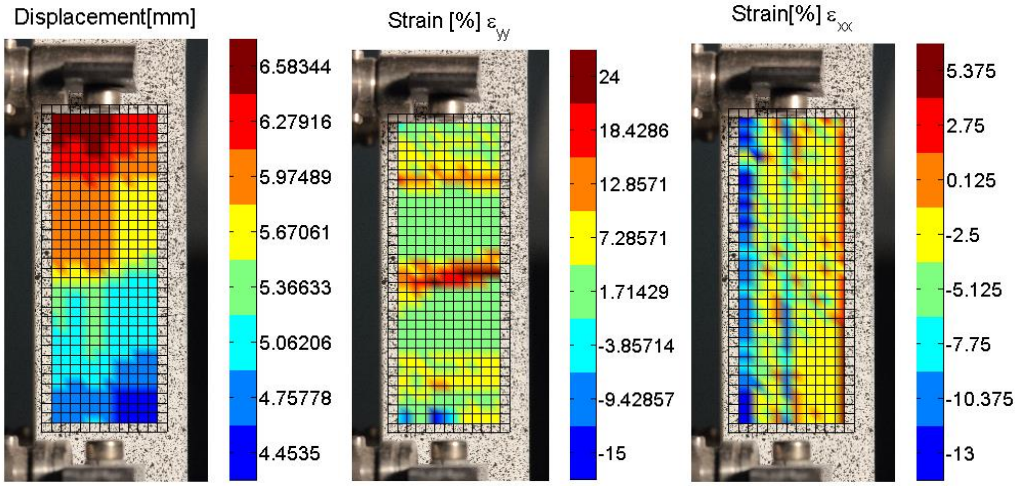

Figure 4-34. Maps of displacement and strain in y and x directions for A4 specimen

Figure 4-35 shows the graphs of strength versus displacement and stress versus strain for the A4 specimen obtained with the RP-PSO and ARPS algorithms using blocks of 100×100 pixels. It is also possible to see the displacement and the strain obtained by the transducer (the black line) referred

as Sensor and *e_Sensor*. Both algorithms behave identically with the calculated displacement slightly higher than the transducer.

The strain for the A4 specimen was calculated from the central zone to the outside with different lengths as illustrated in Figure 4-36. Line L1 only uses information from the 300 central pixels. Lines L2 and L3 use information from the 1100 and 2100 central pixels respectively. Line L4 uses a total of 42 mm, almost the same sample as was analysed by the transducer (40 mm). Line L5 represents the transducer data. L4 and L5 have identical behaviour to Figure 4-35.

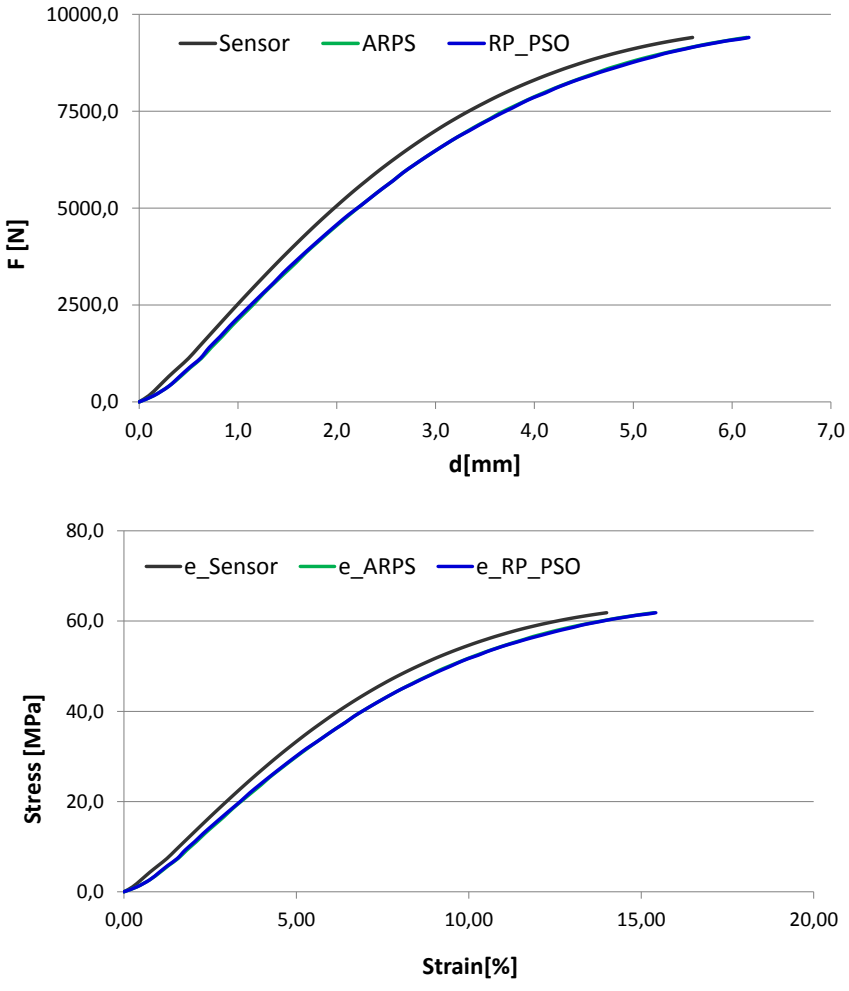

Figure 4-35. Graphs of strength versus displacement (at top) and stress versus strain (at bottom), with blocks of 100×100 pixels, for the A4 specimen

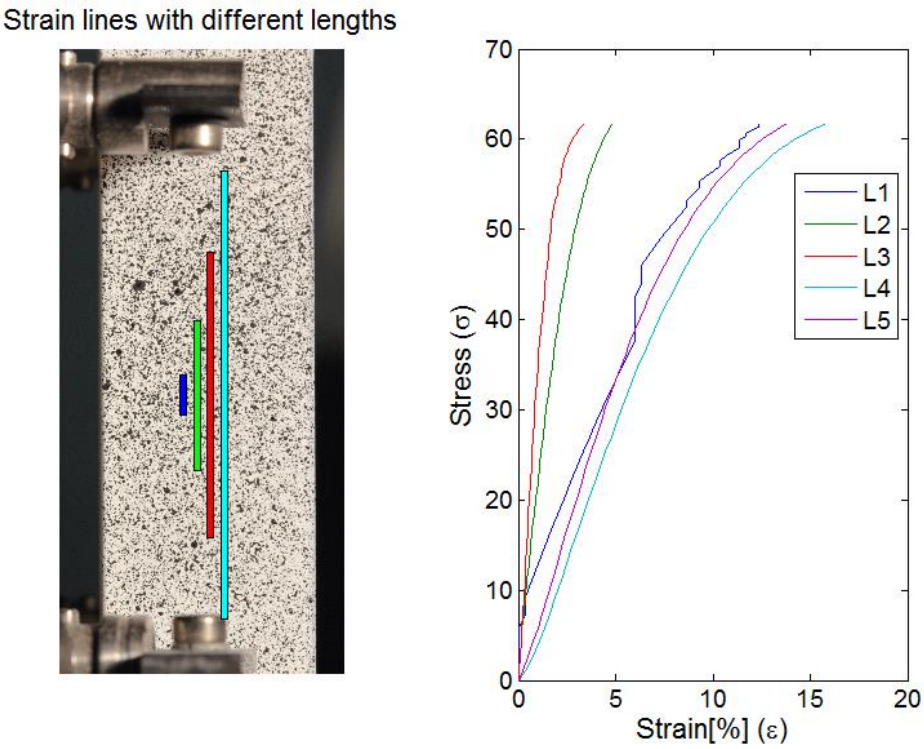

Figure 4-36. Several distributed strain lines with different lengths for the A4 specimen

The strain map at different load stages shows where the biggest strain starts to emerge throughout the sample corresponding to the break zone, showing an advantage in the stress versus strain graph.

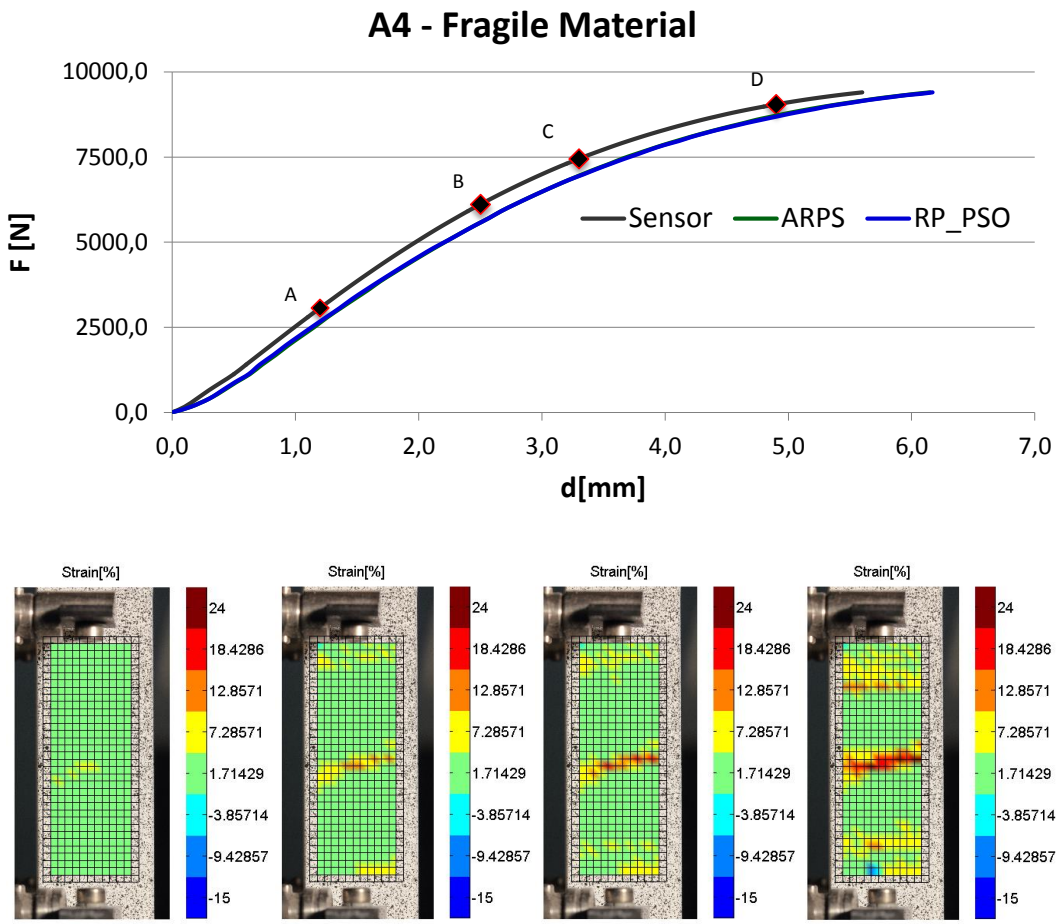

Figure 4-37. A4 evolution of the displacement map and tensile strain component as the charge increases to 9000N.The strain maps of points A to D are shown

In Figure 4-37 it is possible to see the strain map at five different points for the A4 specimen. Point A has 3067 N with 1.20 mm of elongation, point B has 6109 N with 2.50 mm of elongation, point C has 7450 N with 3.30 mm of elongation and point D has 9046 N with 4.90 mm of elongation.

4.2.6.4 B2 Specimen

For the B2 specimen the resolution was 85 pixels/mm. With this ductile material the images were obtained twice and the test speed was higher than the previous one. Figure 4-38 shows the results with 100 pixels per block. The displacement map on the left shows the displacements throughout the specimen.

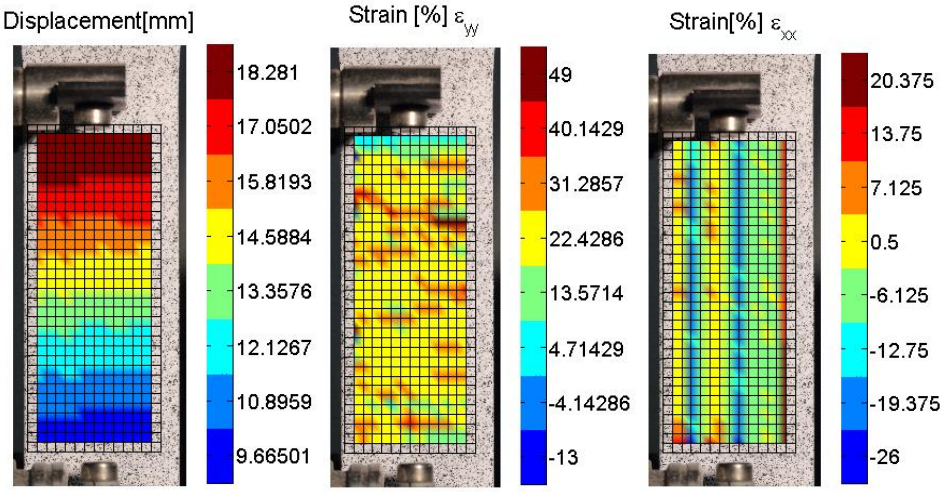

Figure 4-38. Maps of displacement and strain, in y and x directions for the B2 specimen

Figure 4-39 shows the graphs of strength versus displacement and stress versus strain for the B2 specimen, using 100×100 pixels/block. In these graphs it is clear that up to 300 N, the transducer's behaviour is different from the algorithms. In the next section this problem is discussed. For this material the calculated displacement is slightly lower than the transducer.

The strain was calculated over the specimen from the central zone to the outside with different lengths as illustrated in Figure 4-40 for the B2 specimen. Line L1 only uses information from the 300 central pixels. Lines 2 and 3 use information for the 1100 and 2100 central pixels respectively. Line L4 uses a total of 41 mm. Line L5 represents the transducer displacement considering the 40 mm sample length.

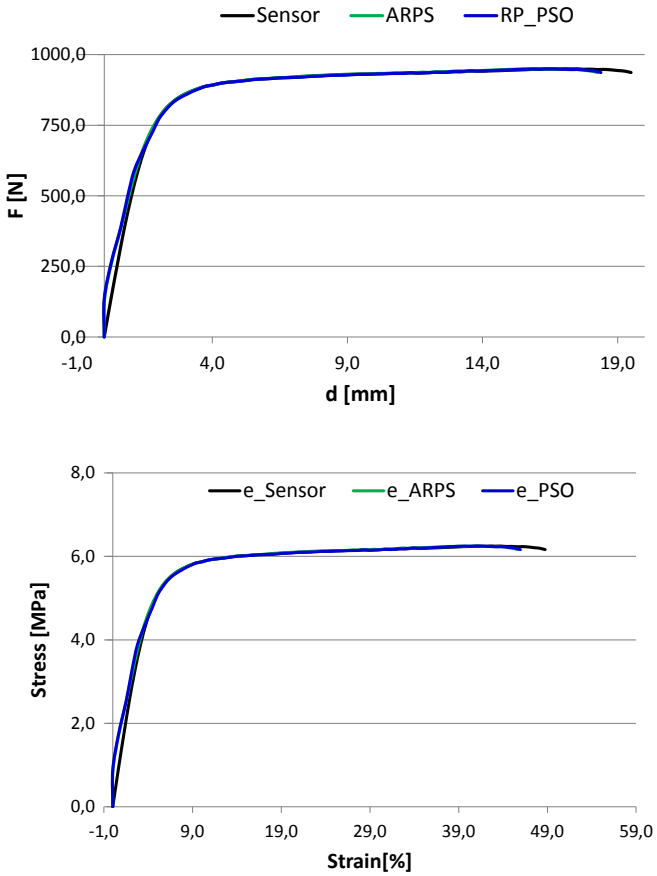

Figure 4-39. Graphs of strength versus displacement and stress versus strain, with 100×100 pixels/block, for the B2 specimen

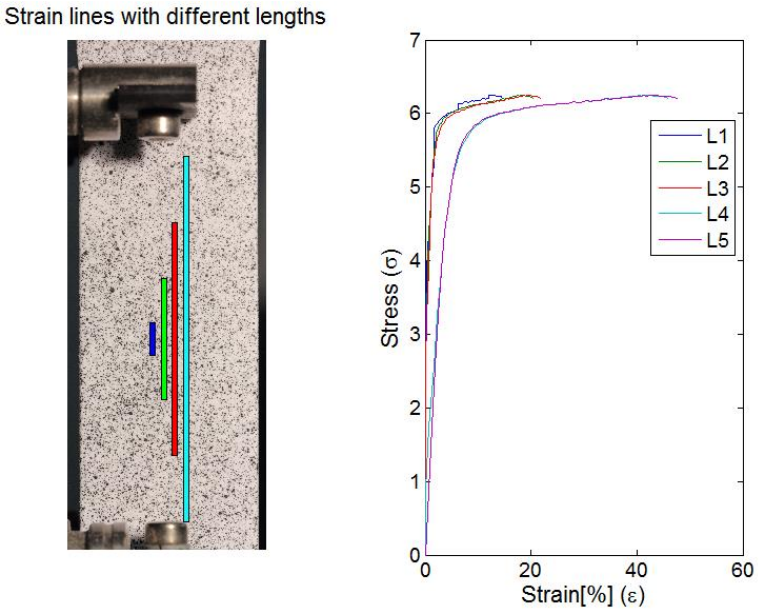

Figure 4-40. Several strain lines with different lengths for B2 specimen

The strain map at different load stages is shown in Figure 4-41. Point A has 919 N with 7.0 mm of elongation, point B has 932 N with 10.25 mm of elongation, point C has 942 N with 14.50 mm of elongation and point D has 943 N with 18.75 mm.

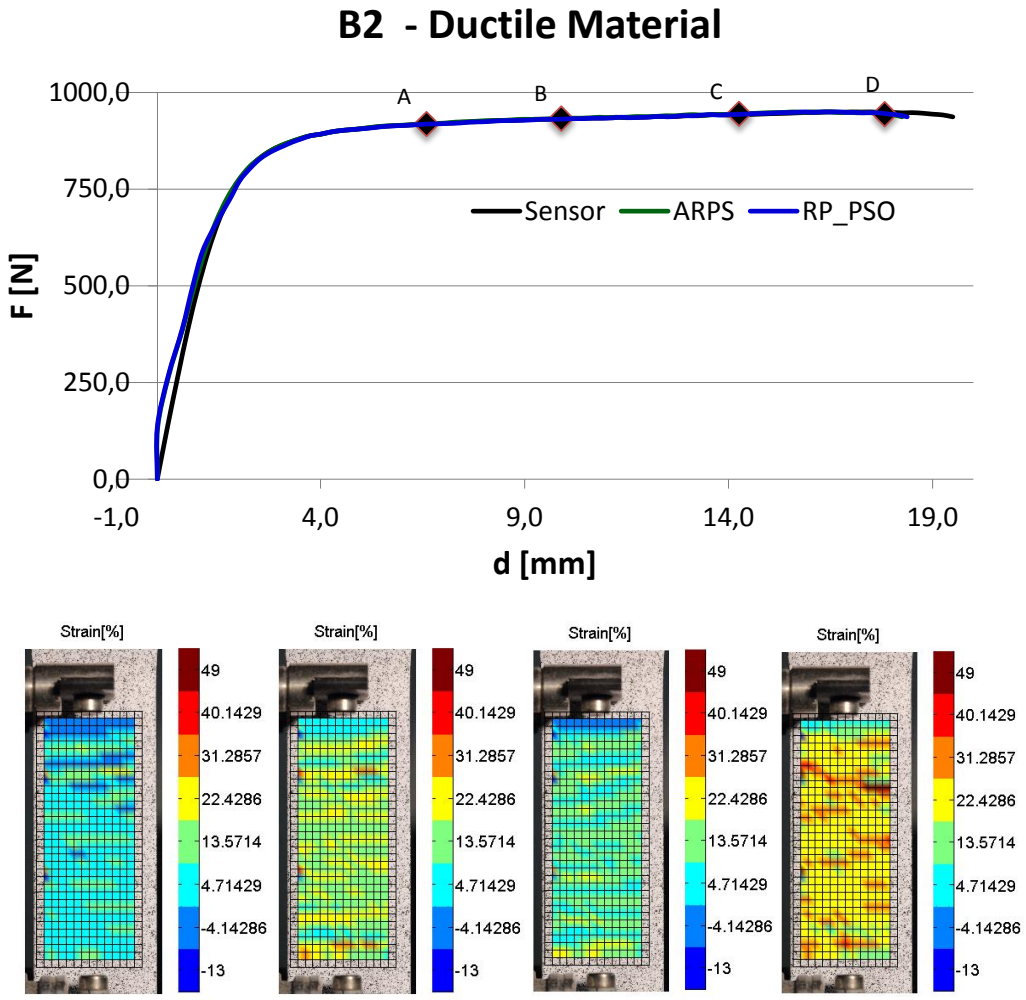

Figure 4-41. B2 evolution of the displacement map and tensile strain component as the charge increases to 943N. The strain maps of points A to D are shown

4.2.6.5 Transducer versus image processing results

In order to validate the results an image Golden Standard (GS) was obtained by manually classifying each image-time series. Figure 4-42 shows the data from the two algorithms, the transducer and the GS data for the two specimens, A4 (top) and B2 (bottom). For the B2 material only the elastic zone graph is shown in order to see the differences between the algorithms.

The GS reference is much closer to the results obtained by the ARPS and the RP-PSO algorithms than to the physical sensor. The transducer error to the GS reference is 12.1% for A4 and 12.4% for B2, which revealed an expected error.

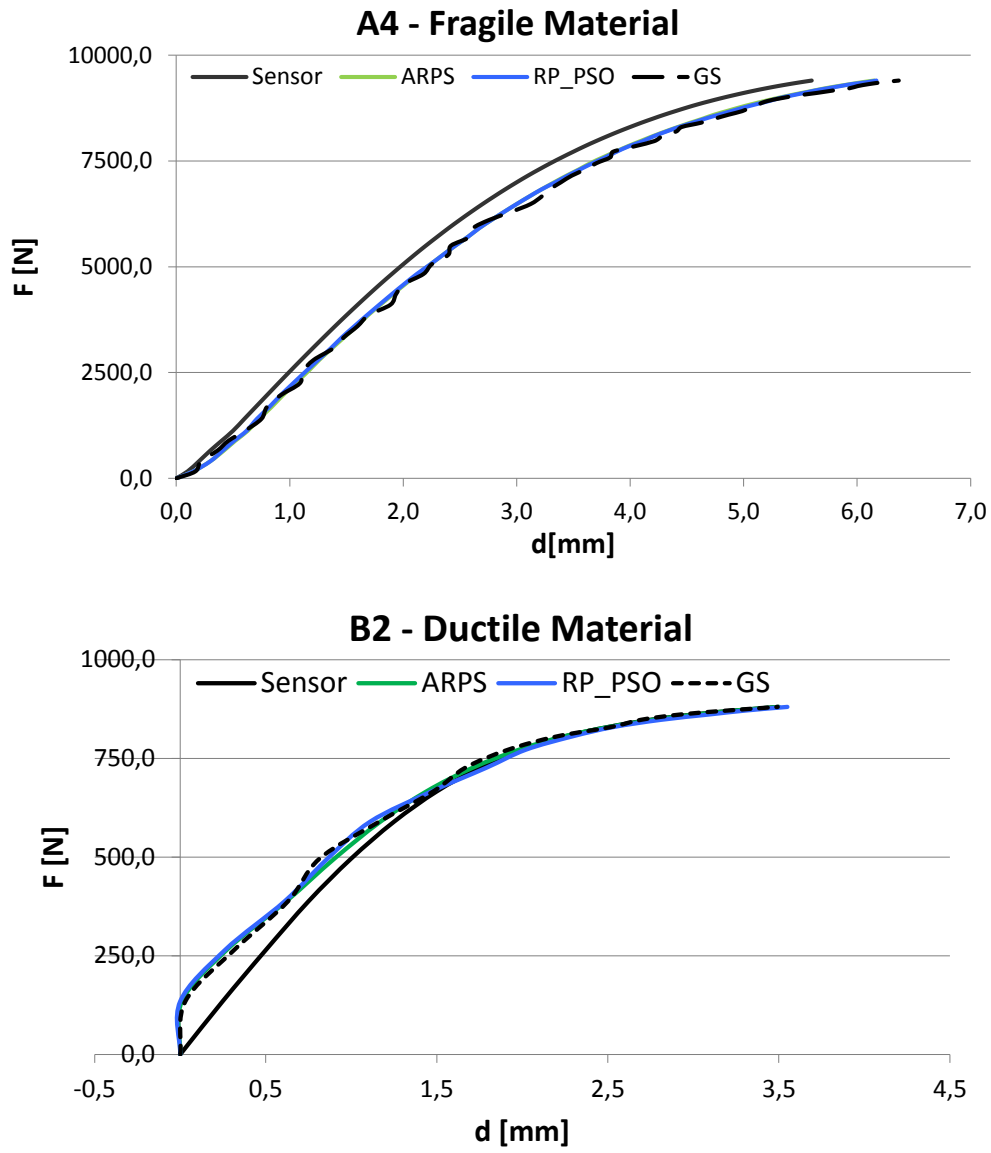

Figure 4-42. Transducer reference versus Image reference for both specimens A4 and B2

The graph in Figure 4-43 shows the difference between using the transducer and the image Golden Standard (GS) data as reference. The black dots are the transducer error when using the GS as the reference value. The fill

marker represents the value shown in Figure 4-32 and the no fill marker is the average error using the GS as reference. The average error using the Gold Standard as reference presents similar errors in both materials. The best result occurs with 100×100 pixels/block.

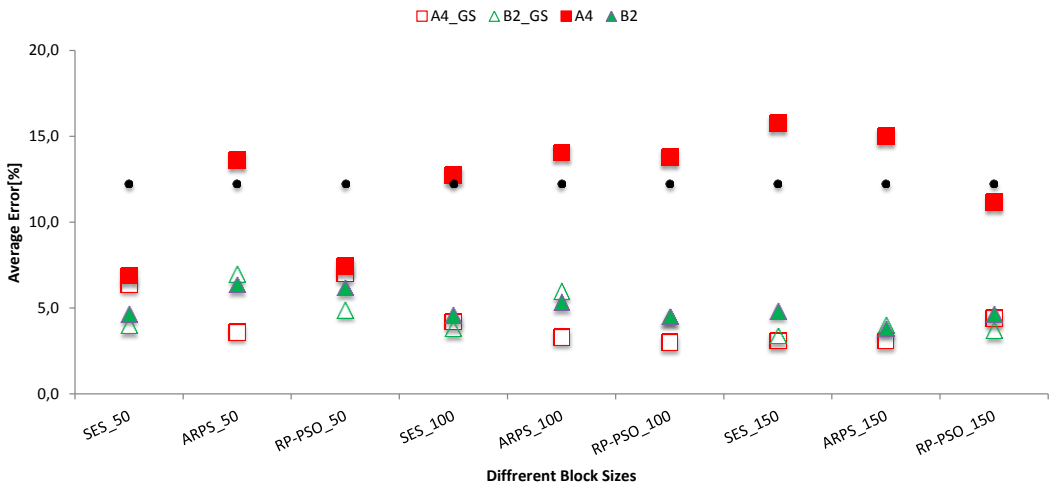

Figure 4-43. Average error for the specimens A4 and B2 using the sensor (fill marker) or the golden standard (no fill marker) as reference value

4.2.7 Pull-Off Tests

Fibre Reinforced Polymer (FRP) materials are used in reinforced concrete and steel structures. The FRP material used in our tests was produced in bar shapes and glued onto the material under test. The structural behaviour between the materials (concrete or steel) and the reinforced bar is the concern in pull-off tests. Analysis of these phenomena with traditional transducers is nowadays beyond the university laboratorie's budget. Using image processing analysis the number of points analysed is no longer an issue. Two LVDT sensors were used to measure the global displacement achieved. Figure 4-44 shows an initial schematic that helps to understand this new test and the best camera position. As this test produced a small displacement it is important to have the best photo resolution. At right a real test image is shown from a CFRP pull-off test on steel. The test was monitored with 2 LVDTs and 4 transducers. The time spent in mounting the sensor acquisition system was considerable.

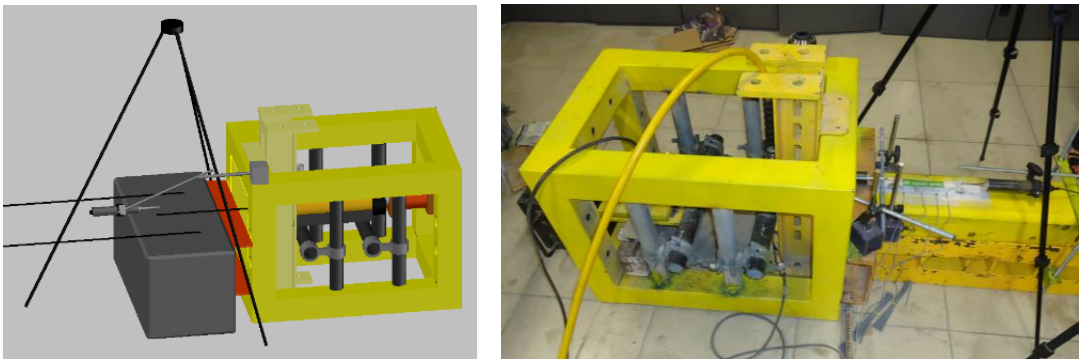

Figure 4-44. A schematic figure of the test equipment and camera position (left) and the real image test (right)

A random pattern was applied to the region of interest. Figure 4-45 shows two examples of this pattern.

Figure 4-45. Pattern applied in CRFP pull-off tests (left: CFRP on steel; right: CFRP on concrete)

In Figure 4-46 and Figure 4-47 the displacement maps are shown. The first is from a CFRP glued on steel and the second on concrete. Axis *X* and *Y* are the CFRP bar dimensions and axis *Z* is the displacement calculated by digital image processing.

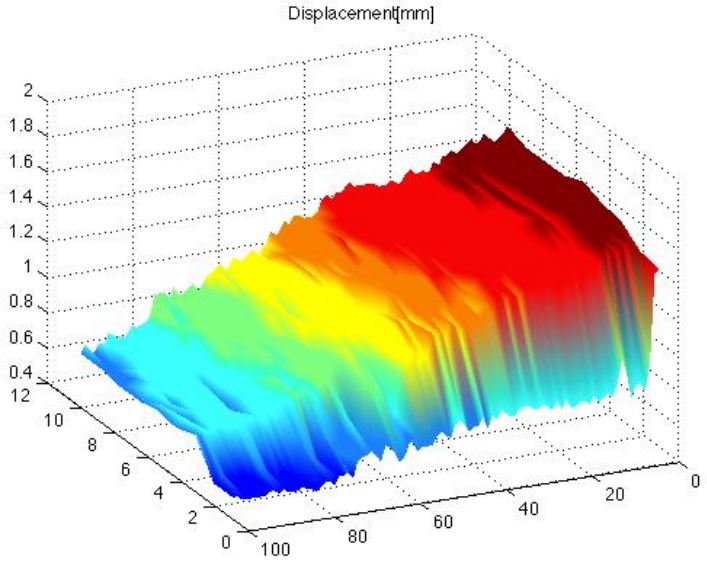

Figure 4-46. Displacement map of steel Pull-Off test

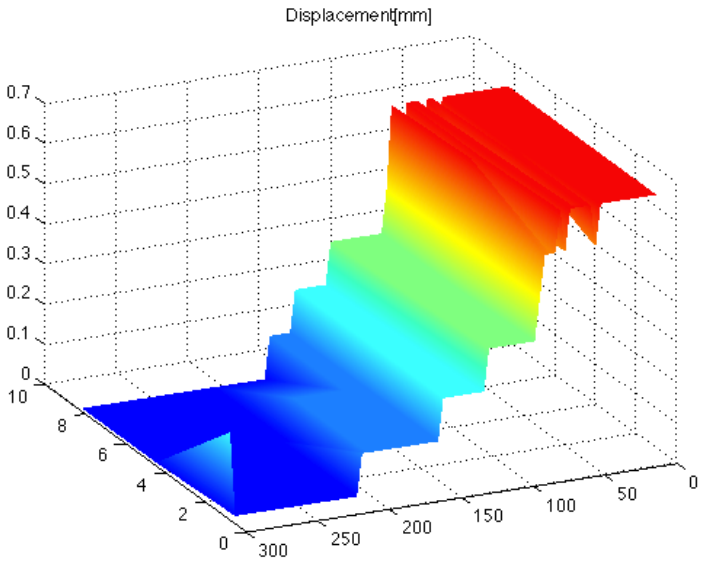

Figure 4-47. Displacement map of concrete Pull-Off test

In some tests no displacement was detected in the central map displacement area while in the surrounding areas it was (Figure 4-48 – left). Another situation that occurs was the observation of a large displacement at the end of the region (Figure 4-48 – right).

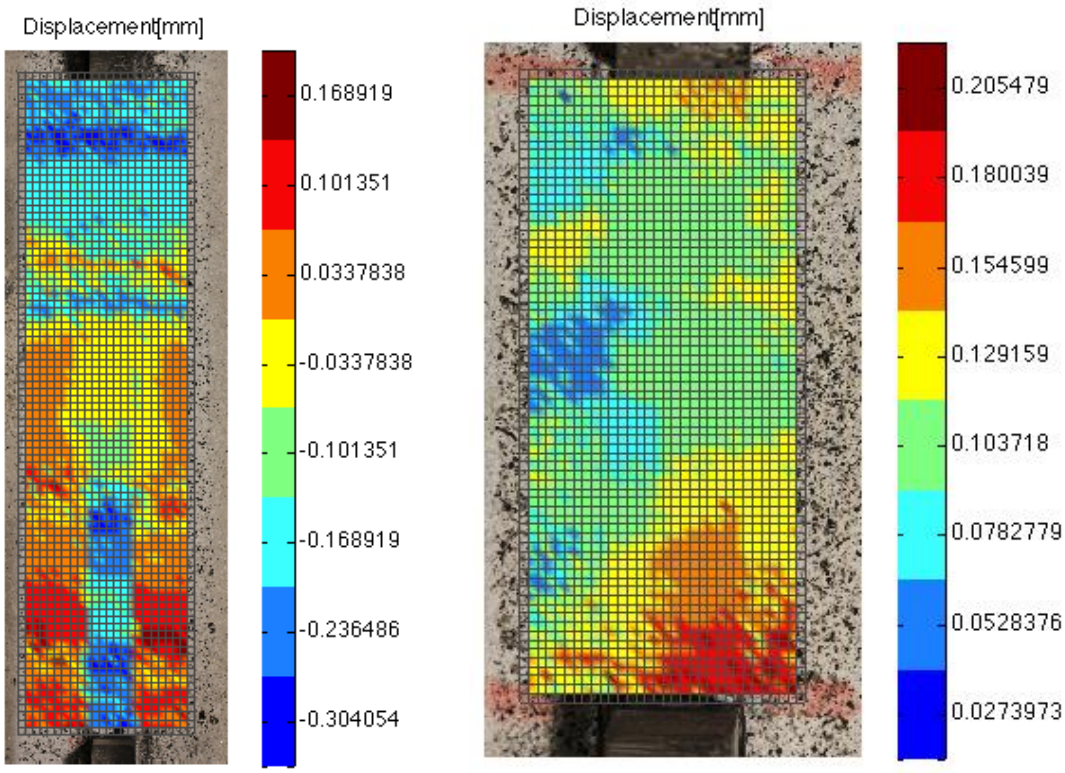

Figure 4-48. Anomalous situation: at left CFP on concrete and at right CRP on steel

4.3 Digital Image Measurements (DIM) Software

The DIM software is an easy platform that allows computation of the results from four of the tests (A4, B2, V5 and V6), each of them with four complete random patterns as can be seen in Figure 4-49. It computes the displacement field based on block matching algorithms. Three different algorithms can be used: the Simple and Efficient Algorithm, the Adaptive Rood Pattern Search and the Rood Pattern - Particle Swarm Optimization.

The general idea for the DIM software was to collect all the isolated program files onto a platform capable of being used for people without particular knowledge of image processing analysis. The user only needs to select the test, the algorithm and the particular parameters and then calculate the data that is needed.

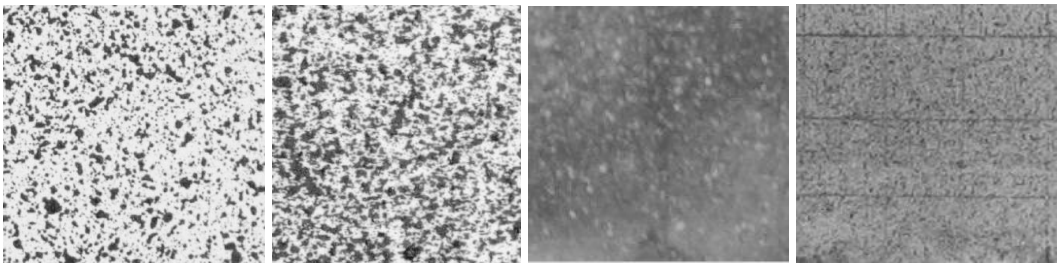

Figure 4-49. Details of the imposed random pattern for the A4, B2, V5 and V6 specimens analysed in the DIM software

The software can use previously processed information or the user can choose some of the parameters: the pixels per block, the algorithm and the region of interest.

Figure 4-50 shows the DIM initial screen where it is possible to choose the test and the number of pixels per block.

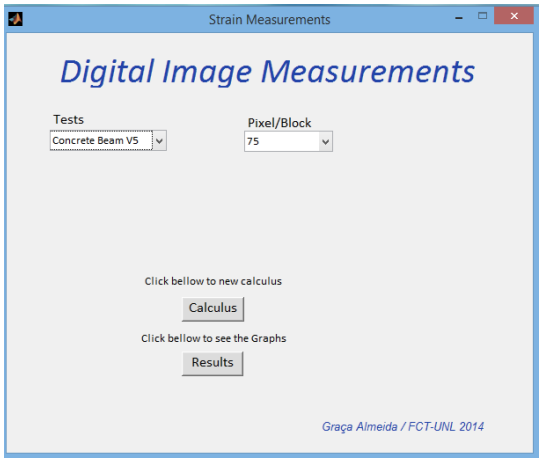

Figure 4-50. DIM front page

After choosing the test and the number of pixels per block the user can calculate the algorithms for a particular ROI (region of interest) choosing the two extreme points of a rectangle or by going directly to the results. In this situation the previous data is used (see Figure 4-51).

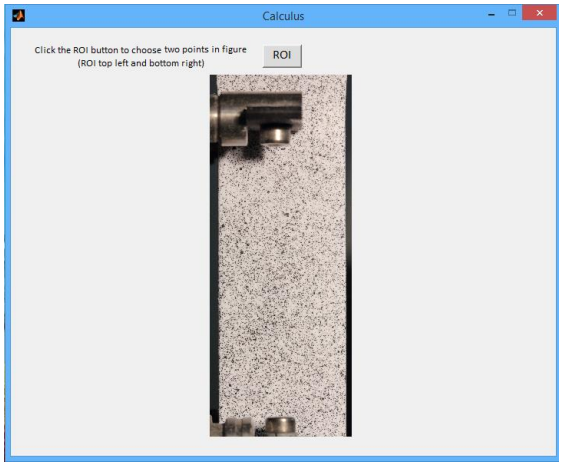

Figure 4-51. The screen for choosing the new region of interest

The result screen allows the user to choose one of the three algorithms as the graph to show (d×t, F×d, motion vectors, displacement map, strain map and strain lines). Some examples of these graphs are in Figure 4-52.

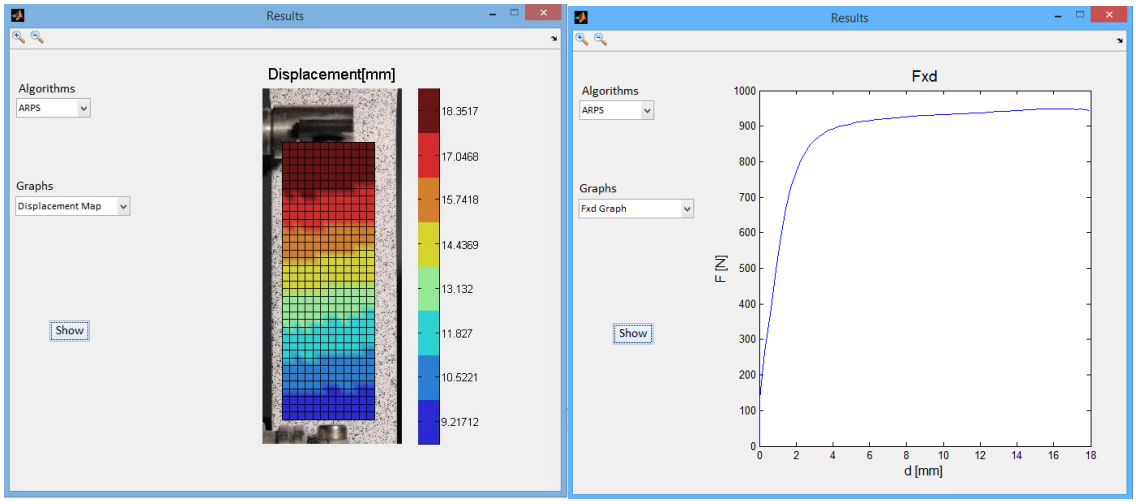

Figure 4-52. Some examples of the graphs of DIM software

The benefit of this software is for students who need to visualize some information that is not presented by the physical sensors, or to analyse a particular small region in more detail.

Chapter 5

Conclusions and Future Work

This section presents a summary of the main issues addressed in this thesis, the contributions of the research developed and the proposals for future work.

5 Conclusions and Future Work

5.1 Thesis Summary

The motivation of this thesis arose from the need to create an alternative method for the calculation of displacements in Civil Engineering load tests. Several tests are done recurrently in Civil Engineering Material Laboratories. However, the time and effort spent in placing all the sensors in the right places, along with the acquisition system, is enormous.

This thesis presents a methodology for Civil Engineering measurements and analysis using image processing techniques. The use of photogrammetry has several advantages over traditional methods: a precise and complete result is rapidly obtained with much lower investment and calibration needs. It is therefore a technique with a good cost/benefit and with an unlimited number of data acquisition points.

Measurements by LVDT sensors on specific target points are point-wise and do not allow obtaining of a complete map of the displacements. Several situations arise when using LVDTs: 1) restriction on the number of devices; 2) restriction of space and difficulties in positioning them; 3) restriction of limits (large displacements). Further, target point measurements cannot calculate the displacements that occur between two closed targets.

In this thesis more than 50 real tests were conducted in collaboration with researchers from the materials laboratory of the Faculdade de Ciências e Tecnologia using a variety of conditions: virtual displacements, video sequence analysis, concrete beams, specimens of Plexiglas, wood and PVC. Images were achieved using a Cannon EOS 400D digital camera with a resolution of 3888×2592 and two 500W spotlights for structured lighting. The specimens were initially prepared with an underlying cover of matt white ink and a superimposed random speckle pattern manually applied using matt black ink.

The proposed approach for displacement calculation was based on block motion algorithms. Besides the already known algorithms, SES and ARPS, two

new algorithms were created: RP-PSO and PSCH. The RP-PSO algorithm uses the ARPS concept for placement of the initial particles and then the rules of the PSO algorithm are applied. The PSCH algorithm uses the pattern histogram as their main feature.

This thesis is a multi-disciplinary collaboration with Civil Engineers. This was extremely important to understand their difficulties and all the issues related to laboratory tests of different materials.

5.2 Conclusions

From the results presented in the previous chapters it is possible to conclude that the objectives of developing a system for displacement measurements were achieved. The various tests prove the benefits of this technique compared to the traditional method. For example, in pull-off tests it is a major advantage to use image processing analysis because of the detailed information that it is possible to acquire. The use of block motion algorithms has proven to be fast and accurate. Despite the fact that commercial software already exists on the market it is very expensive. The efficiency of the algorithms is dependent on several factors such as the speckle pattern, the block size, the search parameters, the image resolution and the interval between images. However, as was shown in this study, it is not difficult to find a good compromise between these values that allows for good results. Larger resolutions produce better results but there is always a compromise between the size of the region of interest and the maximum displacement that can occur in the test.

The ARPS and the RP-PSO algorithms are approximately twice as fast as the SES algorithm. However, the increase in time of the SES algorithm does not correspond to an improvement in accuracy.

With the RP-PSO algorithm, despite having a higher number of computations than the ARPS, the increase in time is negligible. Both algorithms are equivalent in accuracy. RP-PSO in some tests shows a more detailed displacement map.

One of the major problems related to strain measurements with spatial resolution is result validation because the strains caused by the test machine are global and not local. Therefore, only a few points can be compared with the spatial distribution obtained by image processing analysis. To validate the algorithms, the average deviation error was used with the transducer and the Golden Standard data. The comparison between the measurements from the transducers and the measurements from the image processing techniques revealed some minor differences. A deviation of about 12% was obtained in the worst case. However, when the data from the algorithms was compared with the Golden Standard, the average error was in the order of 4%. The comparison of the image processing algorithms with the Golden Standard is relevant since the transducer data also has considerable error.

It should also be mentioned that this work was disseminated in several oral presentations, has been published in four articles in International Conferences and two journal articles that are currently in the review process.

5.3 Future Work

There are a few areas that need further investigation. Some of these methods may be a compromise between improvements versus longer processing time:

- using methods of lighting compensation;
- detecting motion using the block matching algorithms already presented combined with other image processing techniques like optical flow, template matching and iterative optimization;
- using a method for combining features: pixel intensity, histogram, pattern and others;
- development of a software program able to calculate the displacements in real time allowing the grip mounted LVDT sensors to be removed before they can be damaged.

Bibliography

Acharya, Tinku, and Ajoy K Ray. 2005. *Image Processing: Principles and Applications*. Wiley. http://books.google.pt/books?id=oChm86mSnDIC.

Albert, Jörg, Hans-Gerd Maas, Andreas Schade, and Willfried Schwarz. 2002. "Pilot Studies on Photogrammetric Bridge Deformation Measurement Test Facility at Bauhaus University." In *Proceedings 2nd IAG Symposium on Geodesy for Geotechnical and Structural Engineering*, 133–140. Berlin, Germany.

Almeida, G, F Melicio, and J Fonseca. 2012. "Block Matching Algorithms for Load Test Evaluation." In *Proceedings of the Eighth International Conference on Engineering Computational Technology*, edited by B H V Topping. Dubrovnik, Croatia: Civil-Comp Press, Stirlingshire, UK. doi:10.4203/ccp.100.57.

Almeida, G., H. Biscaia, C. Chastre, J. Fonseca, and F. Melicio. 2010. "Displacement Estimation of a RC Beam Test Based on TSS Algorithm." In *Information Systems and Technologies (CISTI), 2010 5th Iberian Conference on*. Santiago de Compostela. http://ieeexplore.ieee.org/xpls/abs_all.jsp?arnumber=5556688.

Almeida, Graça, Fernando Melicio, Carlos Chastre, and José Fonseca. 2011. "Displacement Measurements with ARPS in T-Beams Load Tests." In *IFIP Advances in Information and Communication Technology*, edited by LuisM Camarinha-Matos, 349 AICT:286–293. Springer Berlin Heidelberg. doi:10.1007/978-3-642-19170-1_31. http://dx.doi.org/10.1007/978-3-642-19170-1_31.

Almeida, Graça, Fernando Melicio, and José Fonseca. 2011. "Displacement Measurements with Block Motion Algorithms." In *VIPIMAGE, III ECCOMAS Thematic Conference on Computacional Vision and Medical Processing*. Olhão, Portugal.

Al-Mualla, Mohammed Ebrahim, C. Nishan Canagarajah, and David R. Bull. 2007. *Video Coding for Mobile Communications*. Elsevier Science. http://www.igi-pub.com/reference/details.asp?ID=6974&v=tableOfContents.

Astm. 2014. "ASTM International." http://www.astm.org/SNEWS/SPANISH/SPJF09/nelson_spjf09.html.

Asundi Ananda. 2002. *Matlab for Photometrics A Primer*. Elsevier Science. http://books.google.pt/books?id=COh_Ffy4n-UC&pg=PA39&dq=photoelasticity&hl=pt-PT&sa=X&ei=Dp_eUr2NPMmO7Qa4iIDwCQ&redir_esc=y#v=onepage&q=photoelasticity&f=false.

Bakwad, K.M., S.S. Pattnaik, B.S. Sohi, S. Devi, S. Gollapudi, C.V. Sagar, and P.K. Patra. 2008. "Small Population Based Modified Parallel Particle Swarm Optimization for Motion Estimation." In *2008 16th International Conference on Advanced Computing and Communications*, edited by IEEE, 367–373. Chennai. doi:10.1109/ADCOM.2008.4760475.

Barjatya, Aroh. 2004. "Block Matching Algorithms For Motion Estimation." *IEEE Transactions Evolution Computation*. DIP 6620 Spring 2004 Final Project Paper.

Barranger, Y., P. Doumalin, J. C. Dupré, and a. Germaneau. 2012. “Strain Measurement by Digital Image Correlation: Influence of Two Types of Speckle Patterns Made from Rigid or Deformable Marks.” *Strain* 48 (5): 357–365. doi:10.1111/j.1475-1305.2011.00831.x.

Barranger, Y., P. Doumalin, J.C. Dupré, and a. Germaneau. 2010. “Digital Image Correlation Accuracy: Influence of Kind of Speckle and Recording Setup.” In *EPJ Web of Conferences*, 6:31002. EPJ Web of Conferences. doi:10.1051/epjconf/20100631002.

Bhaskaran, Vasudev, and Konstantinos Konstantinides. 1997. *Image and Video Compression Standards: Algorithms and Architectures*. 2nd ed. Norwell, MA, USA: Kluwer Academic Publishers. http://books.google.co.uk/books?id=dzOV8-sZE9cC.

Biscaia, Hugo C., Carlos Chastre, and Manuel a G Silva. 2013. “A Smeared Crack Analysis of Reinforced Concrete T-Beams Strengthened with GFRP Composites.” *Engineering Structures* 56: 1346–1361. doi:10.1016/j.engstruct.2013.07.010. http://linkinghub.elsevier.com/retrieve/pii/S0141029613003349.

Bornert, M., F. Brémand, P. Doumalin, J. C. Dupré, M. Fazzini, M. Grédiac, F. Hild, et al. 2009. “Assessment of Digital Image Correlation Measurement Errors: Methodology and Results.” *Experimental Mechanics* 49 (3): 353–370. doi:10.1007/s11340-008-9204-7.

Carolin, A, T Olofsson, and B Taljsten. 2004. “Photographic Strain Monitoring for Civil Engineering.” *FRP Composites in Civil Engineering - CICE 2004, Seracino*. doi:10.1201/9780203970850.ch66.

Carvalho, T, C Chastre, H Biscaia, and R Paula. 2010. “Flexural Behaviour Ff RC T-Beams Strengthened With Different FRP Materials.” In *3rd Fib International Congress*. Washington, D.C.

Chastre, Carlos, and Manuel a G Silva. 2010. “Monotonic Axial Behavior and Modelling of RC Circular Columns Confined with CFRP.” *Engineering Structures* 32 (8): 2268–2277. doi:10.1016/j.engstruct.2010.04.001. http://linkinghub.elsevier.com/retrieve/pii/S0141029610001240.

Choi, Sokhwan, and Surendra P. Shah. 1998. *Fracture Mechanism in Cement-Based Materials Subjected to Compression*. *Journal of Engineering Mechanics*. Vol. 124. Reston, VA, ETATS-UNIS: American Society of Civil Engineers. doi:10.1061/(ASCE)0733-9399(1998)124:1(94).

Chu, T. C., W. F. Ranson, and M. a. Sutton. 1985. “Applications of Digital-Image-Correlation Techniques to Experimental Mechanics.” *Experimental Mechanics* 25 (3): 232–244. doi:10.1007/BF02325092.

Cintrón, Rommel, and Victor Saouma. 2008. “Strain Measurements with the Digital Image Correlation System Vic-2D.” *System*. NEES at CU Boulder. http://nees.org/site/resources/pdfs/cintron_final_paper.pdf.

Czaderski, Christoph, and Masoud Motavalli. 2010. “Full-Field Displacements Of CFRP To Concrete Pull-Off Bond Tests.” *Proceedings of the 3rd Fib International Congress – 2010*. Washington, D.C.

Dai, Jian Guo, Tamon Ueda, Yasuhiko Sato, and Kohei Nagai. 2012. “Modeling of Tension Stiffening Behavior in FRP-Strengthened RC Members Based on Rigid Body Spring Networks.” *Computer-Aided Civil and Infrastructure Engineering* 27 (6): 406–418. doi:10.1111/j.1467-8667.2011.00741.x. http://doi.wiley.com/10.1111/j.1467-8667.2011.00741.x.

Gom. 1990. “GOM Optical Measuring Tecniques.” http://www.gom.com/3d-software/aramis-software.html.

Gonzalez, Rafael C., and Richard E. Woods. 2007. *Digital Image Processing*. Pearson/Prentice Hall. doi:10.1049/ep.1978.0474. http://books.google.pt/books?id=8uGOnjRGEzoC.

Hampel, H, and Hans-Gerd Maas. 2009. "Cascade Image Analysis for Dynamic Crack Detection in Material Testing." *ISPRS Journal of Photogrammetry and Remote Sensing,* 64: 345–350. doi:0.1016/j.isprsjprs.2008.12.006. ISPRS\nJournal\nof\nPhotogrammetry\nand\nRemote\nSensing.

Hampel, Uwe, and Hg Maas. 2003. "Application of Digital Photogrammetry for Measuring Deformation and Cracks During Load Tests in Civil Engineering Material Testing." *Optical 3-D Measurement Techniques VI* Volume II: 80–88. doi:0099-1112/06/7201–0000. http://www.dresden-uni.com/die_tu_dresden/fakultaeten/fakultaet_forst_geo_und_hydrowissenschaften/fachrichtung_geowissenschaften/ipf/photogrammetrie/publikationen/pubdocs/2003/2003_Hampel_Maas_Opt3D2003.pdf.

Huang, Jianping, Wanyu Liu, and Xiaoming Sun. 2014. "A Pavement Crack Detection Method Combining 2D with 3D Information Based on Dempster-Shafer Theory." *Computer-Aided Civil and Infrastructure Engineering* 29 (4) (April 26): 299–313. doi:10.1111/mice.12041. http://doi.wiley.com/10.1111/mice.12041.

Hussain, Z. 1991. *Digital Image Processing: Practical Applications of Parallel Processing Techniques*. Ellis Horwood Series in Digital and Signal Processing. Ellis Horwood Limited.

Iyer, Shivprakash, and Sunil K. Sinha. 2006. "Segmentation of Pipe Images for Crack Detection in Buried Sewers." *Computer-Aided Civil and Infrastructure Engineering* 21 (6): 395–410. doi:10.1111/j.1467-8667.2006.00445.x.

Jerabek, M., Z. Major, and R. W. Lang. 2010. "Strain Determination of Polymeric Materials Using Digital Image Correlation." *Polymer Testing* 29 (3): 407–416. doi:10.1016/j.polymertesting.2010.01.005. http://www.sciencedirect.com/science/article/pii/S0142941810000097.

Jianguo, Jiang Jianguo Jiang, Li Xiaolin Li Xiaolin, and Li Min Li Min. 2010. "Research of Image Matching Algorithm Based on Hybrid Particle Swarm Optimization." *Information Technology and Applications (IFITA), 2010 International Forum on* 2: 81–84. doi:10.1109/IFITA.2010.155. http://ieeexplore.ieee.org/lpdocs/epic03/wrapper.htm?arnumber=5634913.

Jin, Tailie, Nam Seo Goo, Sung-Choong Woo, and Hoon Cheol Park. 2009. "Use of a Digital Image Correlation Technique for Measuring the Material Properties of Beetle Wing." *Journal of Bionic Engineering* 6 (3): 224–231. doi:10.1016/S1672-6529(08)60105-5. http://www.sciencedirect.com/science/article/B82XN-4XGBD95-4/2/301dae7001bbc9d3cd593c44b2c40686.

Kennedy, J., and R. Eberhart. 1995. "Particle Swarm Optimization." In *Proceedings of ICNN'95 - International Conference on Neural Networks*, edited by IEEE, 4:1942–1948. Perth, WA, Australia. doi:10.1109/ICNN.1995.488968.

Kennedy, James, and Rui Mendes. 2002. "Population Structure and Particle Swarm Performance." In *Proceedings of the 2002 Congress on Evolutionary Computation, CEC 2002*, edited by IEEE, 2:1671–1676. Honolulu, HI: Evolutionary Computation, 2002. CEC '02. Proceedings of the 2002 Congress on (Volume:2). doi:10.1109/CEC.2002.1004493. Proceedings.

Koljonen, Janne, Olli Kanniainen, and Jarmo T. Alander. 2007. "An Implicit Validation Approach for Digital Image Correlation Based Strain Measurements." *EUROCON 2007 - The International Conference on Computer as a Tool*. Warsaw. doi:10.1109/EURCON.2007.4400299. http://ieeexplore.ieee.org/stamp/stamp.jsp?tp=&arnumber=4400299&isnumber=4400218.

Kurtz, Stephen, Perumalsamy Balaguru, and Jeffrey Helm. 2008. “Experimental Study of Interfacial Shear Stresses in FRP-Strengthened RC Beams.” *Journal of Composites for Construction* 12 (3): 312–322. doi:10.1061/(ASCE)1090-0268(2008)12:3(312).

Lall, P., D. Panchagade, D. Iyengar, S. Shantaram, J. Suhling, and H. Schrier. 2007. “High Speed Digital Image Correlation for Transient-Shock Reliability of Electronics.” In *2007 Proceedings 57th Electronic Components and Technology Conference*, 924–939. Reno, NV. doi:10.1109/ECTC.2007.373908.

Lecompte, D, H Sol, J Vantomme, and a Habraken. 2006. “Analysis of Speckle Patterns for Deformation Measurements by Digital Image Correlation.” In *Spie*, SPIE Proce, Vol. 6341:E1–E6. Proceedings of SPIE. doi:10.1117/12.695276.

Lee, W. T., Y. J. Chiou, and M. H. Shih. 2010. “Reinforced Concrete Beam-Column Joint Strengthened with Carbon Fiber Reinforced Polymer.” *Composite Structures* 92 (1): 48–60. doi:10.1016/j.compstruct.2009.06.011. http://www.sciencedirect.com/science/article/B6TWP-4WNXV2H-1/2/77ef12e92ec55ee23dcfdde505dcd86a.

Liu, Xiaoxiang Liu Xiaoxiang, Weigang Jiang Weigang Jiang, Jianwen Xie Jianwen Xie, and Yitian Jia Yitian Jia. 2009. “An Image Template Matching Method Using Particle Swarm Optimization.” In *Computational Intelligence and Industrial Applications, 2009. PACIIA 2009. Asia-Pacific Conference on*, 1:83–86. doi:10.1109/PACIIA.2009.5406370.

Lu, Jianhua, and Ming .L. Liou. 1997. “A Simple and Efficient Search Algorithm for Block-Matching Motion Estimation.” *IEEE Transactions on Circuits and Systems for Video Technology* 7 (2): 429–433. doi:10.1109/76.564122.

Maas, Hans-Gerd, and Uwe Hampel. 2006. “Photogrammetric Techniques in Civil Engineering Material Testing and Structure Monitoring.” *Photogrammetric Engineering and Remote Sensing* 72 (1): pp 39–45. doi:0099-1112/06/7201–0039.

Nie, Yao, and Kai Kuang Ma. 2002. “Adaptive Rood Pattern Search for Fast Block-Matching Motion Estimation.” *IEEE Transactions on Image Processing* 11 (12): 1442–1449. doi:10.1109/TIP.2002.806251.

Nishikawa, Takafumi, Junji Yoshida, Toshiyuki Sugiyama, and Yozo Fujino. 2012. “Concrete Crack Detection by Multiple Sequential Image Filtering.” *Computer-Aided Civil and Infrastructure Engineering* 27 (1): 29–47. doi:10.1111/j.1467-8667.2011.00716.x. http://doi.wiley.com/10.1111/j.1467-8667.2011.00716.x.

Omran, Mahamed G H, Andries P. Engelbrecht, and Ayed Salman. 2006. *Particle Swarm Optimization for Pattern Recognition and Image Processing*. *Studies in Computational Intelligence*. Vol. 34. doi:10.1007/978-3-540-34956-3_6.

Pan, Bing, Huimin Xie, Zhaoyang Wang, Kemao Qian, and Zhiyong Wang. 2008. “Study on Subset Size Selection in Digital Image Correlation for Speckle Patterns.” In *Optics Express*, 16:7037–7048. doi:10.1364/OE.16.007037. http://www.opticsinfobase.org/oe/abstract.cfm?URI=oe-16-10-7037.

Park, H. S., H. M. Lee, Hojjat Adeli, and I. Lee. 2007. “A New Approach for Health Monitoring of Structures: Terrestrial Laser Scanning.” *Computer-Aided Civil and Infrastructure Engineering* 22 (1) (January): 19–30. doi:10.1111/j.1467-8667.2006.00466.x. http://doi.wiley.com/10.1111/j.1467-8667.2006.00466.x.

Peters, W. H., and W. F. Ranson. 1982. “Digital Imaging Techniques In Experimental Stress Analysis.” In *Optical Engineering*, 21:213427. doi:10.1117/12.7972925. http://opticalengineering.spiedigitallibrary.org/article.aspx?doi=10.1117/12.7972925.

Ranganadham, D., P. Gorpuni, and G. Panda. 2009. “An Efficient Bidirectional Frame Prediction Using Particle Swarm Optimization Technique.” In *2009 International Conference on Advances in Recent Technologies in Communication and Computing*, 42–46. doi:10.1109/ARTCom.2009.87.

Reu, Phillip L, Michael Sutton, Yanqing Wang, and Timothy J Miller. 2009. “Uncertainty Quantification for Digital Image Correlation:” Proceedings of the SEM Annual Conference.

Shi, Y., and R. Eberhart. 1998. “A Modified Particle Swarm Optimizer.” In *1998 IEEE International Conference on Evolutionary Computation Proceedings. IEEE World Congress on Computational Intelligence (Cat. No.98TH8360)*, 69–73. doi:10.1109/ICEC.1998.699146.

Sonka, Milan, Vaclav Hlavac, and Roger Boyle. 2007. *Image Processing, Analysis, and Machine Vision*. Thomson-Engineering.

Sutton, M. A., J. J. Orteu, and H. Schreier. 2009. *Image Correlation for Shape, Motion and Deformation Measurements*. Springer. http://link.springer.com/book/10.1007/978-0-387-78747-3/page/1.

Sutton, MA, WJ Wolters, WH Peters, WF Ranson, and SR McNeill. 1983. “Determination of Displacements Using an Improved Digital Correlation Method.” *Image and Vision Computing*. doi:10.1016/0262-8856(83)90064-1.

Yamaguchi, Tomoyuki, and Shuji Hashimoto. 2006. “Automated Crack Detection for Concrete Surface Image Using Percolation Model and Edge Information.” *IECON Proceedings (Industrial Electronics Conference)*. doi:10.1109/IECON.2006.348070.

Yu, Jian H, Alex J Hsieh, Peter G Dehmer, and James M Sands. 2009. “Real-Time Full-Field Deformation Analysis on the Ballistic Impact of Polymeric Materials Using High-Speed Photogrammetry.” In *Procedings- American Society for Composites; 4; 2797-2805 American Society for Composites Annual Technical Conference; 24th, American Society for Composites*, 9.

Yuan, Xuedong Yuan Xuedong, and Xiaojing Shen Xiaojing Shen. 2008. “Block Matching Algorithm Based on Particle Swarm Optimization for Motion Estimation.” In *2008 International Conference on Embedded Software and Systems*, 191–195. doi:10.1109/ICESS.2008.35.